UNIVERSITAT POLITÈCNICA DE VALÈNCIA

INSTITUTO INTERUNIVERSITARIO DE INVESTIGACIÓN DE RECONOCIMIENTO MOLECULAR Y DESARROLLO TECNOLÓGICO

Design of smart scaffolds for the treatment and prevention of bone infection

PhD. THESIS

Submitted by

Lorena Polo Aguado

PhD. Supervisors:

Dr. José Luis Vivancos Bono
Dr. Elena Aznar Gimeno

Valencia, September 2018

José Luis Vivancos Bono, PhD and Lecturer at the *Universitat Politècnica de València*, and Elena Aznar Gimeno, PhD and researcher at Centro de Investigación Biomédica en Red (CIBER-BBN),

CERTIFY:

That the work *"Design of smart scaffolds for the treatment and prevention of bone infection"* has been developed by **Lorena Polo Aguado** under their supervision in the Instituto de Reconocimiento Molecular y Desarrollo Tecnológico (IDM) de la *Universitat Politècnica de València*, as a thesis Project in order to obtain the international degree of PhD at the *Universitat Politècnica de València*.

Valencia, June 2018.

Dr. José Luis Vivancos Bono   Dr. Elena Aznar Gimeno

A mis padres y a mi hermano.

But the real way to get happiness is by giving out
happiness to other people.
Try and leave this world a little better than you found it
and when your turn comes to die,
you can die happy in feeling that at any rate
you have not wasted your time but have done your best.

R. Baden-Powell

Agradecimientos
Acknowledgements

Bueno… ¡Por fin! No me puedo creer que al fin vaya a escribir los agradecimientos. Me los había dejado para el final, ya que los considero prácticamente la parte más especial de la tesis, y ahora resulta que no sé por donde empezar. Voy a intentar no extenderme, pero también voy a intentar no dejarme a nadie y, sobre todo, no dejar de agradecer mil veces a las personas que han estado a mi lado durante estos cuatro laaargos años. Os prometo que muchos no sois conscientes de lo mucho que me habéis ayudado, y espero que con estas palabras quede un poco más claro.

En primer lugar, me gustaría agradecer al director del IDM, Ramón Martínez Máñez, por haberme ofrecido la oportunidad de formarme, aprender y trabajar en un grupo de investigación como este. Gracias infinitas, por supuesto, a mi director de tesis José Luis Vivancos, por ayudarme en todo lo que has podido y por ofrecerme la posibilidad de colaborar en tus clases (algunas hasta las echo de menos, fíjate). Millones de gracias a mi otra directora de tesis, Elena. Me acuerdo siempre de aquella vez que me llamaste por teléfono para ofrecerme la beca lanzadera del CIBER, porque para mí ese fue el momento donde empezó toda la aventura de la tesis. Mil gracias por escucharme y tranquilizarme cuando estaba histérica (frecuentemente), y por tu apoyo enorme en todo momento. Gracias también a Joserra, por reclutarme y convertirme en una más; a Félix, por ayudarnos a todos aunque a veces no tengas por qué, y al resto de profesores del departamento (Loles, Luis Villaescusa), por echarnos siempre una mano y ser una parte más de este laboratorio. Gracias también a Carmelo y Cristina, por echarme una mano en su laboratorio, y a la profesora María Vallet Regí y a Daniel Arcos, por vuestra ayuda en nuestros proyectos compartidos.

Bueno… y ahora es cuando viene lo gordo. Quiero dar las gracias a todos mis compañeros, y lo pienso hacer uno por uno porque es mi tesis y hago lo

que quiero, básicamente. En primer lugar, quiero dar las gracias al grupito original que me encontré cuando llegué aquí más asustada que nada y sin tener ni idea de este mundo: gracias a Irene y Amelia, mis compis del máster: ¡gracias por recorrer este camino conmigo! Me acuerdo mucho de las aventuras con Irene (el gimnasio fallido, las clases de inglés fallidas, los ensayos fallidos… mecachis), y de los líos con Amelia para ver quién trabajaba por la mañana y por la tarde y quién se quedaba con la mesa del despacho (al final, no se la quedó ninguna…) Gracias también a Cris Marín, Toni, Luis Enrique, María Moragues, por incluirme en vuestros planes. Me acogisteis de maravilla y os prometo que no hay una forma mejor de empezar una tesis.

Gracias también al grupo de "mayores" de ese momento: Lluis, Cris G., Mar, Núria, Edgar, María Ruiz, Carol, Cris T… Me acuerdo cuando nos mirabais a las nuevas y nos decíais preocupados: "¡¿pero estáis seguras de que queréis hacer la tesis?!". Pero al final no os escuchamos y oye, aquí estamos. Y no fuimos los únicos: poco a poco se fue llenando el laboratorio… (igual os suena la historia y tal).

Gracias infinitas a los que marcasteis una época especial: Marta (¡¡te echo muchísimo de menos!! Y no sólo por las gestiones en el lab, pero bueno, ya te lo imaginas…), Bea (gracias por dejarme vivir en tu casa cuando me echaron de la mía, y sobre todo por los tintos de verano!), Luis (eres molt crack allà on vages!), Anita (vuelveeee), Niamh (Nif, my Little Duck!), Mónica (no se me olvida que te debo una clase de muñequitos), y bueno, en resumen, toda la tromba de gente que llegó casi a la vez y que forman esta generación de sufridos doctorandos: Santi (ánimo con tu sprint final), Adrián (suerte en San Diego), Alba (todavía me acuerdo del perro gordo de Barcelona, jajaja), Elisa (¡menos mal que alguien pone orden!), Xente (compi del abandonado lab 2.1), e Iris (no dejes que las células puedan contigo, ¡tú puedes con ellas!). No puedo no acordarme de aquellos momentos de sobresaturación en el 2.6, todos estresados, peleándonos con los equipos, con las mesas divididas entre 10 personas y haciendo turnos de mañanas y tardes para poder caber en el

laboratorio… en aquel momento no tenía mucha gracia, pero ahora me río al recordarlo.

Gracias a todos por tan buenos momentos ☺.

No quiero olvidar tampoco a la sección internacional, que nos ha hecho un poquito más abiertos y más multiculturales. Gracias a Sameh, Hazem, Ismael, Maria Elena, Andy, Tania… Trabajar con gente de otras culturas es un privilegio que no se tiene en todos los trabajos, y me alegro mucho de haber compartido un trocito de lab con vosotros (trocito literal, muchas veces).

También quiero dar las gracias, con mucho cariño, a las nuevas adquisiciones del lab 2.6: Eva y Bea, lo siento, pero para mí seguís siendo las nuevas, jiji. Tened mucha paciencia con Borja y Xente (lo que hay que aguantar…) y mucha suerte con los años que aún os quedan. No me olvido de la sección principesas: Gema, Alejandra, Araceli y Sara R.: ¡mucha suerte también! Y gracias, cómo no, a los postdocs del lab: María, Andrea, Borja y ahora Paula y Juanfran: gracias por vuestra ayuda desinteresada en todo momento y, sobre todo, ¡ÁNIMOOO! El lab 2.6 no puede ir mal si estáis vosotros ☺ Gracias a la sección de la Fe: Sara, Mari Carmen (echaré mucho de menos tus chistes e historias) y Àngela (ànim!! Eres tot un exemple!).

Vorrei anche ringraziare la dottoressa Milena Fini per avermi permesso di trascorrere tre mesi nel suo laboratorio: ho imparato tantissimo e mi è piaciuto molto condividere questi mesi con voi! Un grazie in particolare a Stefania, per la tua pazienza, ed a Elena, per la tua accoglienza in Italia nei primi giorni. Grazie anche a tutta la gente del laboratorio del centro Codivilla-Putti: Laura, Ada, Olga… Ho dei meravegliosi ricordi di Bologna grazie a voi!

Ya puestos, querría dar las gracias a la gente del Servicio de Microscopía, porque son grandes profesionales y me han tratado genial siempre. También, cómo no, quiero dar las gracias al resto de habitantes del Departamento de Química: gracias a Eva, Pablo y Quique. A Vicky y Óscar (suerte en tu nuevo

trabajo) y, sobre todo, a Andrea y Juan Carlos, porque sois geniales. ¡Muchísima suerte en el futuro!

Bueno, parece que ya acabo… me he dejado lo mejor para el final. En definitiva, gente, gracias por todo este tiempo juntos, porque habéis sido una constante durante estos cuatro años, porque prácticamente os he visto más que a mi familia y porque, aunque no lo sepáis, muchas veces me habéis ayudado aunque sea con una sonrisa, con un chiste en el laboratorio, o con una reunión de lamentamiento general en la sala del café. Para el recuerdo quedan la partida de paintball, las comidas internacionales, las cenas del Workshop (aunque me perdiera aquella tan mítica), las tardes de limpieza con la música a tope, las broncas y las reuniones subversivas interminables, los cotilleos clandestinos, el rafting, las cervezas en el Bocho, los volcanes de colores y las tardes esas improductivas que se alargaban inevitablemente… Gracias, en serio. Viéndolo así, parece hasta bonito jajaja.

Gracias a mi familia, por intentar entender este mundillo (sin éxito) y creer siempre en mí.

A Mireia y Arantza, me alegro muchísimo de haber llegado juntas hasta aquí. ¡Ánimo hasta el final!

A mis amigos, que ya sabéis quienes sois pero yo lo pongo igual: Luci, Laura, Laura Ll., Mari, Tamara, Iris, Alberto (¡¡compañero de fatigas!!), Jose y Pepelu… si hemos llegado juntos hasta aquí, ya nos toca juntos para toda la vida. Gracias. ♥

No me olvido de vosotras: Àngels (TODA la vida juntas), Mónica, Lucía, Marta, Javi, Xexu… ¿Qué os puedo decir? Nos vemos en los bares y en las fiestas de los pueblos ☺

Mis agradecimientos más especiales se los voy a dar a una de las mejores personas que me ha regalado esta tesis… a Nati, porque te lo mereces, por ser un cielo de persona y, especialmente, por aguantarme (y lo que te queda…yo de ti me iba de nuevo a Australia jajaja).

Y, por último, esto no habría sido posible sin mis compañeras de piso, Gema y María… sois otro de los grandes regalos del 2015. No me puedo imaginar otras compañeras de piso mejores que vosotras.

Estos cuatro años han sido maravillosos.

Gracias.

Acknowledgements

Resum

La present tesi doctoral, titulada "Disseny de scaffolds intel·ligents per la prevenció i tractament de la infecció òssia", es centra en el desenvolupament de materials híbrids orgànic-inorgànics capaços de realitzar una lliberació controlada de fàrmacs amb propòsits biomèdics.

En el primer capítol, es presenta una introducció general sobre química supramolecular, materials híbrids orgànic-inorgànics i materials porosos. També s'explica extensivament la caracterització i les aplicacions d'aquests materials, ja que estos continguts estan altament relacionats amb el desenvolupament d'aquesta tesi.

En el segon capítol, es presenten tres projectes sobre el disseny de portes moleculars. En el primer, es mostren dos sistemes basats en l'ús d'un vidre mesoporós que actua com a suport inorgànic, carregat i funcionalitzat amb molècules orgàniques per a dur a terme una lliberació controlada de substàncies. La primera porta molecular està formada per amines i adenosín 5'-trifosfat (ATP), i la segona està formada per 3-(trimetoxisilil)propilisocianat unit a polímers de ε-poli-L-lisina. Els dos sistemes s'han caracteritzat per resonància magnètica nuclear en estat sòlid (RMN) i espectroscopia infrarroja per transformada de Fourier (FTIR). També s'han estudiat les propietats bioactives de ambdós materials. Després, ambdues portes moleculars han sigut implementades en sòlids carregats amb l'objectiu de demostrar que es pot realitzar una lliberació controlada de la càrrega. En el primer cas, el suport mesoporós s'ha carregat amb doxorrubicina, i el sistema s'ha validat in vitro amb cèl·lules humanes d'osteosarcoma (HOS). En el segon cas, el suport mesoporós s'ha carregat amb levofloxací i s'ha entapissat amb ε-poli-L-lisina; el sistema s'ha validat amb bacteris *E.coli*.

Resum

Una volta descrits aquests sistemes, es presenta una segona publicació on també s'utilitza la porta molecular d'ATP. En aquest cas, el vidre mesoporós bioactiu que actua com a suport inorgànic té una composició de 80%SiO_2-15%CaO-5%P_2O_5, y s'ha carregat amb levofloxací amb l'objectiu d'aconseguir propietats antibiòtiques. El sòlid s'ha caracteritzat mitjançant les tècniques corresponents, i s'han estudiat les seues propietats bioactives. Finalment, s'han utilitzat bacteris *E.coli* per demostrar que el sòlid posseïx activitat antibiòtica, i que és capaç de dur-la a terme solament en presència de fosfatasa àcida.

El tercer projecte presentat consisteix en un suport de MCM-41 carregat amb un colorant i funcionalitzat amb una seqüència peptídica que actua com a porta molecular. L'estímul utilitzat en aquest cas és la proteasa V8, típica del microorganisme *S. aureus*. El sistema ha sigut corresponentment caracteritzat, i s'han testat les seues propietats de lliberació controlada de substàncies *in vitro*, demostrant l'eficàcia del disseny.

En el tercer capítol, s'ha utilitzat un derivat d'un component d'olis essencials (vanil·lina) per funcionalitzar microesferes i scaffolds de fosfat de calci amb l'objectiu de dotar-los de propietats antibiòtiques. En primer lloc, s'ha sintetitzat y caracteritzat el compost derivat de la vanil·lina, i s'ha unit a la superfície dels materials de fosfat càlcic. Després, s'han estudiar les propietats antimicrobianes d'ambdós materials en presència de bacteris *E.coli*. També s'han dut a terme assajos de citotoxicitat amb cèl·lules tipus fibroblast L929 per demostrar que els sòlids funcionalitzats amb la vanil·lina no són tòxics. Per últim, s'han dut a terme assajos de biocompatibilitat amb cèl·lules humanes tipus-osteoblast MG-63, demostrant que les propietats osteoregeneratives dels materials originals no es veuen modificades després del procés de funcionalització.

En resum, es pot concloure que els resultats obtinguts en aquesta tesi han contribuït al camp dels materials de lliberació control·lada i materials amb

propietats antibacterianes. Els nous dissenys poden ser claus per al desenvolupament de futures aplicacions en la recerca biotecnològica i biomèdica, particularment en les teràpies que traten la infecció i la regeneració òssea.

Resumen

La presente tesis doctoral, titulada "Diseño de scaffolds inteligentes para la prevención y tratamiento de la infección ósea", se centra en el desarrollo de materiales híbridos orgánico-inorgánicos capaces de realizar una liberación controlada de fármacos con fines biomédicos.

En el primer capítulo, se presenta una introducción general sobre química supramolecular, materiales híbridos orgánico-inorgánicos y materiales porosos. También se explica de forma extensiva la caracterización y aplicaciones de estos materiales, ya que estos contenidos están altamente relacionados con el desarrollo de esta tesis.

En el segundo capítulo, se presentan tres proyectos sobre el diseño de puertas moleculares. En el primero, se muestran dos sistemas basados en el uso de un vidrio mesoporoso que actúa como soporte inorgánico, cargado y funcionalizado con moléculas orgánicas para llevar a cabo una liberación controlada de sustancias. La primera puerta molecular está compuesta por aminas y adenosín 5'-trifosfato (ATP), y la segunda está formada por 3-(trietoxisilil)propilisocianato unido a polímeros de ɛ-poli-L-lisina. Los dos sistemas se han caracterizado por resonancia magnética nuclear en estado sólido (RMN) y espectroscopía infrarroja por transformada de Fourier (FTIR). También se han estudiado las propiedades bioactivas de ambos materiales. Después, ambas puertas moleculares se han implementado en sólidos cargados con el objetivo de demostrar se podía realizar una liberación controlada de la carga. En el primer caso, el soporte mesoporoso se ha cargado con doxorrubicina y se ha tapizado con moléculas de ATP. El sistema se ha validado in vitro con células humanas de osteosarcoma (HOS). En el segundo caso, el soporte mesoporoso se ha cargado con levofloxacino y se ha tapizado con ɛ-poli-L-lisina, y el sistema se validado con bacterias *E.coli*.

Una vez descritos estos sistemas, se presenta una segunda publicación donde también se utiliza la puerta molecular de ATP. En este caso, el vidrio mesoporoso bioactivo que actúa como soporte inorgánico tiene una composición de 80%SiO$_2$-15%CaO-5%P$_2$O$_5$, y se ha cargado con levofloxacino con el objetivo de conseguir propiedades antibióticas. El sólido se ha caracterizado mediante las técnicas correspoondientes, y se han estudiado sus propiedades bioactivas. Finalmente, se han utilizado bacterias *E.coli* para demostrar que el sólido posee actividad antibiótica, y es capaz de llevarala a cabo solo en presencia de fosfatasa ácida.

El tercer proyecto presentado consiste en un soporte de MCM-41cargado con un colorante y funcionalizado con una secuencia peptídica que actúa como puerta molecular. El estímulo usado en este caso es la proteasa V8, típica del microorganismo *S. aureus*. El sistema ha sido correspondientemente caracterizado, y se han testado sus propiedades de liberación controlada de sustancias *in vitro*, demostrando la eficiencia del diseño.

En el tercer capítulo, se utiliza un derivado de un componente de aceites esenciales (vanillina) para funcionar microesferas y scaffolds de fosfato de calcio, para dotarlos de propiedades antibióticas. En primer lugar, se ha sintetizado y se ha caracterizado el compuesto derivado de la vanillina, y se ha anclado en la superficie de los materiales de fosfato cálcico. Después, se han estudiado las propiedades antimicrobianas de ambos materiales en presencia de bacterias *E.coli*. También se han llevado a cabo ensayos de citotoxicidad con células tipo-fibroblasto L929 para demostrar que los sólidos funcionalizados con vanillina no son tóxicos. Por último, se han llevado a cabo ensayos de biocompatibilidad con células humanas tipo-osteoblasto MG-63, demostrando que las propiedades osteoregenerativas de los materiales originales no se ven modificadas tras el proceso de funcionalización.

Resumen

En resumen, se puede concluir que los resultados obtenidos a lo largo de esta tesis han contribuido al campo de los materiales de liberación controlada y de los materiales con efecto antibactérico. Estos nuevos diseños pueden ser clave en futuras aplicaciones para la investigación biotecnológica y biomédica, particularmente en terapias para la regeneración y contra la infección ósea.

Abstract

This thesis, entitled "Design of smart scaffolds for the treatment and prevention of bone infection", is focused on the development of smart organic-inorganic hybrid materials capable of perform controlled-delivery of drugs with biomedical purposes.

In the first chapter, a general introduction about supramolecular chemistry, organic-inorganic hybrid materials and porous materials is given. The characterization and applications of porous materials are extensively explained, since those contents are highly related to the developing of this thesis.

In the second chapter, three projects based on the design of gated devices are presented. In the first publication, two gated systems based on the use of a mesoporous silica material as an inorganic support, loaded and functionalized with organic molecules to achieve a controlled drug release are studied. The first molecular gate is composed by amino moieties and adenosine 5'-triphosphate (ATP), and the second one is composed by 3-(triethoxysilyl)propylisocyanate linked to ε-poly-L-lysine polymers. The two systems were characterized by solid state nuclear magnetic resonance (NMR) and Fourier transformed infrared spectroscopy (FTIR). The bioactivity capabilities of the materials were also studied. Then, both molecular gates have been implemented in loaded solids in order to demonstrate their controlled-release capabilities. In a first case, the mesoporous support was loaded with doxorubicin and capped with ATP molecules, and the system has been validated in a human osteosarcoma cell culture test. In a second case, the mesoporous support was loaded with levofloxacin and capped with the ε-poly-L-lysine molecular gates, and the system has been validated with *E.coli* bacteria.

Once these two systems are described, a second project with the ATP molecular gates is presented. In this case, the mesoporous bioactive glass which acts as support has a composition of $80\%SiO_2$-$15\%CaO$-$5\%P_2O_5$, and it

has been loaded with levofloxacin with the purpose of killing bacteria. The solid has been characterized by corresponding techniques, and its bioactive properties have been studied. Finally, *E.coli* bacteria have been used to demonstrate that the solid is able to perform an antimicrobial activity only in the presence of acid phosphatase.

The third project consists of a MCM-41 support loaded with a dye and capped with a peptide sequence. The trigger used in this case is the V8 protease, typical of the microorganism *S. aureus*. The system has been correspondingly characterized, and its drug release properties *in vitro* have been tested, demonstrating the efficiency of the design.

In the third chapter, calcium phosphate microspheres and scaffolds have been functionalized with an essential-oil component derivative in order to achieve antibacterial properties. First, the vanillin-derivative has been synthesized and characterised, and in a second step, it has been attached to the surface of the calcium phosphate materials. Then, the antimicrobial properties of both materials have been tested against *E.coli* bacteria. Cytotoxicity assays with L929 fibroblast-like cells have been performed in order to demonstrate that the functionalized scaffolds did not perform a cytototxic effect. Finally, biocompatibility assays have been made with MG-63 human osteoblast-like cells, demonstrating that the functionalization of the scaffolds with vanillin do not affect their osteoregenerative properties.

To sum up, it can be concluded that the results obtained in this thesis have contributed to the field of stimuli-responsive materials and antibacterial devices. The new designs could be key in the development of future applications in biotechology and biomedical research, particularly in bone infection and bone regeneration therapeutics.

x

Abbreviations and Acronyms

ALP	Alkaline Phosphatase
ALPL	Alkaline Phosphatase (gene)
ANOVA	Analysis of Variance
APase	Acid Phosphatase
APTS	3-Aminopropyl Triethoxysilane
ATCC	American Type Culture Collection
ATP	Adenosine Triphosphate
αTCP	α-Tricalcium Phosphate
BET	Brunauer-Emmett-Teller
bFGF	Basic Fibroblast Growth Factor
BGLAP	Bone Gamma Carboxyglutamate Protein
BJH	Barret-Joyner-Halenda
BMP2	Bone Morphogenetic Protein 2
βTCP	β-Tricalcium Phosphate
CaP	Calcium Phosphate
CDHA	Calcium-Deficient Hydroxyapatite
cDNA	Complementary Deoxyribonucleic Acid
CFU	Colony Formation Units
COL1a1	Collagen Type 1a1 Chain
CP/MAS	Cross-Polarization/Magic Angle Spinning
CPT	Camptothecin
CTABr	n-Cetyltrimethylammonium Bromide
DCPA	Dicalcium Phosphate Anhydrous
DCPD	Dicalcium Phosphate Dihydrate
DMEM	Dulbecco's Modified Eagle's Medium
DMF	Dimethylformamide
DNA	Deoxyribonucleic Acid
DOX	Doxorubicin
EC$_{50}$	Half Maximal Effective Concentration

ECM	Extracellular Matrix
EDC	N-(3-Dimethylaminopropyl)-N'-Ethylcarbodiimide Hydrochloride
EDQM	European Directorate for the Quality of Medicines
EDTA	Ethylendiaminetetraacetic Acid
EDX	Energy-Dispersive X-ray Analysis
EISA	Evaporation-Induced Self-Assembly
EOC	Essential Oil Component
ɛ-PL	E-poly-L-Lysine
EthD-1	Ethidium Homodimer
FBS	Fetal Bovine Serum
FESEM	Field Emission Scanning Electron Microscopy
FTIR	Fourier-Transform Infrared Spectroscopy
HAp	Hydroxyapatite
HOS	Human Osteosarcoma
Hyal-1	Hyaluronidase 1
IGF-I	Insulin-like Growth Factor
LB	Luria-Bertani
LCT	Liquid Crystal Templating
LDH	Lactate Dehydrogenase
MBG	Mesoporous Bioactive Glass
MCM	Mobile Crystalline Materials
MCPA	Monocalcium Phosphate Anhydrous
MCPM	Monocalcium Phosphate Monohidrate
MCS	Mesoporous Calcium Silicate
MH	Metformin Hydrochloride
MSA	Mesoporous Silica Alumina
MSN	Mesoporous Silica Nanoparticles
N3	3-[2-(2-Aminoethylamino)ethylamino]propyl-Trimethoxysilane
NCO	3-(Triethoxysilyl)propylisocyanate

NMR	Nuclear Magnetic Resonance
PBS	Phosphate Buffered Saline
PCR	Polymerase Chain Reaction
PTFE	Polytetrafluoroethylene
qPCR	Quantitative Polymerase Chain Reaction
RFU	Relative Fluorescence Units
rhBMP2	Recombinant Human Bone Morphogenetic Protein 2
rhTGFβ1	Recombinant Human Transforming Growth Factor β1
RNA	Ribonucleic Acid
$[Ru(bpy)_3]^{2+}$	Tris(Bipyridine)Ruthenium(II) Chloride
SEM	Scanning Electron Microscopy
SFB	Simulated Body Fluid
SPSS	Statistical Package for the Social Sciences
TEA	Triethylamine
TEM	Transmission Electron Microscopy
TGA	Thermogravimetric Analysis
TGF-β	Transforming Growth Factor
TMS	Tetramethylsilane
TTCP	Tetracalcium Phosphate
UV	Ultraviolet
VEGF	Vascular Endothelial Growth Factor

Table of contents

2

1. General introduction

This PhD thesis is focused on the design and use of silica-based materials with biomedical purposes. For a further understanding of the contents, a general introduction is presented to set down the basis of supramolecular chemistry, organic-inorganic hybrid materials and porous materials.

1.1 Supramolecular Chemistry

"Atoms are letters, molecules are the words, supramolecular entities are the sentences and the chapters".

The term "supramolecular chemistry" was coined for the first time in 1978 by Jean-Marie Lehn, who defined a "supermolecule" as an organized complex entity that is created from the association of two or more chemical species held together by intermolecular forces.[1] "Supramolecular Chemistry" would comprise the study of these complex entities and their intermolecular bonding. The studies and contribution of J.M. Lehn and his colleagues Charles Pedersen

---

[1] J. M. Lehn, *Pure Appl. Chem.* **1978**, *50*, 871-892.

and Donald Cram to this new field were recognized with a well-deserved Nobel prize in 1987, and implied the opening of a new field of study.[2,3]

Luckily, the late coining of the term does not mean that supramolecular chemistry did not exist hundreds of years before. Actually, supramolecular chemistry can be found from the very first stages of the Earth: from the hydrogen bonds in water molecules, to the complex system enzyme-substrate existing in the complicated biology of human body.[4] Intermolecular interactions include hydrogen bonding, metal coordination, hydrophobic forces, van der Waals forces, π-π interactions and electrostatic effects. These different types of bonding allow the molecules to join and organize in great complex structures, contributing to create the macroscopic world we are used to see. Other example of supramolecular arrangement lead us to the formation of cell membranes with all the receptors, the formation of double stranded DNA, and the phenomena of protein folding. What is more: supramolecular chemistry is not only present in the interior of our bodies; we can also find it in each aspect of our daily life. Pharmaceutics or the fabrication of plastic in polymer industry are examples of how the study and use of supramolecular chemistry has improved our life quality.[5]

Seen that, it can be expected that supramolecular chemistry had started to being studied far before the 1970s, though it had not properly been given a name. We found that the fundaments of supramolecular chemistry date back to the late 19th century.[6] For example, Alfred Werner developed the idea of coordination chemistry in 1893.[7] Villiers and Hebd discovered cyclodextrines

---

[2] J. M. Lehn, *Angew. Chem. Int. Ed. Engl.* **1988**, *27*, 89-112.

[3] J. M. Lehn, *Supramolecular Chemistry*, Ed. VCH, **1995**; J.-M. Lehn, Nobel lecture, 1987.

[4] F. M. Menger. *Proc Natl Acad Sci U.S.A.* **2002**; *99*, 4818–4822.

[5] P. J. Cragg. *Supramolecular Chemistry: From Biological Inspiration to Biomedical Applications.* Ed. Springer, **2010**.

[6] C. A. Schalley, *Analytical Methods in Supramolecular Chemistry.* WILEY-VCH, **2007**.

[7] A. Werner, *Zeitschr. Anorg. Chem.* **1893**, *3*, 267-330.

in 1891,[8] and found that were molecules which could host a guest-molecule, a model which would be properly defined by Emil Fischer in 1894 as the *lock-and-key* concept.[9] Even Wolf and his coworkers introduced the term "Übermolekül" to refer the coordination between dimers of carboxylic acids.[10] However, it was not until the formal definition of Supramolecular Chemistry given by Lehn when the field arose as a discipline and started to settle the foundations for the sophisticated chemistry we know nowadays.[1]

Currently, this non-covalent bond chemistry comprises a wide area of study which is also connected with other disciplines as physics, materials science, biology and, as stated in this PhD thesis, nanomaterials and biomedicine. Each of these subjects have contributed to increase the spectra of study of supramolecular chemistry.

Supramolecular chemistry deals with three big areas, and the first one considers **molecular recognition chemistry**. Molecular recognition can be defined as the binding between a substrate molecule and a receptor molecule.[11] Thus, a given molecule would recognize its partner molecule in a selective way, and would bind to it to form a host-guest complex. A pretty example of molecular recognition in nature can be found in the already mentioned Fischer *lock-and-key* model (**Figure 1.1**).[12]

According to Fischer, the *lock* or *host* would be an enzyme with a determined key hole or active site, while the *key* or *guest* would be a specific substrate. Only the correctly sized key would fit in the key hole, which means that only a specific substrate, and no other, will bind with the enzyme,

---

[8] a) A. Villiers, C. R. Hebd, *Seances Acad. Sci.* **1891**, *112*, 435; b) A. Villiers, C. R. Hebd, *Seances Acad. Sci.* **1891**, *112*, 536-538.

[9] a) E. Fischer, *Ber. Deutsch. Chem. Ges*, **1894**, *27*, 2985-2993; b) J. P. Behr, *The Lock and Key Principle. TheState of the Art – 100 Years On*, Wiley, **1994**.

[10] K. L. Wolf, H. Frahm, H. Harms, Z. *Phys. Chem. (B)*, **1937**, *36*, 237-287.

[11] D.J. Cram, *Angew. Chem. Int. Ed.*, **1988**, *27*, 1009-1020.

[12] D.J. Cram, J.M. Cram, *Science*, **1974**, *183*, 803-809.

according to the molecular recognition principle. This mechanism is the base of plenty biochemical reactions in the living organisms.
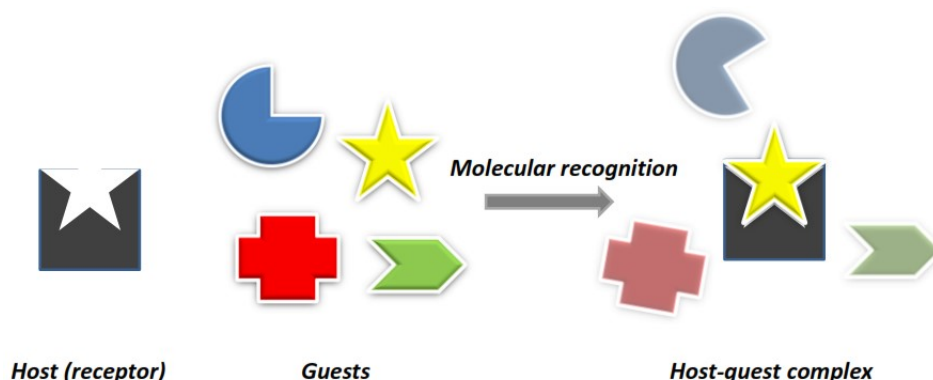

Figure 1.1. Schematic representation of the process of molecular recognition: only one guest is able to bind to the host.

The second field of study is focused on the **chemistry of molecules built to specific shapes**. Supramolecular advances have achieved the design and synthesis of geometric supermolecules with interesting features, like fullerenes, carbon nanotubes or rotaxanes, which have important applications in industry and research, since they are used in microelectronics, solar cells, energy storage…[13] Although medium supermolecules have drawn big attention over the last years, their study is not the scope of this PhD thesis.

Finally, supramolecular chemistry is also related with the study of the **chemistry of self-assembly** from numerous molecules. Molecular self-assembly is the spontaneous formation of supermolecules with specific shapes and characteristics, composed by molecules bonded through non-covalent interactions.[14] Micelles, membranes or vesicles are examples of self-assembled

---

[13] M. Prato, *J. Mater. Chem.*, **1997**, *7*, 1097-1109.

[14] a) G. M. Whitesides, J. P. Mathias, C. T. Seto, *Science,* **1991**, *254*, 1312-1319; b) D. Philp, J. F. Stoddart, *Angew. Chem.* **1996**, *108*, 1243-1286.

systems. But, as before, chemistry of self-assembly is not found only in living bodies: films, gels, nanostructures and polymers are all formed by molecular self-assembly.

The issues treated in this PhD thesis are directly related with supramolecular chemistry, especially with molecular recognition chemistry and chemistry of self-assembly. The synthesis and characterization of nanoscopic mesoporous materials is complemented with the bonding and functionalization with organic molecules and supermolecules. Moreover, the stimuli responsive gated materials developed in this thesis concur with molecular recognition, as the presented systems have been designed for being selective and accurate.

1.2 Hybrid materials

The implementation of organic entities with inorganic materials yields the opportunity to take profit of both the advantages of organic and inorganic compounds. These multicomponent systems are referred as organic-inorganic hybrid materials, and usually the combination of their constituents brings along a synergic effect.[15]

A large number of organic-inorganic hybrid materials with far different applications can be found in literature.[16] Particularly, the trend of incorporating functional molecules in a tridimensional scaffolding has resulted in innovative systems in the fields such those that will be seen along this introduction.[17,18,19]

---

[15] A.B. Descalzo, R. Martínez-Máñez, F. Sancenón, K. Hoffman, K. Rurack, *Angew. Chem.Int*, **2006**, *45*, 5924-5948.

[16] K. Rurack, R. Martínez-Máñez, *The supramolecular chemistry of organic-inorganic hybrid materials*, Wiley, **2010**.

[17] M. Comes, M. D. Marcos, R. Martínez-Máñez, F. Sancenón, J. Soto, L. A. Villaescusa, P. Amorós, D. Beltrán, *Adv. Mater.* **2004**, *16*, 1783-1786.

[18] M. Comes, G. Rodríguez-López, M. D. Marcos, R. Martínez- Máñez, F. Sancenón, J. Soto, L. A. Villaescusa, P. Amorós, D. Beltrán, *Angew. Chem. Int. Ed.* **2005**, *44*, 2918-2922.

This thesis will focus in the functionalization of porous materials with functional entities, with the purpose of developing new hybrid nanodevices as controlled release systems for biomedical applications.

1.3 Porous materials

Porous materials are those materials which present a porous architecture. Is not easy to give a proper classification of porous substances due to their wide nature, so it has been selected the classification given by the IUPAC (International Union of Pure and Applied Chemistry), based on pore sizes. According to that, pores sizes can be classified in three categories: micropores, mesopores and macropores (see **Figure 1.2**). Microporous materials would be those with pores smaller than 2 nm. Mesoporous materials would comprise those materials with pores between 2 nm and 50 nm, and macroporous materials would have large pores bigger than 50 nm.[20]
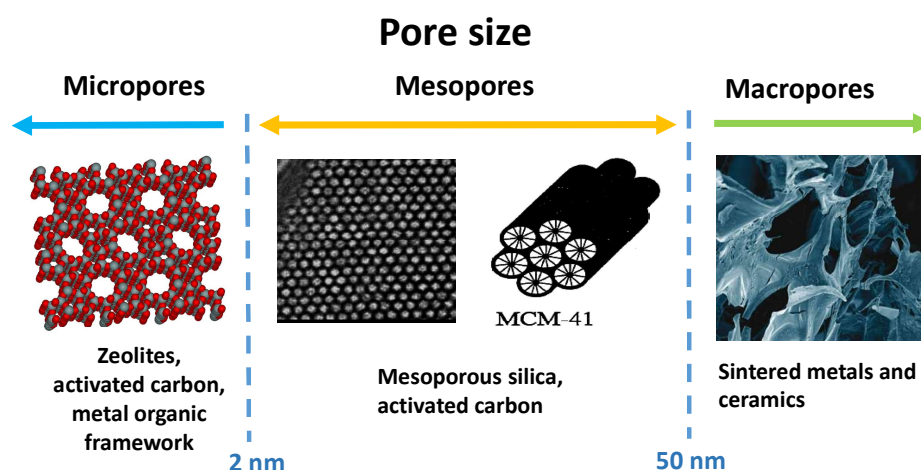

Figure 1.2. Porous materials with different pore size.

---

[19] C. Coll, R. Martínez- Máñez, M. D. Marcos, F. Sancenón, J. Soto, *Angew. Chem. Int. Ed.* **2007**, *46*, 1675-1678.

[20] IUPAC, "Manual of symbols and terminology", *Pure Appl. Chem.*, **1972**, *31*, 578-638.

Applications of porous materials are wide ranging. Particularly, microporous materials have great importance in fields as catalysis, and the most popular materials with micropores are crystalline aluminosilicates called zeolites. Their narrow pore distribution and small micropores imply high surface areas which make them suitable for catalysis; however, their small size also brings along many limitations.[21]

On the other hand, bigger pore distributions of mesoporous materials make them valid for more varied applications, as catalysis as well,[22] filtration and separation methods,[23] gas adsorption and storage,[24] enzyme immobilization,[25] tissue regeneration,[26] drug delivery[27] and chemical and biochemical sensing.[28] Finally, macroporous materials as amorphous metallic oxides are also used in catalysis, industry and tissue regeneration field.[29]

In this thesis, great importance is given to mesoporous silica materials due to their particular characteristics. Their capabilities as drug delivery systems and the easy functionalization of their surface make them appropriate to implement molecular gates for biomedical applications. Apart from that, the

[21] J. Weitkamp, *Solid State Ionics,* **2000**, *131*, 175.

[22] D.E. De Vos, M. Dams, B.F. Sels, P.A. Jacobs, *Chem. Rev.,* 2002, *102*, 3615

[23] X. Liu, Y. Du, Z. Guo, S. Gunasekaran, C. B. Ching, Y. Chen, S .J. Leong, Y. Yang, *Microporous Mesoporous Mater.*, **2009**, *122*, 114.

[24] M. Kruk, M. Jaroniec, *Chem. Mater.*, **2001**, *13*, 3169. b) A. Corma, M. Moliner, M. J. Díaz-Cabañas, P. Serna, B. Femenia, J. Primo, H. García, *New J. Chem.*, **2008**, *32*, 1338.

[25] M. Vallet-Regí, M. Colilla, I. J. Izquierdo-Barba, *Biomed. Nanotechnol.*, **2008**, *4*, 1.

[26] I. Slowing, B. G. Trewyn, S. Giri, V. S.–Y. Lin, *Adv. Funct. Mater.*, **2007**,*17*, 1225.

[27] M. Vallet-Regí, F. Balas, D. Arcos, *Angew. Chem., Int. Ed.*, **2007**, *46*, 7548. b) K. A. Kilian, T. Bocking, K. Gaus, J. King-Lacroix, M. Gal, J. J. Gooding, *Chem. Commun.*, **2007**, 1936.

[28] A. Jane, R. Dronov, A. Hodges, N. H. Voelcker, *Trends Biotechnol.*, **2009**, *27*, 230.

[29] A. R. Boccaccini, J. J. Blaker, V. Maquet, R. M. Day, R. Jerome, *Mater. Sci. Eng. C*, **2005**, *25*, 23–31.

functionalization of other porous materials as calcium phosphates has also been carried out in this thesis. In the next sections **3.1** and **3.2**, an extensive explanation of mesoporous and macroporous materials is given, with the purpose to facilitate the understanding of the thesis goals and the comprehension of the subsequent chapters.

1.3.1 Mesoporous silica materials

Mesoporous materials have been studied since 1970. In literature can be found some publications and patents about the synthesis of materials with mesoporous structures, but they presented a wide pore distribution and irregular channels that made them unsuitable for various applications.[30] It was not until 1992 that the Mobil Research and Development Corporation presented the synthesis of the mesoporous materials such as we know today. With narrow pore distribution and high ordered pores with a size between 2 and 10 nm, the group of these innovative materials was called the family of M41S.[31]

M41S materials are composed by an amorphous silica network arranged in a mesoporous structure with ordered pores and a large specific surface area between 500 m^2/g and 1000 m^2/g. Their pore volume is large, within the order of 1 cm^3/g, and they present also high chemical inertness and thermal stability. In addition, the synthesis of those materials is simple and reproducible, based on inexpensive and non-hazardous precursors.[32] All these advantages made this new type of materials very popular in the area of inorganic chemistry and catalysis, and researchers were promptly aware of their high potential and new applications began to rise due to their excellent properties.

---

[30] W. Li, D. Zhao, *Chem. Commun.*, **2013**, *49*, 943.

[31] J. S. Beck, J. C. Vartuli, W. J. Roth, M. E. Leonowicz, C. T. Kresge, K. D. Schmitt, C. T. W. Chu, D. H. Olson, E. W. Sheppard, S. B. Mccullen, J. B. Higgins, J. L. Schlenker, *J. Am. Chem. Soc.*, **1992**, *114*, 10834-10843.

[32] C. T. Kresge, M. E. Leonowicz, W. J. Roth, J. C. Vartuli, J. S. Beck, *Nature*, **1992**, *359,* 710-712.

One of the goals the researchers had been trying to reach was the control of size and distribution of the pores. The synthesis of these new materials is based on the presence of a structural directing agent, also called template. The organic molecules of the template usually arrange in a determined structure, that functions as a central structure around which an inorganic precursor polymerizes.[33] In this case, silica precursor was arranged around surfactant micelles following what we call a liquid crystal templating mechanism. Template agents were also used in the synthesis of microporous zeolites; the difference now was that they were no longer single, solvated organic molecules or metal ions, but self-assembled supramolecular species.[34] These templates would arrange in a different manner depending on factors as molecular size, temperature, pH, etc., allowing silica condensation upon different mesoporous structures with different characteristics. The best-known representatives of this kind of materials are depicted in the **Figure 1.3** and include Mobile Crystalline Materials as MCM-41, whose pores are distributed in a hexagonal arrangement; MCM-50, with lamellar distribution of pores, and MCM-48, whose pores are arranged upon a cubic distribution.[35,36]

Despite being the most popular, pure silica mesoporous materials are not the only. Apart from the M41S family, other mesoporous materials were studied and discovered during the 90s. Mesoporous materials made of transition metals require a more challenging procedure for researchers, since the hydrolysis and arrangement of non-silica precursors are more difficult to

---

[33] Zeid A. ALOthman, *Materials,* **2012**, *5*, 2874-2902.

[34] K. Song, J. Guan, Z. Wang, C. Xu, Q. Kan, *Appl. Surf. Sci.* **2009**, *255*, 5843–5846.

[35] C. T. Kresge, W. J. Roth, *Chem. Soc. Rev.,* **2013**, *42*, 3663.

[36] J. C. Vartuli; W.J. Roth, T. F. Degnan, Mesoporous materials (M41): From discovery to application. In: Schwarz J.A., Contescu C.I., Putyera K., editors. Dekker Encyclopedia of Nanoscience and Nanotechnology. Taylor and Francis; New York, NY, USA: **2008**. pp. 1797–1811.

control. Synthesis of mesoporous supports made of alumina, titanium, zirconia or gold are extensively described in literature.[37,38,39,40]
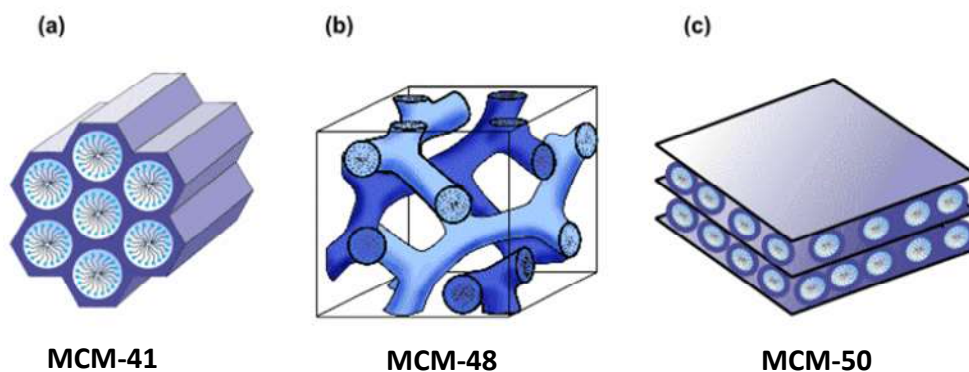

Figure 1.3. Scheme of the M41S family: hexagonal structure (a), cubic structure (b) and lamellar structure (c).

While some researchers were determined to synthesize metallic mesoporous materials, other carried out further studies of silica mesoporous networks. As a consequence, they soon focused in the modification of silica networks with metallic components, obtaining new ceramics as mesoporous silica-alumina (MSA),[41] mesoporous calcium silicate (MCS)[42] or Na_2O-CaO-SiO_2 glasses.[43] Though a large number of ceramics and glasses were synthesized among this period of time, the ones of greatest interest for the developing of this PhD thesis are Mesoporous Bioactive Glasses.

[37] Y. Ren, Z. Ma, P. G. Bruce, *Chem. Soc. Rev.*, **2012**, *41*, 4909–4927.

[38] H. F. Yang, D. Y. Zhao, *J. Mater. Chem.*, **2005**, *15*, 1217–1231.

[39] A. H. Lu, F. Schuth, *Adv. Mater.*, **2006**, *18*, 1793–1805.

[40] T. Valdes-Solis, A. B. Fuertes, *Mater. Res. Bull.*, **2006**, *41*, 2187–2197.

[41] Z. Vít, O. Šolcová, *Microporous and Mesoporous Materials*, **2006**, *96*, 197-204.

[42] C. Y. Huang, T. H. Huang, C. T. Kao, Y. H. Wu, W. C. Chen, M. Y. Shie, *J Endod.,* **2017**, *43*, 69-76.

[43] H.M. Kim, F. Miyaji, T. Kokubo, C. Ohtsuki, T. Nakamura, *J. Am. Chem. Soc,* **1995***,* 78, 2405–2411.

Bioactive glasses were discovered by Larry Hench in 1969. With the Vietnam War as historic context, one of the scopes of scientists was to find a material able to be implanted into the human body without causing any rejection. With this goal in mind, Hench found out the best $Na_2O-CaO-P_2O_5-SiO_2$ composition on the first try, and called his newly created material 45S5 Bioglass.[44] This was the first material that was not only biocompatible with human tissues, but also interacted with them to encourage healing. The discovery inspired researchers to think about new strategies to treat body injuries, which set the bases for the regenerative medicine such as we know it today.

Since then, glass ceramics with $CaO-P_2O_5-SiO_2-MO$ (M= Na, Mg, etc.) compositions have been greatly studied and used in clinical applications. Such materials are able to bond with living bone and promote healing due to their bioactive behaviour. Bioactivity is the main property of materials which allow bone regeneration, and consists of the capability of the material to chemically interact with body tissues.[45] That is: once a bioactive material is grafted into a living organism, the contact with physiological fluids can promote the formation of an apatite-like phase on the surface of the implant. This new formed phase is similar to the inorganic bone matrix and is capable to bond to bone tissue, allowing the healing of injuries and the refilling of bone defects. Both the composition and structure of bioactive materials are important in bioactive processes, and the increase of the specific surface area and pore distribution of bioactive glasses would enhance the apatite deposition process. For this reason, Zhao et al. proposed the synthesis of the first mesoporous bioactive glass in 2004.[46]

---

[44] L. L. Hench, R. J. Splinter, W. C. Allen, T. K. Greenlee, *J.Biomed. Mater. Res.,* **1971**, *2*, 117.

[45] L. L. Hench, *J. Am. Ceram. Soc.*, **1998**, *81*, 1705.

[46] X. Yan, C. Yu, X. Zhou, J. Tang, D. Zhao, *Angew. Chem. Int. Ed.*, **2004**, 43, 5980 –5984.

The discovery of mesoporous bioactive glasses opened up new pathways for bioregenerative medicine. The possibility of controlling porosity, pore size and internal pore architecture helped to understand bioactive processes and allowed the design of better bone regenerative materials. Moreover, the presence of mesoporous channels allowed that, as MCM-41, the mesoporous bioactive glasses were also suitable for the delivery of growth factors or drugs.[47]

1.3.1.1 Synthesis of mesoporous materials

As stated previously, the opportunity of controlling pore characteristics in porous structures was crucial for the development of new materials. In this section, more detailed information about the synthesis of mesoporous silica materials will be given.

First, two main components are necessary for the building of a high ordered porous structure with homogeneous porous dimensions:
   -A structural directing agent or template, which will act as a mold to arrange the material structure.
   -A polymeric precursor or precursors, which will condensate around the directing agent and form the final rigid framework.

In the synthesis of M41S materials, cationic molecules as alkyltrimethylammonium surfactants were used as structure directing agents.[31] Depending on factors such as concentration, temperature or pH solution, these molecules organized themselves in different structures called micelles. The formation of a determined micellar structure in a surfactant aqueous solution depends also on the nature of the surfactant species. The length of the

---

[47] C. Wu, J. Chang, *Journal of Controlled Release*, **2014**, *193*, 282–295.

hydrophobic carbon chain and the hydrophilic head group are also determining in the final phase arrangement.[48]

M41S synthesis is carried out under specific pH conditions, where cationic surfactants are able to self-assemble forming a hexagonal structure. In the next step, silicate precursor species like tetraethylorthosilicate (TEOS) form a sol-gel and condensate around the template, forming a mesoporous mesophase composed by the interaction of the organic and inorganic components. The final mesoporous framework with hexagonal arrangement is formed, according to the mechanism that was called Liquid Crystal Templating (LCT).[49] Finally, in order to obtain the desired mesoporous solid, a compulsory step of calcination or extraction should be carried out with the purpose to remove the organic template and provide empty mesopores. The whole process is represented in **Figure 1.4**. In this way, this process provides a final material with specific features which are difficult to achieve by a traditional synthetic route, since the final solids present high homogeneity not only in the size of the pores, but also in their shape and periodicity.
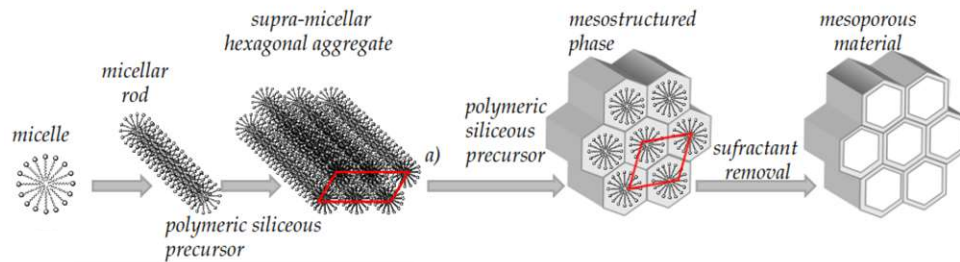

Figure 1.4. Schematic representation of the synthesis of MCM-41.

In the case of mesoporous bioactive glasses, researchers used triblock copolymers like Poly(Oxyethylene)-Poly(Oxypropylene)Poly(Oxyethylene) as

---

[48] F. di Renzo, H. Cambon, R. A. Dutarte, *Microporous Mater.* **1997**, *10*, 283–286.

[49] C. Y. Chen, H. Y. He, W. Z. Zhou, J. Klinowski*, Microp. Mater.*, **1993**, *2*, 17-26.

structure directing agents. For the synthesis of SiO_2-CaO-P_2O_5 framework, TEOS, calcium nitrate and tritethylphosphate (TEP) were used as silica, calcium and phosphor sources. Once added the precursor species to the reaction mixture, a process called evaporation-induced self-assembly (EISA) was undergone. EISA process was based on the preferential evaporation of the solvent, which progressively made the solution richer in non-volatile constituents and encouraged the mesophase to be formed. The next step was the condensation of silica and phosphor framework with entrapped Ca^{2+} ions, forming the mesoporous structure.[49] As with M41S materials, final extraction or calcination would also be needed in order to obtain empty mesopores.

1.3.1.2 Functionalization of mesoporous materials

One of the most important features of silica mesoporous materials is the possibility of achieving different surface characteristics and pore volumes by making small variations in the synthesis route. But this is only a small part of the wide potential this kind of materials can offer. Apart from studying the textural properties of mesoporous silica and finding applications, researchers were promptly aware that the presence of silanol (Si-OH) groups on their surface made them optimal candidates for surface modification, which opened up the possibility for the preparation of new organic-inorganic hybrid materials.[50,51,52]

The surface of mesoporous silica materials is full of structural defects in the form of silanol groups (Si-OH). These groups, as commented before, have the possibility of easily react with trialkoxysilane derivatives with the form (R'O)-Si-R, giving as a result an inorganic solid functionalized with organic moieties.[53] The new properties of the hybrid nanocomposite will be defined by the

[50] I. Slowing, B. G. Trewyn, V. S.-Y. Lin, *J. Am. Chem. Soc.*, **2006**, *128*, 14792-14793.

[51] R. Anwander, I. Nagl, M. Widenmeyer, *J. Phys. Chem. B.*, **2000**, *104*, 3532-3544.

[52] X. Zhang, D. Zeng, N. Li, J. Wen, X. Jiang, C. Liu, Y. Li, *Scientific Reports*, **2016**, *6*, 19361.

[53] M. Luechinger, R. Prins, G. D. Pirngruber, *Microporous and Mesoporous Materials*, **2005**, *85*, 111-118.

chemical nature of the functional groups contained on the selected trialkoxysilane. Thus, the desired features of functionalized materials can be easily selected according to the kind of molecules to be anchored on their surface.[54]

There are two main processes which allow the modification of mesoporous silica surfaces (see **Figure 1.5**):

❖ **Co-condensation procedure**: this procedure is carried out during the synthesis of the inorganic support, and consists of the incorporation of the selected alkoxysilane group both on the surface of the silica framework and inside the inner surface. According to this mechanism, the alkoxysilane carrying the functional group of interest must be added to the synthesis suspension at the beginning of the reaction. In aqueous medium, alkoxy groups are hydrolysed, concurrently to the silica network condensation, and silicon coming from the alkoxysilane becomes a part of the amorphous silica wall, with the organic group R still bonded to it.[55]

This method leads to a homogeneous distribution of selected functional groups covering all the silica surface.[56] However, the one-step incorporation of organic entities can accomplish structural modifications in the silica framework, and can make complicate the control of pore characteristics. Moreover, adding an organic compound to the surface of the material during the synthesis itself means that no calcination will be possible in order to remove the organic template. This restricts the removal to the surfactant to an extracting method.

---

[54] F. Hoffmann, M. Cornelius, J. Morell, M. Fröba, *Angew. Chem., Int. Ed.* **2006**, *45*, 3216−3251.

[55] Y. R. Han, J. W. Park, H. Kim, H. Ji, S. H. Lim, C. H. Jun, *Chem. Commun.*, **2015**, *51*, 17084-17087.

[56] M. Ghorbani, S. M. Nowee, N. Ramenzanian, F. Raji, *Hydrometallurgy Volume,* **2016**, *161*, 117-126.

❖ **Grafting procedure**: this procedure is carried out after the synthesis of the inorganic support, and consists on the reaction of a selected trialkoxysilane with the surface of the material. Thus, the solid is treated with the selected trialkoxysilane derivative in the presence of an anhydrous solvent and under inert atmosphere, in order to avoid silanol condensation caused by humidity. The alkoxy groups present in the trialkoxysilane react with free silanol groups on the surface of the material, and organic functional groups are attached to the surface of the solid by covalent bonds.[57,58]
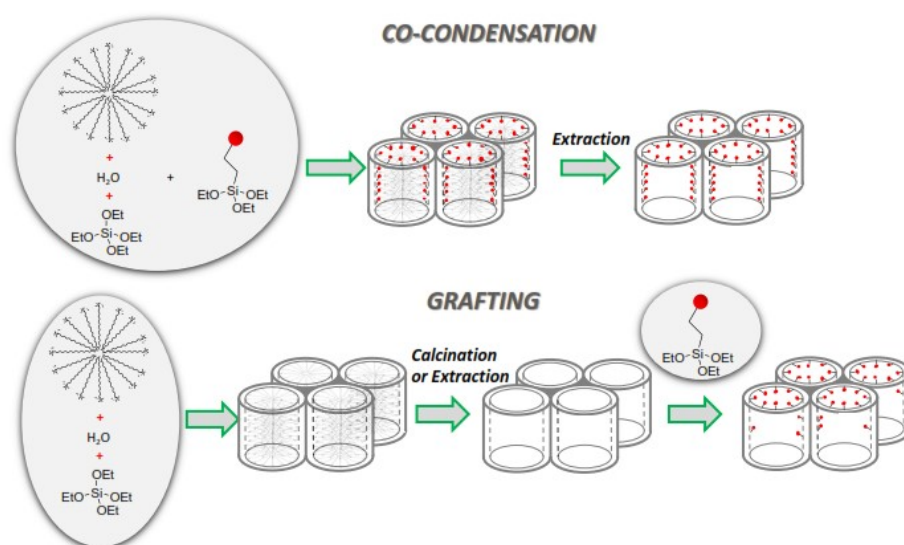

Figure 1.5. Schematic representation of the functionalization procedures for mesoporous materials.

[57] H. I. Meléndez-Ortiz, Y. Perera-Mercado, J. A. Mercado-Silva, Y. Olvares-Maldonado, G. Castruita, L. A. García-Cerda , *Ceramics International*, **2014**, *40*, 9701-9707.

[58] A. Bento, J. P. Lourenço, A. Fernandes, M. L. Cerrada, M. Rosario Ribeiro, *Chem. Cat. Chem.*, **2013**, *5*, 966 – 976.

This method is based on a post-synthesis treatment, which allows calcination as a form to eliminate the organic surfactant. Moreover, it does not modify the mesoporous structure nor pore properties. For these reasons, grafting is the most used procedure to obtain functionalized mesoporous materials.

Although grafting is the method used in this thesis for the synthesis of organic-inorganic hybrid materials, there are another ways which allow the modification of the original silica network. In relation with mesoporous bioactive glasses, it is of wide importance the possibility of entrapping ions or metals within the silica net in order to achieve specific properties.[59] In these cases, the method consists of a one-step synthesis and the ion precursor is added at the same time as the silica and other precursors. In this way, silica condensation is performed and metal ions are entrapped inside, acting as network modifiers. Since the ions are not part of the silica network, they can be slowly released in an aqueous media, exhibiting interesting properties when in contact with physiological fluids.[60,61,62]

Surface functionalization of materials and properties derived from these procedures are fundamental in this PhD thesis. An extensive explanation about characterization and applications of functionalized solids is available in sections 1.4 and 1.5, in order to provide the basic notions for the understanding of this thesis.

[59] A. Hoppe, N. S. Güldal, A. R. Boccaccini, *Biomaterials*, **2011**, *32*, 2757-2774.

[60] V. Aina, A. Perardi, L. Bergandi, G. Malavasi, L. Menabue, C. Morterra, D. Ghigo, *Chem. Biol. Interact.*, **2007**, *167*, 207-218.

[61] S. Murphy, D. Boyd, S. Moane, M. Bennett, *J. Mater. Sci. Mater. Med.*, **2009**, *20*, 2207-2214.

[62] H. Zreiqat, Y. Ramaswamy, C. Wu, A. Paschalidis, Z. Lu, B. James, O. Birke, M. McDonald, D. Little, C. R. Dunstan, *Biomaterials*, **2010**, *31*, 3175-3184.

1.3.2 Calcium phosphates

Though silica mesoporous materials are highly suitable for achieving the aims of this thesis, other biomaterials have also been studied. With similar properties to mesoporous bioglasses, calcium phosphates are one the most used ceramic materials for bone tissue regeneration.[63][64] These materials are composed by calcium cations (Ca^{2+}) together with orthophosphate (PO_4^{3-}), metaphosphate (PO_3^-), or pyrophosphate ($P_2O_7^{4-}$) anions, and sometimes hydrogen (H^+) or hydroxide (OH^-) ions. Particularly, apatites are calcium phosphates with an atomic ratio Ca/P between 1.5 and 1.67, and are extensively used in bone prosthesis due to its similarity to natural bone matrix and its excellent properties.[65]

Calcium phosphates have been studied for several centuries. However, it was at the end of the 18th century when the Swedish chemist and metallurgist Johan Gottlieb Gahn discovered that CaP was present in bones. At the end of the 18th century and the beginning of the 19th, different calcium phosphates as monocalcium phosphate monohydrate (MCPM), monocalcium phosphate anhydrous (MCPA), dicalcium phosphate anhydrous (DCPA, monetite), and dicalcium phosphate dihydrate (DCPD, brushite) were discovered and studied, as well as calcium-deficient hydroxyapatite (CDHA), α tricalcium phosphate (αTCP) and β tricalcium phosphate (βTCP), which were discovered a bit later.[66] More detailed studies started to appear in this period, focused on bone structure, composition, properties and formation (also called biomineralization).[67] The Ca/P molar ratio of these compounds and their formula can be seen in **Table 1.1**.

---

[63] N. Eliaz, N. Metoki, *Materials*, **2017**, *10*, 334.

[64] R.J. Turner, J.C. Renshaw, A. Hamilton, *ACS Appl. Mater. Interfaces*, **2017**, *9*, 31401-31410.

[65] S. V. Dorozhkin, *Prog. Biomater.*, **2016**, *5*, 9–70.

[66] A. Aikin, C. R. Aikin, *A Dictionary of Chemistry and Mineralogy, Vol. II*, **1807**.

[67] B. Parr, *The London Medical Dictionary, Vol. I*; Wentworth Press: London, UK, **1809**.

Table 1.1. Different types of calcium phosphates. Reproduced from *Biomatter.*, **2011**, *1*, 121-64.[68]

Ca/P molar ratio	Compound	Formula
0.5	Monocalcium phosphate monohydrate (MCPM)	$Ca(H_2PO_4)_2·H_2O$
0.5	Monocalcium phosphate anhydrous (MCPA or MCP)	$Ca(H_2PO_4)_2$
1.0	Dicalcium phosphate dihydrate (DCPD), mineral brushite	$CaHPO_4·2H_2O$
1.0	Dicalcium phosphate anhydrous (DCPA or DCP), mineral monetite	$CaHPO_4$
1.33	Octacalcium phosphate (OCP)	$Ca_8(HPO_4)_2(PO_4)_4·5H_2O$
1.5	α-Tricalcium phosphate (α-TCP)	$α-Ca_3(PO_4)_2$
1.5	β-Tricalcium phosphate (β-TCP)	$β-Ca_3(PO_4)_2$
1.2-2.2	Amorphous calcium phosphates (ACP)	$Ca_xH_y(PO_4)_z·nH_2O$, $n = 3–4.5$; 15–20 % H_2O
1.5-1.67	Calcium-deficient hydroxyapatite (CDHA or Ca-def HA)[e]	$C−x(HPO_4)_x(PO_4)_{6−x}(OH)_{2−x}(0 < x < 1)$
1.67	Hydroxyapatite (HA, HAp or OHAp)	$Ca_{10}(PO_4)_6(OH)_2$
1.67	Fluorapatite (FA or FAp)	$Ca_{10}(PO_4)_6F_2$
1.67	Oxyapatite (OA, OAp or OXA)[f], mineral voelckerite	$Ca_{10}(PO_4)_6O$
2.0	Tetracalcium phosphate (TTCP or TetCP), mineral hilgenstockite	$Ca_4(PO_4)_2O$

[68] S.V. Dorozhkin, *Biomatter.*, **2011**, *1*, 121-64.

Concurrently, surgeons started to use CaPs in order to treat some diseases. At the beginning of the 20th century, carbonate apatites were discovered, and first attempts to fabricate synthetic calcium phosphates were made in order to use them with a medical purpose.[69] Materials made of CaP were not only biocompatible, but had the special feature of enhancing bone formation, and this phaenomena was deeply studied since the last half of the 20th century. Terms as osteoinduction and osteointegration, related to bone regeneration capabilities, will be explained in section 1.5 of this thesis.

In 1969, the first implant made of hydroxyapatite (HAp, $Ca_{10}(PO_4)_6(OH)_2$)) was reported.[70] Since the beginning of the 1980s, HAp was started to be used in dentistry and orthopaedics, enduring a commercial boom and becoming one of the most used bioceramics in the world. CaP coatings, films and layers were also commercialized during this period, as well as CaP-based biocomposites and hybrid materials, which consolidated the industry of bone regeneration devices.

1.3.2.1 *Synthesis of calcium phosphates*

Since calcium phosphates are ideal for bone regenerative processes, their synthesis has become one of the major concerns of scientists in the last decades. However, the existence of such a big number of different types and compositions of calcium phosphates makes it difficult to define a single synthesis method. For this reason, this PhD thesis will focus on the synthesis of hydroxyapatite, which is the material that was used during the present research.

Synthetic HAp is, from a crystallographic point of view, the calcium phosphate most similar to natural bone apatite. The relationship between the molar amount of calcium and phosphorous (Ca/P ratio) in synthetic HAp has

[69] F. H. Albee, *Bone-Graft Surgery*, W.B. Saunders Company, **1915**.

[70] J. E. Cravens, *Dent. Cosmos.,* **1876**, *18*, 463–469.

been found to be 1.67, which fits with the Ca/P ratio of natural hydroxyapatite.[67] For this reason, considerable efforts have been made in order to synthesize stoichiometric hydroxyapatite, sometimes shaped in specific ways as fibers, nanoparticles, composites or microspheres as function as their different applications.

In this thesis, only general procedures for the synthesis of hydroxyapatite will be described.[71] Different methods for hydroxyapatite synthesis can be found in literature: precipitation,[72] hydrothermal and solvothermal processing,[73] sol-gel,[74] solid state[75] and emulsion,[76] but only the most frequently used are going to be explained.

❖ **Precipitation**: also called wet precipitation or chemical precipitation, is one of the most used methods to obtain hydroxyapatite. A selected phosphates specie (e.g. H_3PO_4) is added to a water solution containing a calcium precursor (e.g. $Ca(OH)_2$). The reaction is carried out at room temperature. Since final composition of the material is dependent on the solution pH, temperature, and the concentration of starting species, exhaustive control of these parameters should be carried out in order to obtain the desired product. Moreover, posterior high temperature heat treatment may be needed to maximize the percentage of crystalline phase in the precipitated calcium phosphate. Finally, precipitated powders must be

[71] A. K. Nayak, *Int. J. ChemTech. Res.*, **2010**, *2*, 903-907.

[72] I. Mobasherpour, M. S. Heshajin, A. Kazemzadeh, M. Zakeri, *J. Alloys Compd.* **2007**, *430*, 330-333.

[73] Y. Yang, Q. Wu, M. Wang, J. Long, Z. Mao, X. Chen., *Cryst. Growth Des.*, **2014**, *14*, 4864–4871.

[74] D. M. Liu, W. T. Troczynski, W. J. Tseng, *Biomaterials*, **2001**, *22*, 1721-1730.

[75] V. H. Arkin, L. Meenu, I. Manjubala, U. N. Kumar, *Int. J. ChemTech Res.*, **2015**, *8*, 264-267.

[76] S. Bose, S. K. Saha, *Chem. Mater.*, **2003**, *15*, 4464-4469.

typically calcined at 400 – 600 °C to refine the crystal structure. This method is one of the most used due to its simple procedure and the ready availability and inexpensiveness of reactants.

❖ **Hydrothermal and solvothermal processing**: contrarily to precipitation method, hydro and solvothermal processing allows the possibility of a strict control of process parameters. The method involves the heating of a solution containing initial reactants into a sealed vessel or autoclave. There, the solvent can be heated above its boiling point, performing changes in the reaction solution which favour the formation of hydroxyapatite crystals. The achievement of a constant temperature enables regulation of reaction parameters as nucleation, growth and ageing of the solid. This method is one-step, which means that does not require a post heating treatment in order to crystallise the hydroxyapatite, in contrast to other methods. Hydro and solvo thermal process is also cheap and easy to endure; however, few attempts of synthesizing hydroxyapatite with this method can be found in literature.

Though hydroxyapatite is one of the calcium phosphates which are most used in industry and research, scientists are still focused on creating new methods and improving the old ones in order to achieve total control of parameters involving hydroxyapatite formation. Powder features as crystallinity, ratio Ca/P, porosity or particle size are decisive for the future capabilities of the material, and controlling these characteristics is fundamental for getting tailor-made materials for specific and intelligent applications.

1.3.2.2 Modification of calcium phosphates

As occurs with previously mentioned mesoporous materials, researchers have also studied the possibility of modifying a calcium phosphate surface with the purpose to enhance their features or achieve a specific function. The wide number of strategies for the synthesis of calcium phosphates allows the possibility of achieving different chemical and physical properties by making specific changes in the synthetic route. This allows to obtain of tailored materials with specific characteristics which may go beyond bone regeneration and get into different fields as drug delivery,[77] antibacterial capabilities[78] or antitumoral features.[79] Apart from that, also post-synthesis modifications are possible thanks to the phosphates and hydroxyl groups of the surface of CaP materials, which allow the grafting of diverse molecules on the surface of CaP materials with the purpose of achieving a more complex material behaviour. Both methods are extensively explained below for a better understanding.

❖ **Ion substitution**. Calcium phosphates usually form a crystalline network with ions arranged in a specific way. In the case of hydroxyapatite, its particular structure makes it easy to substitute calcium, hydroxyl and phosphate ions with other ions of similar size. As it can be seen in **Figure 1.6**, a hydroxyapatite elementary cell is formed by hydroxyl groups arranged at the edges of the elementary cell, two types of calcium cations (Ca I and Ca II), and phosphate ions which build unit cells and determine the structure.[80] This arrangement allows ion substitution; for example, the locations of hydroxyl ions may be occupied by Cl⁻ or F⁻, or the location of calcium cations can by

[77] S. S. Syamchand, G. Sony, *Microchim Acta,* **2015**, *182*, 1567.

[78] Y. Lin, Z. Yang, J. Cheng, *Journal of Rare Earths*, **2007**, *25*, 452-456.

[79] W. Yanhua, H. Hao, Y. Li, S. Zhang, *Colloids and Surfaces B: Biointerfaces*, **2016**, *140*, 97-306.

[80] J. C. Elliott, *Structure and Chemistry of Apatites and Other Calcium Orthophosphates*, Elsevier, **1994**.

occupied by Mg^{2+}, Mn^{2+} or Sr^{2+} ions.[81] This kind of exchange can be total (in the case of OH-F and Ca-Sr) or partial, depending on the size of ions exchanged. Moreover, substitution of ions with different charges is also possible: it is possible to exchange a phosphate ion (PO_4^{3-}) with a carbonate (CO_2^{3-}), with the positive charge being balanced by the release of a calcium (Ca^{2+}) and a hydroxyl (OH^-). Ion exchange in hydroxyapatite structure, even in a small percentage, can accomplish substantial changes in biological, physicochemical and mechanical properties of the material. Substitution with several ions has been studied to have meaningful application in tissue regeneration field.[82]
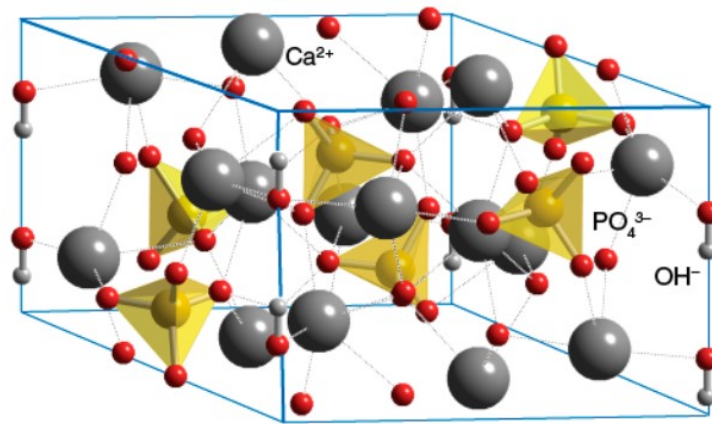

Figure 1.6. Unit cell of hexagonal HAp (space group *P63/m*). Reprinted from *Materials*, **2017**, *10*, 334.

[81] S. Kannan, F. Goetz-Neunhoeffer, J. Neubauer, J. M. F. Ferreira, *J. Am. Ceram. Soc.*, **2008**, *91*, 1–12.

[82] J.T.B. Ratnayake, M. Mucalo, G.J. Dias, *J. Biomed. Mater. Res. B Appl. Biomater.*, **2017**, *105*, 1285-1299.

For example, Mn^{2+} ions have been proved to favour osteoblasts proliferation and material biocompatibility. On the other hand, ions as silver (Ag^+), copper (Cu^{2+}), and zinc (Zn^{2+}) have been proved to possess important antimicrobial behaviour.[83,84] The ion substitution process is carried out during hydroxyapatite synthesis. Ion exchange can be carried out by using a precursor containing the desired ion which will substitute original ions. Then, a sintering process must be applied in order to consolidate the structure.[85]

❖ **Surface modification**. The modification of calcium phosphates surface can be achieved by the reaction of free hydroxyl groups with specific molecules. Just as it happens with silica materials, free OH^- groups of calcium phosphates are able to react with trialkoxysilanes, and a great number of molecules containing interesting functional groups can be grafted to the surface of the material. Thus, hybrid organic-inorganic materials with interesting applications can be obtained again. For example, several studies have achieved the modification of HAp surface with APTS, a trialkoxysilane that can be conjugated with different molecules for getting different surface charges, which is important for particle dispersion in a liquid media.[86] Though grafting processes may be really helpful to obtain new properties for calcium phosphate materials, few bibliography dealing with surface modification has been found.

---

[83] S. Samani, S. M. Hossainalipour, M. Tamizifar, H. R. Rezaie, *J. Biomed. Mater. Res. A*, **2013**, *101*, 222–230.

[84] Y. Li, J. Ho, C. P. Ooi, *Mater. Sci. Eng. C*, **2010**, 30, 1137–1144.

[85] J. Kolmas, E. Groszyk, D. Kwiatkowska-Różycka, *BioMed Res. Int.*, **2014**, Article ID 178123.

[86] S. Wang, S. Wen, M. Shen, R. Guo, X. Cao, J. Wang, X. Shi, *Int. J. Nanomed.*, **2011**, *6*, 3449–3459.

To sum up, both modification methods provide new strategies for improving the original properties of calcium phosphates. During the development of this PhD thesis, the second strategy has been accomplished for the design of a hybrid material with innovative capabilities.

1.4 Characterization of porous materials

As seen previously, synthetic procedures for obtaining porous materials have been widely studied. However, controlling the steps and parameters of the synthesis is not enough to guaranty the quality of the obtained material. Characterization methods allow to know and evaluate the properties of synthesized materials, giving essential information about their structure, porosity, composition, etc., and serving as a way of controlling their quality and functionality.

Many techniques are available for porous materials characterization depending on the properties to be known. Silica mesoporous materials are of great importance in this thesis, so that techniques for the study of porosity, structure and surface properties are explained below. Moreover, organic-inorganic hybrid materials were also prepared within the development of this thesis, so that techniques applied to this kind of materials are described too.

1.4.1 Techniques for the study of textural properties

For a good characterization of mesoporous materials, it is compulsory to study their textural properties. Nitrogen adsorption-desorption isotherms provide meaningful importance about parameters as surface area, pore size, pore volume or pore shape.[87] Isotherms are obtained depending on the amount of nitrogen that porous solids are able to adsorb among a certain range of pressure: specific porosities result in specific curves.

---

[87] C. G. Sonwane, S. K. Bhatia*, J. Phys. Chem. B*, **2000**, *104*, 9099–9110.

Figure 1.7A shows the six types of known isotherms, representing the volume of adsorbed N_2 versus the increment of P/P_0 values.[88] As it can be observed in every curve, the volume of adsorbed nitrogen increases with the increase of P/P_0 values. In this way, it has been studied that Type I isotherms are typical of microporous solids, where the high adsorption energy of the micropores allows the pores to be be filled with the N_2 at low pressures. Contrarily, Type II isotherms are typical of non-porous solids or macroporous materials, since the amount of adsorbed nitrogen remains low and almost constant with the rise of P/P_0, due to the low specific area of these solids. Type III isotherm is typical of those solids which are not able to perform gas adsorption, while type IV isotherm is typical of mesoporous materials. Type V isotherms are typical of porous materials which had a low interaction with the adsorbate. Lastly, type VI isotherms are not commonly obtained, since they are typical of very homogenous surfaces.[89]

Particularly, **Figure 1.7B** shows an adsorption-desorption isotherm which is typical of mesoporous solids. As it can be observed, the amount of adsorbed N_2 increases in a smooth way when P/P_0 is lower than 0.5. This occurs because a small amount of N_2 is adsorbed on the surface of the solid, covering the interstitial spaces between particles. When the P/P_0 is higher than 0.5, capillary condensation occurs inside the pores, and the N_2 starts to be adsorbed inside the pores, which is represented by a sharp leap in the adsorption curve. At higher values of P/P_0, the adsorbed volume of N_2 remains constant since there is no more empty space to fill.

The presence of the hysteresis loop also gives information about the pore.[90] The type H1 hysteresis loop (found in Tipe IV isotherms) is typical of solids with narrow pore distribution composed by cylindrical, regular pores. The type

---

[88] S. Brunauer, L. S. Deming, W. S. Deming, E. Teller, *J. Am. Chem. Soc.,* **1940**, *62*, 1723.

[89] S. J. Gregg, K.S.W. Sing, Adsorption, Surface Area and Porosity, Second Edition, **1982**, Academic Press.

[90] R. Defay, I. Prigogine, Tension Superficielle et Adsorption, Dunod, Paris (**1951**).

H2 hysteresis loop (found in Type V isotherms) is typical of porous inorganic oxides. Moreover, this technique can also measure the surface area of materials through the application of the Brunauer-Emmett-Teller (BET)[91] method to the adsorption isotherm, and the pore size distribution by means of the Barrett-Joyner-Halenda (BJH)[92] method.
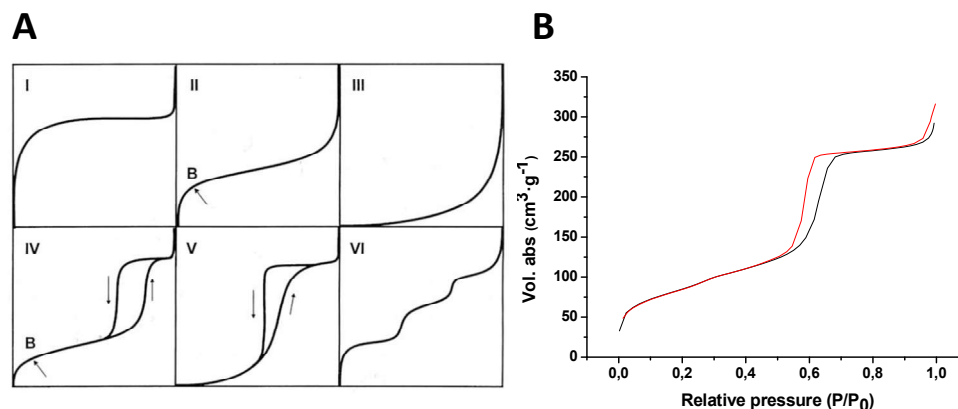
Figure 1.7. The six types of adsorption-desorption isotherms according to the IUPAC classification (A) and the adsorption-desorption isotherm typical of mesoporous materials (B).

If the use of a mesoporous support implies a loading, functionalization or modification step, it is important to check that the mesoporous structure is preserved during the processing. Powder X-ray diffraction (PXRD) is a technique which analyses the arrangement of a material.[93] For each crystalline material, a specific diffraction pattern is given, which allows to know the exact structure of every solid. This occurs by means of the following procedure[94]: when a sample is irradiated with X-rays, the interaction of the incident rays

[91] S. Brunauer, P.H. Emmett, T. Teller, *J. Am. Chem. Soc.*, **1938**, *60*, 309.

[92] E.P. Barrett, L.G. Joyner, P.P. Halenda, *J. Am. Chem. Soc.* **1951**, *73*, 373.

[93] L. A. Solovyov, O. V. Belousov, R. E. Dinnebier, A. N. Shmakov, and S. D. Kirik, *J. Phys. Chem. B*, **2005**, *109*, 3233–3237.

[94] D. A. Skoog, F.J. Holler, Crouch, S.R. Principles of Instrumental Analysis. Sixth Edition, Thomson Brooks/Cole, **2007**, USA.

with the sample produces constructive interference (and a diffracted ray) when conditions satisfy Bragg's Law ($n\lambda = 2d \sin \theta$). This law is related to the angle in which the rays are dispersed, and to the lattice spacing in a crystalline sample. Thus, the sample is scanned at different values of 2θ angles. When the geometry of the incident X-rays impinging the powder sample satisfies the Bragg Equation, constructive interference occurs and a peak in intensity occurs. The recompilation and treatment of these data creates a diffractogram, which is specific for each kind of crystalline sample.[95,96] Thus, it is possible to identify the crystalline structure of a material by the comparison between an obtained diffractogram and a known pattern. In the case of hydroxyapatite (**Figure 1.8A**), the diffractogram shows several peaks which correspond to characteristic plans of the crystalline structure, and gives information about the ordination of the atoms into the lattice.[97]

In the case of mesoporous materials, no crystalline structure can be identified since they are formed by an amorphous network of silica. However, in the case of ordered mesoporous solids, the periodicity of the pores can be detected by powder X-ray technique.[98] For this, lower values of 2θ angles are needed. In this way, the cubic, hexagonal or lamellar mesoporous structures correspond with specific patterns appearing at low angle values.[99] **Figure 1.8B** shows the diffractogram of MCM-41, which is an ordinated mesoporous solid with hexagonal arrangement. There can be observed four typical peaks, which can be indexed as the (100), (110), (200) and (210) Bragg peaks of a P6 space

[95] D.L. Bish, J.E. Post, Modern Powder Diffraction. Reviews in Mienralogy, **1989**, Mineralogical Society of America.

[96] D. M. Moore, R. C. Reynolds, X-Ray diffraction and the identification and analysis of clay minerals. 2nd Ed. Oxford University Press, **1997**, New York.

[97] R. K. Brundavanam, G. E. J. Poinern, D. Fawcett, *American Journal of Materials Science*, **2013**, *3*, 84-90.

[98] B. P. Feuston, J. B. Higgins, *J. Phys. Chem.,* **1994**, *98*, 4459−4462.

[99] L. A. Solovyov, *Chem. Soc. Rev.*, **2013**, 42, 3708.

group, confirming the hexagonal distribution of the pores.[100] Powder X-ray diffraction has been widely use during the research of this PhD thesis, since allows the easy and quick characterization of the prepared materials.

This technique allows to verify that the corresponding materials have been correctly synthesized, and that their ordered have not been altered upon functionalization and modification processes, which is highly helpful in materials science research.
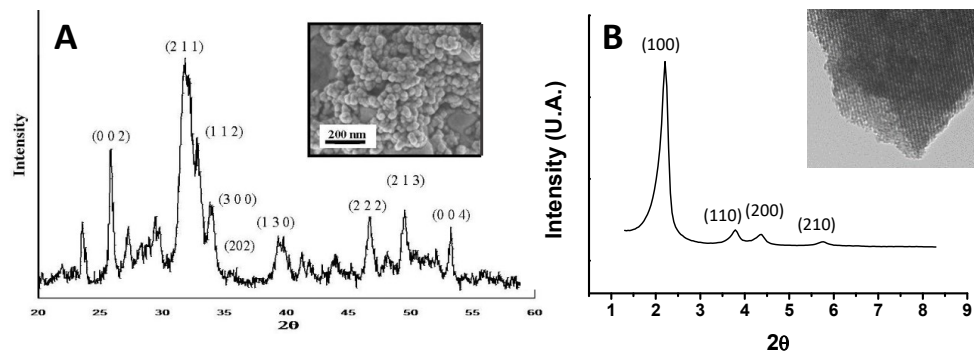

Figure 1.8. Typical X-ray diffraction patterns of hydroxyapatite (A) and MCM-41 (B). (A) reproduced from *American Journal of Materials Science*, **2013**, *3*, 84-90.

Also, electron microscopy techniques allow the visualization of materials structure.[101] These techniques are based on the incidence of a beam of electrons over a sample for the obtaining of visual information of each studied material.[102] For example, in Transmission Electron Microscopy (TEM), a beam of electrons is transmitted through the sample, and this allows the formation of a specific image which shows the particular structure of the material. Transmission electron microscopy is known to have a significantly high resolution, which allows the obtaining of precise and defined images. In the case of mesoporous solids, nanometric channels are easily observable, despite to their small size of only 2 or 3 nm. In this way, a wide scan of the whole

---

[100] Y. Ishii, Y. Nishiwaki, A. Al-zubaidi, S. Kawasaki, *J. Phys. Chem. C*, **2013**, *117*, 18120–18130.

[101] O. Terasaki, T. Ohsuna, S. Inagaki, *Catalysis Surveys from Japan*, **2000**, *4*, 99-106.

[102] D. S. Lee, T. K. Liu*, J. Sol-Gel Sci. Technol*, **2002**, *24*, 69–80.

sample can be made, in order to check the shape and regularity of the mesoporous channels, and the homogeneity over the sample.[103]

On the other hand, techniques as Scanning Electronic Microscopy (SEM) and Field Emission Scanning Electronic Microscopy (FESEM) provide a clear image of the surface of the solids, where possible damage or inconvenience can be seen.[104] These techniques are based on the scanning of a sample with a beam of electrons, and the signals produced by their interaction contain information about the sample's surface topography and composition. This technique is really helpful to accurately study the surface of a material, providing important information for the research.[105]

1.4.2 Techniques for evaluation of organic matter

In the case of organic-inorganic hybrid materials, it is interesting to determine the amount of organic matter or even to know the composition of the organic part. For this, thermogravimetric analysis (TGA) and elemental analysis can be performed. Thermogravimetry is a technique which measures the weight changes experimented by a sample upon a progressive heating process. A thermogravimetric curve is obtained, which shows the amount of matter that has been consumed at a specific temperature and allows the quantification of organic matter present in the material. Complementary, elemental analysis measures the composition of oxygen, nitrogen, carbon, sulphur or phosphorus present in a sample, which not only allows to determine the amount of organic matter, but also allows to know the exact composition. Interestingly, the scanning electronic microscopy technique can be coupled with energy dispersive X-ray spectroscopy, which also allows the quantification of single elements in a sample, but is more adequate for those elements with high atomic mass.

---

[103] X. Huang, N. P. Young, H. E. Townley, *Nanomater. Nanotechnol.*, **2014**, *4*, 2.

[104] 2. C.T. Kresge, M.E. Leonowicz, W.J. Roth, J.C. Vartuli, J.S. Beck, *Nature,* **1992**, *359*, 710.

[105] C.Y. Chen, H.X. Li, and M.E. Davis, *Micro. Mater.*, **1993**, *2*, 27.

Fourier-transform infrared spectroscopy (FTIR) is also useful for the characterization of organic matter attached to a material surface. This technique provides a spectra typical of each organic component, which show typical signals representing functional groups and bond types. This technique is useful to verify the formation of new covalent bonds and that the molecule of interest is indeed present in a sample.

In this PhD thesis, all these techniques have been used for the characterization of the designed materials, together with other exceptional techniques. As commented previously, validation and characterization of porous materials is fundamental to test the correct formation of starting materials and their quality, and also to verify that they are not modified upon each procedural step. This is essential to guarantee the correct performance of the designed systems and the attainment of the aims of this thesis.

1.5 Applications of porous materials

After the exposure of the synthesis procedures and characterization techniques of porous materials, some applications of this kind of materials are explained below. Since the great variety of porous materials comprise a wide range of applications in many different fields, we are only focusing on those related to the aims of this thesis.

As seen previously, both silica mesoporous materials and calcium phosphates have been extensively used in the field of tissue regeneration.[106] Their bone regenerating capabilities and high biocompatibility with human body has caused the industry to focus on this kind of materials, which commercialise a great number of devices oriented to biomedicine and dentistry. However, silica mesoporous materials are not only useful in bone regeneration industry. Actually, this thesis is mainly focused on more recent

---

[106] A. Fassio, M. Rossini, O. Viapiana, L. Idolazzi, E. Vantaggiato, C. Benini, D. Gatti, *Curr. Pharm. Des.*, **2017**, *23*, 6241-6250.

advances regarding mesoporous materials, like the use of this materials as drug nanocarriers,[107] drug delivery systems[108] or molecular-gated nanodevices which perform controlled release of selected substances.[109]

In this section, some applications of porous materials are shown, stressing the importance of molecular-gated systems similar to those which have been developed in this thesis.

1.5.1 Bone regeneration applications

As commented previously, both mesoporous bioactive glasses and calcium phosphate materials have been used for biomedical purposes in tissue regenerative medicine. This is due to their osteoconductive, osteointegrative and osteoinductive properties,[110] related to the processes of bone healing. O**steoconduction** is the possibility of hosting bone tissue cells and enhance their growth on the surface of the material. Textural properties as a specific porosity and wide specific surface are fundamental for favouring cell adhesion; moreover, the ability of these kind of materials of adsorbing extracellular matrix proteins also helps the cells to nest on the surface of the implant.[111] The term **osteointegration** refers to the ability of these materials to integrate into the living bone: a direct interface between old bone and the implant must be formed in order to provide mechanical stability and avoid detachment.[112,113] A

[107] M. Vallet-Regí, F. Balas, D. Arcos, *Angew. Chem. Int. Ed.*, **2007**, *46*, 7548–7558.

[108] S.W. Song, K. Hidajat, S. Kawi, *Langmuir*, **2005**, *21*, 9568–9575.

[109] E. Aznar, M. Oroval, L. Pascual, J. R. Murguía, R. Martínez-Máñez, F. Sancenón, *Chem. Rev.* **2016**, *116*, 561-718.

[110] T. Albrektsson, C. Johansson, *Eur. Spine J.*, **2001**, *10*, 96–101.

[111] Wilson-Hench J, Osteoinduction. In: Williams DF (ed) Progress in biomedical engineering, vol 4. Definitions in biomaterials, **1987**, Elsevier, Amsterdam, p 29.

[112] P.I. Brånemark, B.O. Hansson, R. Adell, U. Breine, J. Lindström, O. Hallén, A. Öhman, *Scand. J. Plast. Reconstr. Surg.*, **1977**, *11*, 1–175.

[113] A. Ghanem, S.V. Kellesarian, T. Abduljabbar, N. Al-Hamoudi, F. Vohra, F. Javed, *Implant Dent.*, **2017**, *26*, 770-777.

good anchorage and mechanical strength are important in the surgery effectivity, since it can play a role in the success or failure of the implant. Lastly, **osteoinduction** would be the ability of a material for enhancing the recruitment of progenitor cells and stimulate them to develop into the bone-forming cell lineage.[114,115] Moreover, as stated before, this kind of materials are **biocompatible**, which means that do not arise a negative response of the organism once implanted. And they are also **bioactive**, which means that are able to enhance not only bone-cells proliferation, but also the creation of new inorganic-phase bone. Bioactive processes start with Ca^{2+} ions leaking from the silica framework and undergoing an exchange with body H^+ ions. In a physiological media, calcium ions are capable of react with phosphates and form the crystalline apatite layer.[116,117]

In this context, Polak and coworkers studied how the Bioglass 45S5 stimulates osteoblast turnover and enhance bone formation in vitro. Human primary osteoblasts were seeded on a Bioglass substrate, and it was demonstrated that this material has the ability to stimulate the growth and osteogenic differentiation of human primary osteoblasts, which is directly correlated with the formation of the bone.[118] In another case, Xiao and coworkers compared the bone regenerative capabilities of mesoporous bioglasses with those of normal bioglasses, and concluded that MBG scaffolds had better physiochemical properties (mechanical strength, in vivo apatite mineralization, Si ion release and pH stability) than bioglass. Moreover, they

---

[114] R.W. Young, *Clin. Orthop. Rel. Res.*, **1963,** *26*, 147–156.

[115] J. Xie, C. Peng, Q. Zhao, X. Wang, H. Yuan, L. Yang, K. Li, X. Lou, Y. Zhang, *Acta Biomater.*, **2016**, *29*, 365-379.

[116] L. Hench, J. M. Polak, *Science,* **2002**, *295*, 1014.

[117] L. Robinson, K. Salma-Ancane, L. Stipniece, B.J. Meenan, A.R. Boyd, *J. Mater. Sci. Mater. Med.,* **2017**, *28*, 51.

[118] I.D. Xynos, M.V.J. Hukkanen, L.D.K. Buttery, L.L. Hench, J.M. Polak., *Calcif. Tissue Int.*, **2000**, *4*, 321-329.

demonstrated that mesoporous bioglasses improved in vivo osteogenesis, and induced a slightly higher rate of new bone formation in bone defects and greater synthesis of type I collagen than bioglass scaffolds.[119] **Figure 1.9** shows the different steps of osteoblast differenciation and subsequent bone formation. The first step consists of the recruiting of mesenchymal cells on the surface of the bone-regenerative material, in the presence of platelet derived growth factor (PDGF), bone morphogenic proteins (BMP) and transforming growth factor (TGF). The second step includes mesenquimal cells differentiation into a bone lineage cell, as pre-osteoblasts and osteoblasts, and the third step would consist of bone formation thanks to the action of osteoblasts, whose objective is the construction of new bone tissue.[120]

---

[119] C. Wu, Y. Zhang,, Y. Zhou, W. Fan, Y. Xiao, *Acta Biomaterialia*, **2011**, *7*, 2229-2236.

[120] F. Sharmin, C. McDermott, J. Lieberman, A. Sanjay, Y. Khan, *J. Orthop. Res.*, **2017**, 35, 1086-1095.
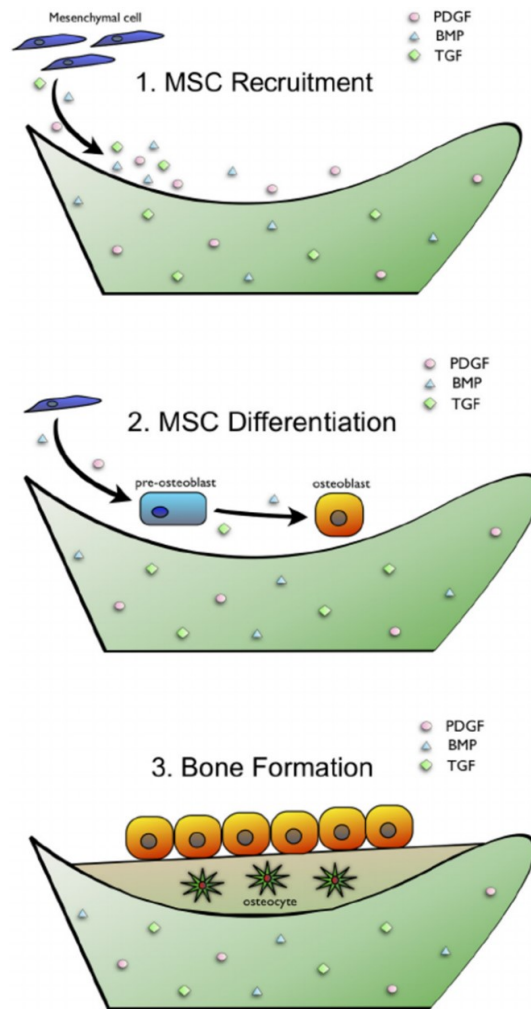
Figure 1.9. Steps of the bone-forming process carried out by and osteoinductive material: recruitment of mesenchymal cells (1), differentiation of mesenchymal cells into a bone cell lineage (2), formation of ectopic bone in vivo (3). Reproduced with the permission of SAGE journals.[121]

Deep research has been done in order to enhance these properties and improve prosthesis implant conditions. The synthesis of different

---

[121] R.J. Miron, Y. Zhang, *Journal of dental research*, **2012**, *91*, 736-744.

tridimensional structures called *scaffolds* used for the filling of structural defects and the study of cell colonization and bone growing has been of great interest in the field of regenerative biomedicine: the ability to control the different degrees of porosity and particular structural features of these devices has helped to the improvement of essential parameters as cell nesting, bone healing and implant attachment to the healthy bone.[122,123,124]

1.5.1.1 Drug delivery

However, other functionalities have been developed seizing the porous nature of these materials. One of them is the ability of acting as nanocarriers and delivery systems, to allow the local release of substances that fight surgery complications and enhance bone healing. The mesoporous structure of MBGs allows the loading of high amounts of drugs (antibiotics, anti-inflammatories or antitumoral substances) or bioactive species (growth factors or even nucleic acids for gene therapy), and their subsequent release in a physiological environment.[125] Cargo encapsulation and its posterior release can be helpful to avoid typical problems as poor water-solubility of drugs, delivery of substances in a non-specific way, or difficulties for the transcytosis of drugs across the endothelial and epithelial barriers.

In this context, Zhang and coworkers[126] developed a dexamethasone-loaded scaffold with the purpose of enhancing osteogenic capabilities, while Xiao and coworkers used dimethyloxallyl glycine with the same objective.[127] These

---

[122] T. Winkler, F. A. Sass, G. N. Duda, K. Schmidt-Bleek, *Bone Joint Res.,* **2018**, *7*, 232–243.

[123] C. Li, T.F. Cheung, V.C. Fan, K.M. Sin, C.W. Wong, G.K. Leung, *Surg. Innov.,* **2017**, *24*, 82-88.

[124] M. L. Ramiro-Gutierrez, J. Will, A. R. Boccaccini, A. Diaz-Cuenca, *J. Biomed. Mater. Res. A.*, **2014**, *102*, 2982-2992. .

[125] M. Vallet-Regi, A. Ramila, R. P. del Real, J. Perez-Pariente, *Chem. Mater.*, **2001**, *13*, 308-311.

[126] C. Wu, R. Miron, A. Sculeaan, S. Kaskel, T. Doert, R. Schulze, Y. Zhang, *Biomaterials*, **2011**, *32*, 7068–7078.

[127] C. Wu, W. Fan, J. Chang, Y. Xiao, *J. Mater. Chem.*, **2011**, *21*, 18300–18307.

substances were shown to enhance alkaline phosphatase (ALP) activity and bone-related gene expressions of osteoblasts, which means that were able to improve considerably the bone healing.[128] Apart from drugs, osteogenic growth factors have also been loaded into mesoporous structures. Recombinant human bone morphogenetic protein (RhBMP2)[129] or basic fibroblast growth factor (bFGF)[130] have been proved to show good results in the repairing of bone defects and enhancement of cell proliferation (see **Figure 1.10**).
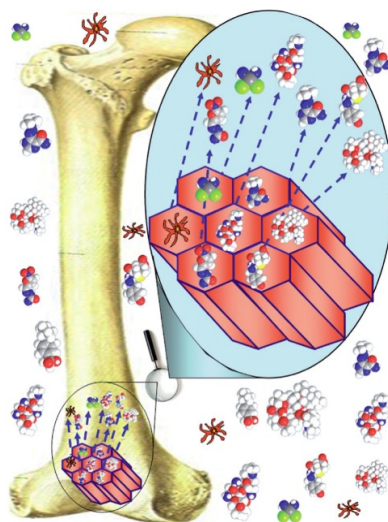
Figure 1.10. Schematic diagram a mesoporous scaffold releasing substances for the enhancement of bone growth.[131] Reproduced with the permission of Wiley-WCA.

Angiogenesis is also of great importance in bone tissue engineering, since the formation of new blood vessels around the implanted material is essential

---

128 M. Yuasa, T. Yamada, T. Taniyama, T. Masaoka, W. Xuetao, T. Yoshii, M. Horie, H. Yasuda, T. Uemura, A. Okawa, S. Sotome, *PLoS One.*, **2015**, *10*, 1-23.

129 C.Dai, H.Guo, J.Lu, J.Shi, J.Wei, C.Liu, *Biomaterials*, **2011**, *32*, 8506–8517.

130 R.A. Perez, A. El-Fiqi, J.H. Park, T.H. Kim, J.H. Kim, H.W. Kim, *Acta Biomater.*, **2013**, *10*, 520–530.

131 M. Vallet-Regi, *Chem. Eur. J.* **2006**, *12*, 5934–5943.

for the regeneration of tissues. For this reason, vascular endothelial growth factor (VEGF) has been effectively released from MBG scaffoldings, and it has been proved that its encapsulation helps to maintain its biologic activity.[132] Apart from this, release of antibiotics as gentamicin, tetracycline and ampicillin, or anticancer drugs as doxorubicin has been also studied with antimicrobial and antitumoral purposes respectively, providing encouraging results. Gene delivery has also been triggered by Kim et al., who loaded a BMP2 plasmid DNA in a mesoporous glass and achieved high expression of bone-related genes, with the consequent production of bone sialoprotein, osteopontin and osteocalcin which enhanced bone regeneration.[133]

Calcium phosphates are also promising in regards to drug delivery. In this case, loaded substances can be retained into the porous network of CaP materials, and be eluted thanks to their progressive degradation. In this context, C. S. Adams et al. prepared titanium rods and coated them with vancomycin-loaded CaP.[134] These devices were proved to reduce infection in an in vivo rat model thanks to the eluted drug. Other antibiotics as amoxicillin, clavulanic acid and erythromycin have also been delivered from HAp materials.[135] As happens with mesoporous bioglasses, calcium phosphates are also adequate for the release of growth factors as rhBMP2[136] and recombinant human transforming growth factor β1 (rhTGFβ1).[137] Moreover, gene delivery

[132] C.Wu, W.Fan, J.Chang, Y.Xiao, *J. Biomater. Appl.*, **2013**, *28*, 367-364.

[133] T.H. Kim, R.K. Singh, M.S. Kang, J.H. Kim, H. W. Kim, *Nanoscale*, **2016**, *8*, 8300-8311.

[134] C. S. Adams,V. Antoci Jr., G. Harrison, P. Patal, T. A. Freeman, I. M. Shapiro, J. Parvizi, N. J. Hickok, S. Radin, P. Ducheyne, *J. Orthop. Res.*, **2009**, *27*, 701–709.

[135] M.P. Ferraz, A.Y. Mateus, J.C. Sousa, F.J. Monteiro, *J. Biomed. Mater. Res. A*, **2007**, *81*, 994–1004.

[136] A.Sachse, A.Wagner, M.Keller, O.Wagner, W.-D.Wetzel, F.Layher, R.A.Venbrocks, P.Hortschansky, M.Pietraszczyk, B.Wiederanders, H.J.Hempel, J.Bossert, J.Horn, K.Schmuck, J.Mollenhauer., *Bone*, **2005**, *37*, 699–710.

[137] J. W.M. Vehof, M. T.U. Haus, A. E. De Ruijter, J. A. Jansen, P. H.M. Spauwen, *Clin. Oral Implants Res.*, **2002**, *13*, 94–102.

has also been achieved by Curtin and coworkers, who created a collagen-nanoHAp bone scaffold for delivering genes which could induce the expression of BMP-2 and VEGF in vitro and in vivo.[138]

1.5.1.2 Ion exchange

Apart from drugs, the particular structure of mesoporous materials and calcium phosphates makes them suitable to perform ion exchange. Recently, different therapeutic ions have been incorporated into MBG networks without affecting their original structures. These modified networks have the ability of releasing the ions to the media, with significant functional effects on osteogenesis, cementogenesis, angiogenesis and anti-bacterial activity. For example, Li-MBG scaffolds are able to promote bi-lineage regeneration of osteochondral defects thanks to the Li^+ release,[139] while release of divalent ions as Sr, Zn, Mg and Cu have been found to stimulate osteogenic differentiation of human bone marrow stroma cells and human periodontal ligament cells.[140] At the same time, the release of Co and Cu ions from MBG scaffolds has been shown to enhance VEGF secretion and thus angiogenesis capacity.[141] Relating to anti-bacterial properties of some ions, Ag-containing MBG showed a great antibacterial effect against *Staphylococcus aureus*, while Cu-releasing scaffolds were able to inhibit the growing of *Escherichia coli* thanks to its antibacterial effect.[142]

Calcium phosphates are also able to release ions thanks to their ability to perform ion exchange: due to their crystalline structure, calcium cations are

---

[138] C. M. Curtin, E. G. Tierney, K. McSorley, S.-A. Cryan, G. P. Duffy, F. J. O'Brien, *Adv. Healthc. Mater.*, **2015**, *4*, 223-227.

[139] P. Han, C. Wu, J. Chang, Y. Xiao, *Biomaterials*, **2012**, *33*, 6370–6379.

[140] C. Wu, Y. Zhou, C. Lin, J. Chang, Y. Xiao, *Acta Biomater.*, **2012**, *8*, 3805–3815.

[141] C. Wu, Y. Zhou, M. Xu, P. Han, L. Chen, J. Chang, Y. Xiao, *Biomaterials*, **2013**, *34*, 422–433.

[142] N. Gargiulo, A.M. Cusano, F. Causa, D. Caputo, P.A. Netti, *J. Mater. Sci. Mater. Med.*, **2013**, *24*, 2129–2135.

susceptible to be substituted by therapeutic ions with a similar shape. For example, in vitro studies showed that Zn release stimulates the osteoblastic production of growth factors, i.e., insulin-like growth factor (IGF-I) and transforming growth factor (TGF-β),[143] as well as Mn^{2+}[144] and Sr^{2+},[145] which showed similar results. Contrarily, Ag^{+}[146] ions have been released for achieving antimicrobial properties, as well as Cu^{2+}[147], Zn^{2+}[148] and Ce^{3+}.[149]

1.5.2 Gated materials

1.5.2.1 General considerations about molecular gates

As seen previously, recent advances in biomedicine have considered the use of mesoporous silica materials for the construction of delivery systems.[117] Antibiotics, growth factors, antitumoral drugs or even genes have been loaded into the pores of this kind of materials with therapeutic purposes. However, drug delivery has been proved to be not always efficient. The lack of control over delivery processes often results in a burst of drug release, which elevates its concentration over recommendable levels and endures adverse reactions as increased antibiotic resistance or liver and renal complications.[150] Moreover, after the initial burst of drug, sustained release during long periods of time is hardy achievable.

For this reason, nowadays innovative designs which deal with the controlled delivery of substances are becoming more and more popular. In this type of

---

[143] X. Wang, A. Ito, Y. Sogo, X. Li, and A. Oyane, *Acta Biomaterialia*, **2010**, *6*, 962–968.

[144] Y. Li, J. Widodo, S. Lim, C. P. Ooi, *J. Mater. Sci.*, **2012**, *47*, 754–763.

[145] W. Querido, A.L. Rossi, M. Farina, *Micron.*, **2016**, *80*, 122–134.

[146] N. Rameshbabu, T.S.S. Kumar, T.G. Prabhakar, V.S. Sastry, K.V. Murty, K.P.Rao, *J. Biomed. Mater. Res. A*, **2007**, *3*, 581–591.

[147] V. Stanić, S. Dimitrijević, J. Antić-Stanković, M. Mitrić, B. Jokić, I. B.Plećaš, S. Raičević, *App. Surf. Sci.*, **2010**, *256*, 6083–6089.

[148] X. Chen, Q.L.Tang, Y.J. Zhu, C.L. Zhu, X.P.Feng, *Mater. Lett.*, **2012**, *89*, 233–235.

[149] Y. Lin, Z. Yang, and J. Cheng, *J. Rare Earth.*, **2007**, *25*, 452–456.

[150] A.H. Faraji, P. Wipf, *Bioorg. Med. Chem.*, **2009**, *17*, 2950–2962.

systems, mesoporous silica materials are often used as an inorganic scaffolding, where the drug of interest is stored. Then, the surface of the solid is functionalized with specific molecules which will entrap the loaded substance and act as a gatekeeping. These specific capping entities are called **molecular gates**,[16] and can be defined as an architectural nanoscopic structure which can be triggered by an external stimulus and change its state (closed or open) to achieve a controlled release of the loaded cargo. In **Figure 1.11**, a scheme of a typical gated material is shown. The pores of the mesoporous material are filled with the drug of interest, and the outlets of the pores are functionalized with the corresponding molecular gate. Under normal conditions, the closed state of the molecular gate will keep the cargo inside the pores, avoiding its release. The presence of a specific stimulus would trigger substantial changes in the molecular gate (as hydrolysis, conformation change, etc.), and the loaded substance would be released in a stimuli-responsive way.[151]
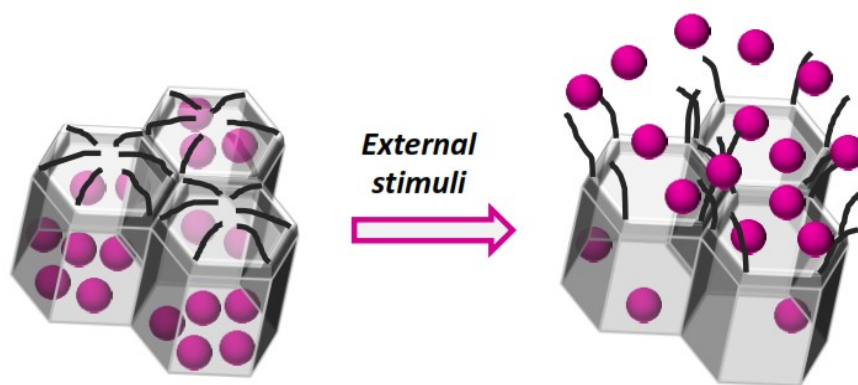

Figure 1.11. Schematic representation of a molecular-gated system.

The first example of a molecular-gated design was reported by Fujiwara and coworkers in 2003.[152] The system consisted of mesoporous silica nanoparticles

---

[151] K.K. Cotí, M. E. Belowich, M. Liong, M. W. Ambrogio, Y. A. Lau, H. A. Khatib, J. I. Zink, N. M. Khashab, J. F. Stoddart, *Nanoscale,* **2009**, *1*, 16.

[152] a) N. K. Mal, M. Fujiwara, Y. Tanaka, Y. *Nature,* **2003**, *421*, 350. b) N. K. Mal, M. Fujiwara, Y. Tanaka, T. Taguchi, M. Matsukata, *Chem. Mater.* **2003**, *15*, 3385.

(MSN) loaded with a dye and implemented with coumarin derivatives in the outlets of the pores. When irradiated with a wavelength higher than 310 nm, the formation of a cyclobutane derivative between coumarin monomers was induced, and the delivery of the dye was prevented due to their bulky structure. In contrast, when irradiated with wavelengths lower than 310 nm (concretely 250 nm), the cyclobutane dimer was cleaved and the monomers separated, allowing the release of the dye.

After this demonstration, a great number of nanoscopic gated systems have been developed during the last years. Supramolecular assemblies,[153] inorganic nanoparticles[154] or polymers[155] have been selected as gatekeeping entities, while several stimuli as pH,[156] light,[157] redox potential,[158] temperature[159] or target (bio)molecules[160] have been used as triggers. These specific stimuli provoke the subsequent changes in the capping entities, inducing a convenient hydrolysis, shifting or conformational change which allow the release of previously

---

[153] a) T. D. Nguyen, Y. Liu, S. Saha, K. C. F. Leung, J. F. Stoddart, J. I. Zink, *J. Am. Chem. Soc.* **2007**, *129*, 626. b) R. Liu, Y. Zhang, P. Y. Feng, *J. Am. Chem. Soc.* **2009**, *131*, 15128.

[154] a) E. Aznar, M . D. Marcos, R. Martinez-Manez, F. Sancenon, J. Soto, P. Amoros, P. Guillem*, J. Am. Chem. Soc.*, **2009**, *131*, 6833, b) Y. Yang, Y. Lin, D. Di, X. Zhang, D. Wang, Q. Zhao, S. Wang, *J. Colloid Interface Sci.*, **2017**, *508*, 323-331.

[155] a) R. Liu, X. Zhao, T. Wu., P. Y. Feng*, J. Am. Chem. Soc.* 2008, *130*, 14418. b) C. L. Zhu, X. Y. Song, W. H. Zhou, H. H. Yang, X. R. Wang, *J. Mater. Chem.,* **2009**, 19, 7765

[156] a) J.T. Lin, J.K. Du, Y.Q. Yang, L. Li, Da.W. Zhang, C.L. Liang, J. Wang, J. Mei, G.H. Wang, *Mat. Sci. Eng. C*, **2017,** *81*, 478-484. b) S. Angelos, Y.–W. Yang, K. Patel, J. F. Stoddart, J. I. Zink, *Angew. Chem. Int. Ed.*, **2008**, *47*, 2222.

[157] a) E. Johansson, E. Choi, S. Angelos, M. Liong, J. I. Zink, *Sol-Gel Sci. Technol.*, **2008**, *46*, 313. b) J. Lai, X. Mu, Y. Xu, X. Wu, C. Wu, C. Li, J. Chen, Y. Zhao, *Chem. Commun.,* **2010**, *46*, 7370.

[158] X. Chen, H. Sun, J. Hu, X. Han, H. Liu, Y. Hu, *Colloids Suf. B*, **2017**, *152*, 77-84.

[159] F. Yu, H. Wu, Y. Tang, Y. Xu, X. Qian, Q. Zhu, *Int. J. Pharm*, **2018**, *536*, 11-20.

[160] a) C. Coll, R. Casasús, E. Aznar, M. D. Marcos, R. Martínez-Máñez, F. Sancenón, J. Soto, P. Amorós, *Chem. Commun.*, **2007**, 1957. b) A.H. Teruel, C. Coll, A.M. Costero, D. Ferri, M. Parra, P. Gaviña, M. González-Álvarez, V. Merino, M.D. Marcos, R. Martínez-Máñez, F. Sancenón, *Molecules*, **2018**, *23*, 375.

entrapped cargos. In a further step, these systems have been adapted to accomplish particular purposes as molecular sensing or therapeutic finalities.

In this section, a brief summary of stimuli-responsive nanodesigns organized by the triggering on selective stimuli as pH, light, redox potential and temperature changes are shown. In the next section, marked importance will be given to those systems based on the response to specific bio(molecules), which are usually designed for biomedical applications.

1.5.3.2 Types of gated systems

As commented previously, the first design of a gated system was based on the use of a **light-sensitive molecular gate**. Since then, numerous studies to achieve a light-mediated mass transport have been reported. One example of a light-mediated mechanism was conceived by Jiang et al.[161] In this system, the external surface of MSNs was functionalized with 3-Aminopropyl Triethoxysilane (APTS) and perfluorodecyltriethoxy-silane, and then a suitable spiropyran derivative was attached to the amino groups through the formation of an amide bond (**Figure 1.12**). Pores were loaded with fluorescein. PBS suspensions of the prepared nanoparticles at pH 7.2 showed negligible fluorescein release due to the formation of a hydrophobic layer, which protected the surface from being wet by aqueous solution. However, under UV-light irradiation, spiropyran moieties isomerized to their merocyanine charged form. This changed the character of the layer around pores from hydrophobic to hydrophilic, and as a result, the surface was wetted with the subsequent dye release.

This system was also tested in cells, by the synthesis of the same design loaded with a cytotoxic drug. Camptothetin (CPT) loaded capped MSNs were internalized in HeLa and EA.hy926 cells by endocytosis and a clear decrease in cell viability was observed upon UV-light irradiation.

---

[161] L. Chen, W. Wang, B. Su, Y. Wen, C. Li, Y. Zhou, M. Li, X. Shi, H. Du, Y. Song, L. Jiang, *ACS Nano,* **2014**, *8*, 744-751.
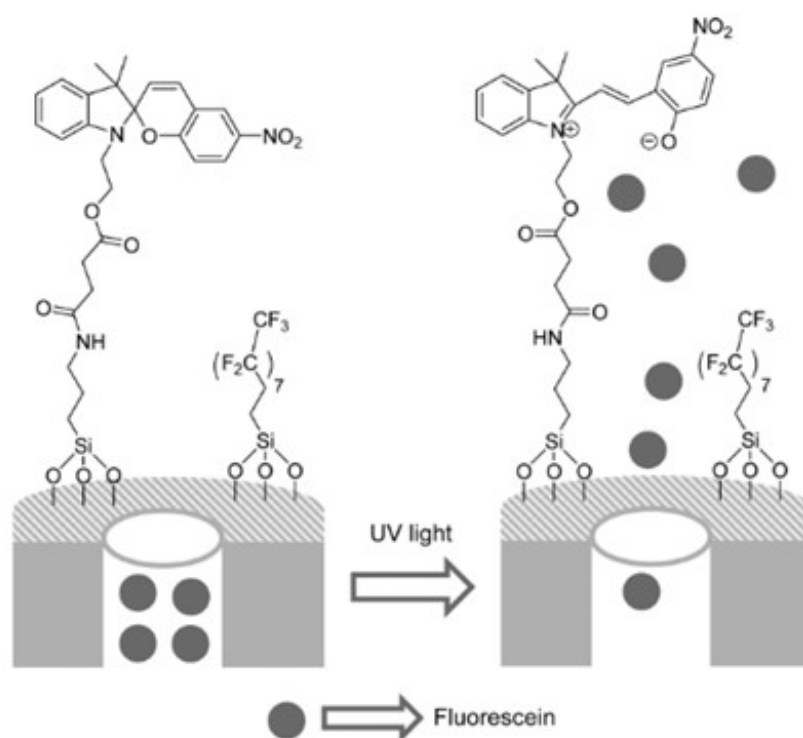
Figure 1.12. Schematic representation of a MSN loaded with flourescein, funcionalized with a perfluorohydrocarbon chain and capped with a spiropyran derivative. Reprinted with permission from (Chem.Rev., 2016, 116, 561-718). Copyright (2016) American Chemical Society.

Apart from light, other stimuli of different nature have been used for the design of molecular-gated systems. While some researchers used light as an external stimuli which can be easily controlled, other focused in the biological reactions taking place inside the cells, as redox and pH changes. One of the first **redox-responsive molecular gates** was designed by Lin. et al, who used CdS nanocrystals bonded to a disulphide linker to cap the pores of mesoporous silica nanoparticles.[162] In a first step, the authors synthesized

---

[162] C. Y. Lai, B. G. Trewyn, D. M. Jeftinija, K. Jeftinija, S. Xu, S. Jeftinija, V. S. Y. Lin, *J. Am. Chem. Soc.*, **2003**, *125*, 4451-4459.

mercaptopropyl-modified MSNs and functionalized the surface with 2-(pyridyldisulfanyl)ethylamine. Then, pores were loaded with ATP or vancomycin and capped with mercaptoacetic acid-coated Cds nanocristals. Cargo release was inhibited until the addition of a reducing agent, which cleaved the disulphide bridge, freeing the Cds nanoparticles and allowing ATP or vancomycin release (see **Figure 1.13**).
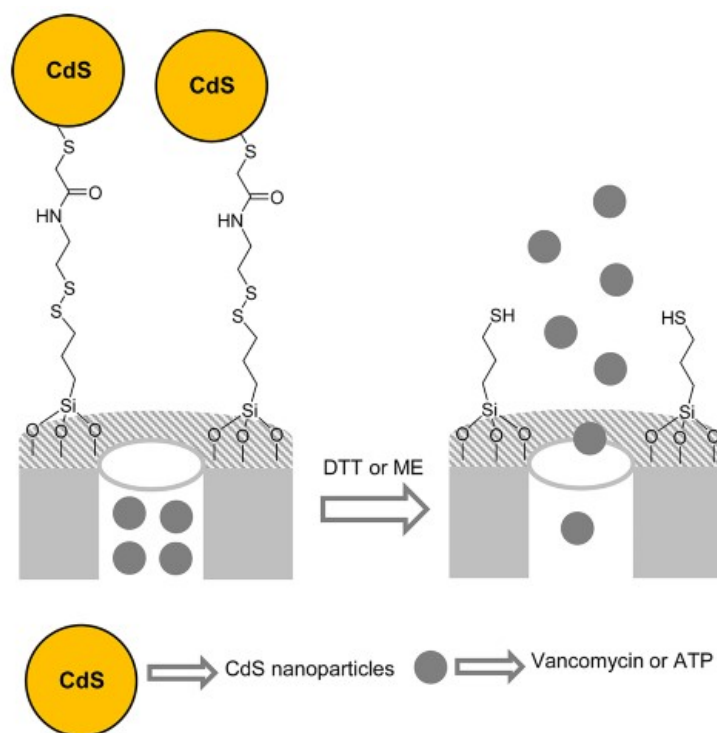

Figure 1.13. Schematic representation of a mesoporous material loaded with vancomycin or ATP and capped with CdS nanocrystals bonded to a disulphide linker. Reprinted with permission from (Chem.Rev., 2016, 116, 561-718). Copyright (2016) American Chemical Society.

This method presents interesting applications in biomedicine, since redox changes at an intracellular level could be easily triggered for the treatment of diverse diseases. For example, cancer cells usually present increased concentrations of redox-active molecules, and treatment with molecular-gated

nanoparticles would favour the killing thanks to this redox-responsive mechanism.

On the other hand, also pH changes have been used as an internal stimuli for the on-command release of drugs. Acidic pH is often typical of damage scenarios like tumor presence, tissue inflammation or tissue infection. For this, molecular gates that would open under acidic conditions would be a great tool towards the treatment of several pathologies. In a first example, Quan and coworkers developed a **pH-responsive molecular gate** using mesoporous silica nanoparticles as an antitumoral carrier for selective delivery in the colon.[163] MSNs were loaded with doxorubicin and capped with polyacrylic acid acting as a gatekeeping entity (**Figure 1.14**). Thus, in gastric environment (pH = 2.0), doxorubicin molecules were encapsulated in the pore channels since the pore outlets were capped with collapsed PAA. In contrast, in colonic environment (pH = 7.6), a fast release was observed because of the removal of capping.
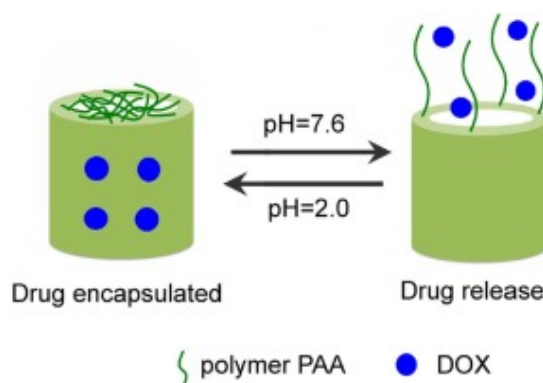

Figure 1.14. Schematic representation of a mesoporous support loaded with doxorubicin and capped with polyacrilic acid. Reprinted with permission of Elsevier.

---

[163] B.Tian, S. Liu, S. Wu, W. Lu, D. Wang, L. Jin, B. Hu, K. Li, Z. Wang, Z. Quan, *Colloids Surf. B*, **2017**, *154*, 287-296.

Another pH-driven gate with potential applications in bone infection environments is the one designed by Lin and co-workers, who developed a pH-responsive system based on a mesoporous bioglass loaded with metformin hydrochloride (MH) and coated with hydroxyapatite.[164] At a physiological pH, hydroxyapatite was stable and acted as a barrier which avoided drug release. However, in acid environments caused situations of bone damage (bone metastases, infection), hydroxyapatite was degraded, unblocking the pores and allowing drug release (**Figure 1.15**).
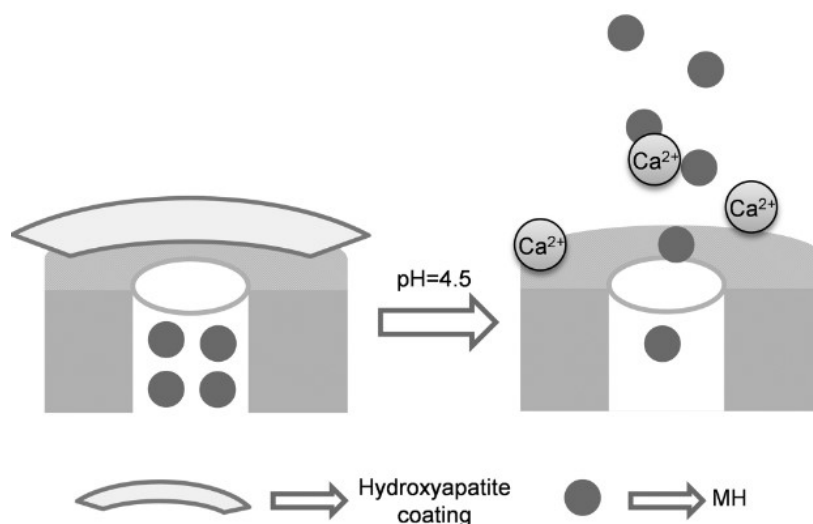
Figure 1.15. Schematic representation of a mesoporous bioglass loaded with metformin hydrochloride and coated with hydroxyapatite. Reprinted with permission from (Chem.Rev., 2016, 116, 561-718). Copyright (2016) American Chemical Society.

Other kind of gated designs are based in the increase of **temperature** as external stimuli. Abnormal increase of temperature in located zones of the body can be caused by infectious processes or tumor presence, but also in common situations as postsurgical inflammation. Thus, the design of gated

---

[164] C. Yang, W. Guo, L. Cui, D. Xiang, K. Cai, H. Lin, F. Qu, *Mater. Sci. Eng. C.*, **2014**, *36*, 237-243.

systems able to open with the increase of temperature would be a good approach to treat these pathologies or prevent further complications. One example of temperature-driven molecular gates was designed by R. Martínez-Máñez and co-workers, who prepared a new tailor made thermoresponsive hybrid system using paraffins as capping agents.[165] There, mesoporous silica nanoparticles (MSNs) were loaded with a dye and functionalized with octadecyltrimethoxysilane molecules. Then, the nanoparticles were covered with a paraffin, which sealed the outlets of the pores and avoid dye release at room temperature. However, with the increase of the temperature beyond the melting point (42 °C), the paraffin melted and uncap the pores, letting the dye to be released (**Figure 1.16**).

The system was also tested in a cellular *in vitro* model: the same design was synthesized, using doxorubicin as cargo. The nanoparticles were then added to human cervix carcinoma HeLa cells. The results showed that, the sample incubated at 42 °C exhibited features of doxorubicin-induced cell death, whereas those incubated at 37 °C showed healthy cells.

---

[165] E. Aznar, L. Mondragón, J.V. Ros-Lis, F. Sancenón, M. D. Marcos, R. Martínez-Máñez, J. Soto, E. Pérez-Payá, P. Amorós*, Angew. Chem. Int. Ed.* **2011**, *50*, 11172.
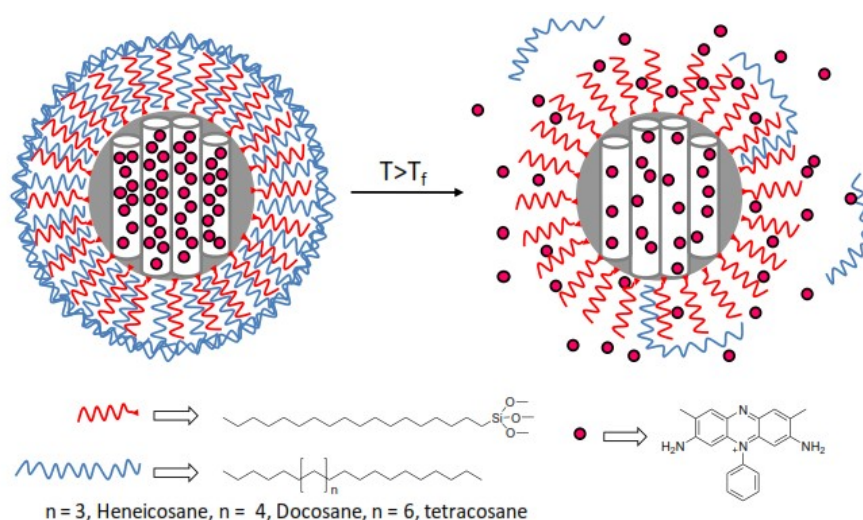
Figure 1.16. Schematic representation of a temperature-responsive molecular gate composed of octadecyltrimethoxysilane and paraffins. Reproduced with permission of Wiley-WCA.

Another thermos-responsive gated system was also conceived by Kim et al.[166] In this case, the pores of the MSNs were loaded with DOX, and the surface of the material was functionalized with propylamine. Then, the final nanoparticles were coated with a temperature sensitive poly(ethylene glycol)/poly (epsiloncaprolactone) (PEG/PCL) multiblock copolymer (**Figure 1.17**). When the temperature was lower than 45 °C, the copolymer blocked the entrance to the pores and the release of entrapped DOX from the nanoparticles was negligible. However, at a temperature above 45 ºC, the melting of the crystalline structure of PLC unblocked the pores and allowed a remarkable drug release.

---

[166] I.H. Cho, M.K. Shim, B. Jung, E. H. Jang, M.J. Park, H.C. Kang, J.H. Kim, *Microporous Mesoporous mater.*, **2017**, *253*, 96-101.
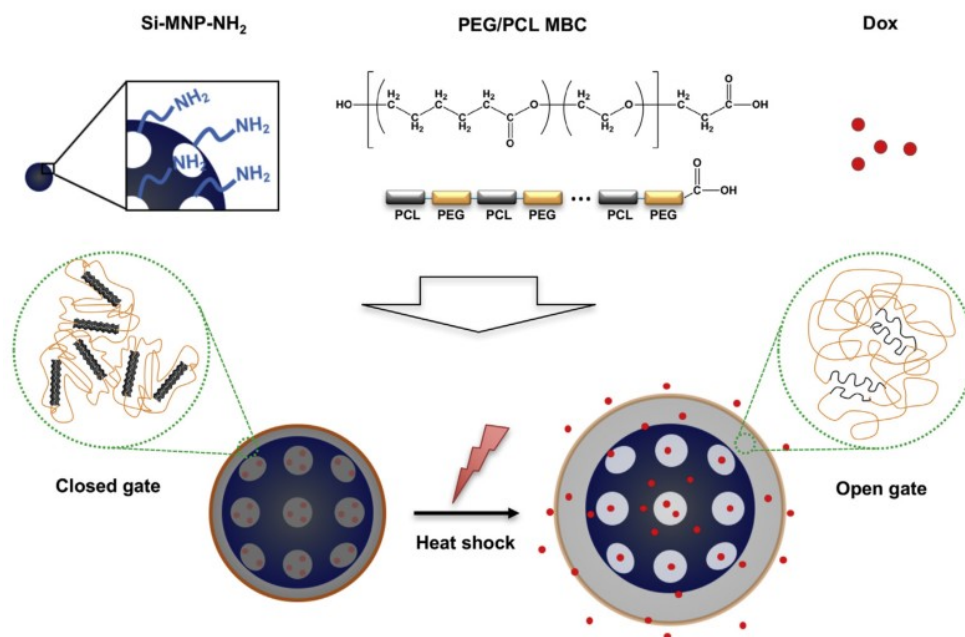
Figure 1.17. Schematic representation of a temperature-responsive molecular gate composed of MSNs loaded with DOX and coated with a thermosensitive copolymer. Reproduced with permission of Elsevier Inc.[166]

The last type of molecular gates are those which are open in the presence of stimuli as enzymes and biomolecules. An easy example of enzyme-responsive molecular gates was provided by Qu and co-workers, who prepared MSNs capped with hyaluronic acid.[167] The MSNs were loaded with Rhodamin B and then capped with the polysaccharide through an amidation. They investigated the performance of the capped nanoparticles in the presence of lysosomal enzyme hyaluronidase-1 (Hyal-1), an enzyme found in tumor microenvironments (**Figure 1.18**). In the absence of this enzyme, the hyaluronic acid molecules remained undamaged and avoided the leakage of the dye. Only when the Hyal-1 enzyme was added to aqueous suspensions of the capped MSNs, the release of Rh B was observed. Apart from acting as a cap,

---

[167] Z. W. Chen, Z. H. Li, Y.H. Lin, M.L. Yin, J.S. Ren, X.G. Qu, *Chem. Eur. J.,* **2013**, *19*, 1778.

hyaluronic acid was also used to target tumors, since the principal receptor for HA (which is CD44) is known to be overexpressed in several cancer cell lines. The authors demonstrated that these gated nanoparticles were effectively directed to cancer cells, and after that, they prepared the same hyaluronic acid gated nanoparticles loaded with doxorubicin for killing tumor cells with promising results.
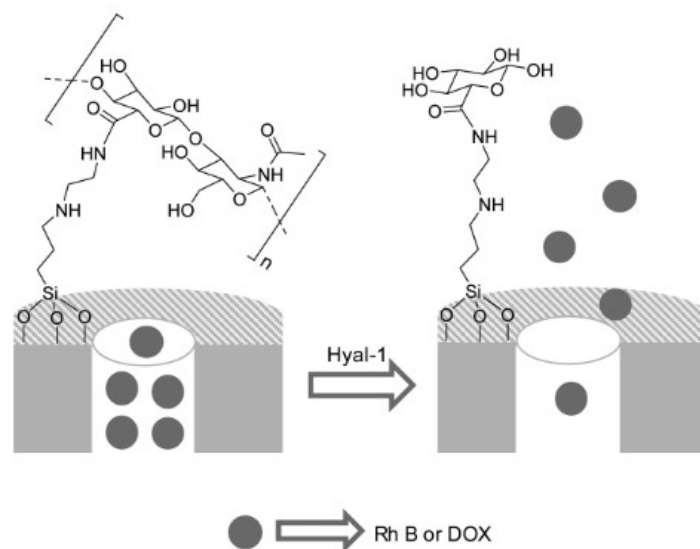

Figure 1.18. Schematic representation of an enzyme-driven molecular gate. Reprinted with permission from (Chem.Rev., 2016, 116, 561-718). Copyright (2016) American Chemical Society.

Another enzyme-responsive system was designed by Martínez-Máñez and coworkers.[168] In this case, MSNs containing oleic acid-coated magnetic nanoparticles were synthesized and loaded with safranin O or hydrocortisone. Then, the pores of the nanoparticles were capped with a bulky azo derivative bearing urea moieties. Aqueous suspensions of both solids at pH 7.4 showed negligible payload release whereas a marked delivery was observed in the

---

[168] A.H. Teruel, E. Pérez-Esteve, I. González-Álvarez, M. González-Álvarez, A.M. Costero, D. Ferri, M. Parra, P. Gaviña, V. Merino, R. Martínez-Máñez, F. Sancenón, *J. Controlled release*, **2018**, *281*, 58-69.

presence of sodium dithionite due to the rupture of the azo bonds (**Figure 1.19**) Besides, a moderate cargo release was observed at acidic pH due to the hydrolysis of the urea bonds that linked the azo derivative onto the external surface of theinorganic scaffolds.
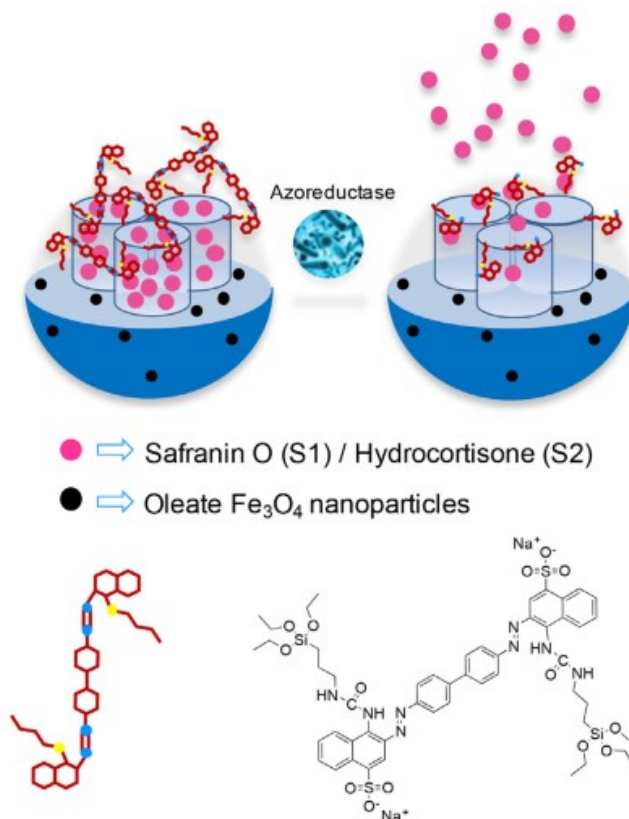

Figure 1.19. Schematic representation of azoreductase-driven molecular gate.[168] Reproduced with permission of Elsevier Inc.

This system was tested in an in vivo model of colitis, and it was demonstrated that a high release of the cargo was observed in the colon (where the azoreductase enzymes are present). Moreover, the controlled release of hydrocortisone was able to reduce inflammation in the injueried colon tissue.

1.5.3.3. Gated systems applied to infection processes

As one of the aims of this thesis is the design of molecular-gated systems which would act in an infection environment, it is convenient to review those systems which are already found in bibliography. Most of them use different kinds of biomolecules as capping entities, like peptides,[169] saccharides,[170] DNA and RNA strands,[171] etc., and these gates are cleaved or displaced upon different internal stimuli, as pH changes or the presence of specific enzymes.

One of these infection-fighting systems was created by Martínez-Máñez et al. in 2013, and used gated mesoporous silica nanoparticles in order to enhance the antimicrobial power of determined drugs.[172] **Figure 1.20** shows the schematic representation of the design. The authors prepared the MSNs and loaded them with a dye, and afterwards functionalized the external surface with a n-[(3 trimethoxysilyl)propyl] ethylendiaminetriacetic acid trisodium salt. This salt provided the nanoparticles with a negative charge over all the surface, and allowed the attachment of cationic polymer ε-poly-L-lysine (ε-PL), which also has antimicrobial power, by electrostatic interactions. Under normal conditions, the bulky polymer blocked the entrance to the pores, acting as a molecular gate and avoiding cargo release. In the presence of gram negative-bacteria as *E.coli*, ε-PL polymer was displaced due to their preferential attraction to the negatively charged bacterial wall, unblocking the entrance to the pores and allowing dye release.

---

[169] C. De la Torre, L. Domínguez-Berrocal, J.R. Murguía, M.D. Marcos, R. Martínez-Máñez, J. Bravo, F. Sancenón, *Chem. Eur. J*, **2018**, *24*, 1890-1897.

[170] A. Agostini, l. Mondragón, A. Bernardos, R. Martínez-Máñez, M.D. Marcos, F. Sancenón, J. Soto, A. Costero, C. Manguan-García, R. Perona, M. Moreno-Torres, R. Aparicop-Sanchis, J.R. Murguía, *Angew. Chem. Int. Ed.* **2012**, *51*, 10556.

[171] a) A. Schossbauer, S. Warncke, P. M. E. Gramlich, J. Kecht, A. Manetto, T. Carell, T. Bein, *Angew. Chem.Int. Ed.*, **2010**, *49*, 4734. b) M. Selvamani, A. Ribes, M. Anusuyajanakiraman, V. Narayanan, J. Soto, R. Martínez-Máñez, E. Aznar, *Supramolecular Chemistry*, **2017**, *29*, 776-783.

[172] L. Mondragón, N. Mas, V. Ferragud, C. de la Torre, A. Agostini, R. Martínez-Máñez, F. Sancenón, P. Amorós, E. Pérez-Payá, M. Orzáez. *Chem. Eur. J.* **2014**, *20*, 5271 − 5281.[108]
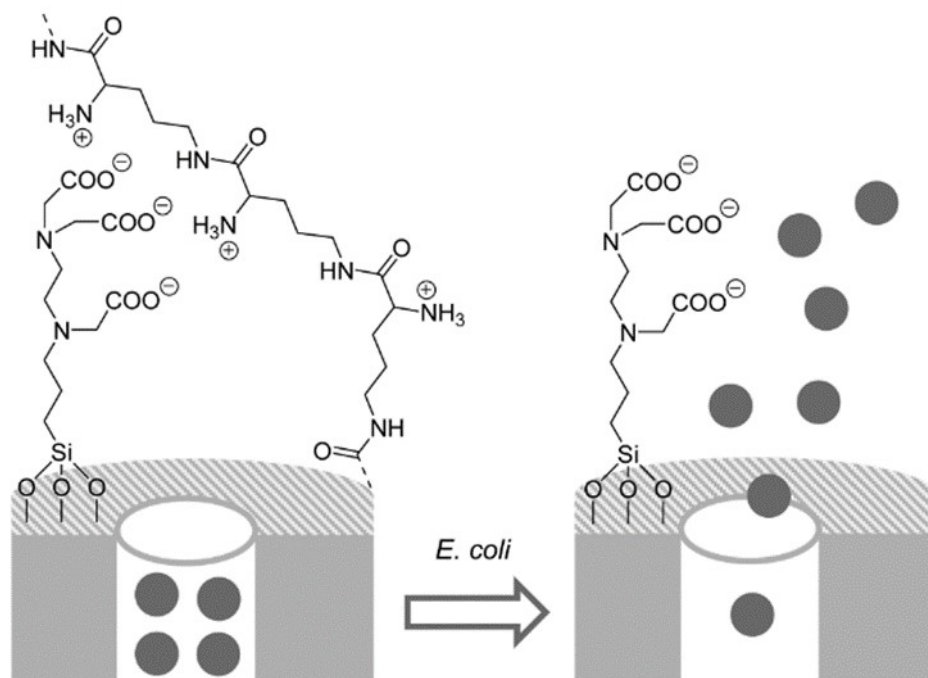
Figure 1.20. Schematic representation of a porous support loaded with vancomycin and capped with ε-poly-L-lysine molecular gates. Reprinted with permission from (Chem.Rev., 2016, 116, 561-718). Copyright (2016) American Chemical Society.

The system was also tested *in vitro* using vancomycin as cargo, showing interesting results: free vancomycin was not effective against gram-negative bacteria, because their external negative-charged wall serves as a protective barrier against certain kinds of antibiotics. However, when vancomycin was encapsulated in ε-PL-gated nanoparticle, the ε-PL binding to the bacteria caused serious damage to the bacterial wall, which allowed the vancomycin to gain access into the cell. In this way, a synergic effect was obtained, since the antibiotic activity of the vancomycin was reinforced by the antimicrobial activity of ε-PL molecules, and the activity of the two compounds together caused higher damage than the individual activity of each of them.

Another system designed to act in an infection scenario is the described below. In this case, mesoporous silica nanoparticles were embedded into a tridimensional scaffold in order to explore future applications in bone tissue regeneration.[173] For this, mesoporous silica nanoparticles were loaded with a dye and functionalized with with 3-[2-(2-aminoethylamino)ethylamino] propyl-trimethoxy silane. Then, adenosine 5'-triphosphate disodium salt hydrate was added. Coordination of ATP with the grafted polyamines (through electrostatic interactions and hydrogen bonds) induced pore closure and inhibited dye release. Thus, the molecular gate was closed under normal conditions, but in the presence of an enzyme called acid phosphatase (APase), the ATP molecules were hydrolysed and the cargo was released (**Figure 1.21**).

---

[173] N. Mas, D. Arcos, L. Polo, E. Aznar, S. Sánchez-Salcedo, F. Sancenón, A. García, M. D. Marcos, A. Baeza, M. Vallet-Regí, R. Martínez-Máñez, *Small*, **2014**, *10*, 4859-4864.
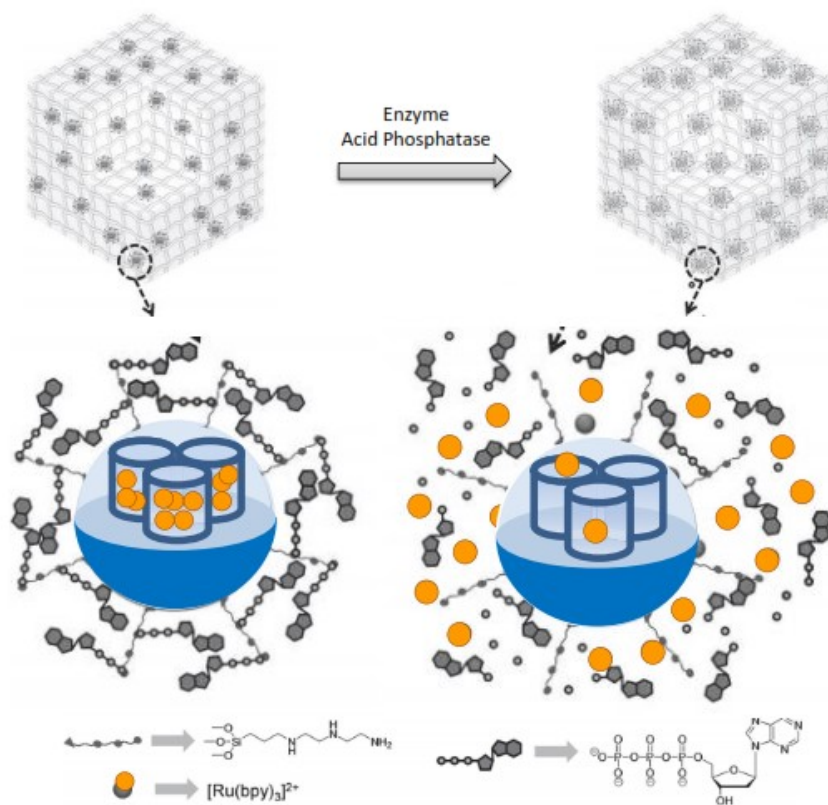
Figure 1.21. Schematic representation of a tree-dimensional scaffold containing enzyme-responsive nanoparticles. Reproduced with permission of Wiley-WCA.

Acid phosphatase is an enzyme present in the organism and its function is the cleavage of phosphate bonds. An abnormal increase in the APase concentration has been related to the presence of bone metastases. Moreover, this enzyme is also present in bone remodelling processes, specifically during osteoclast resorption. The presence of an infection can unbalance the remodelling process and enhance osteoclast resorption, with the consequent rise in the APase concentration and the progressive loss of bone mass. Thus, higher concentrations of APase can also be a marker of bone infection situations. The incorporation of the MSNs in the macroporous gelatine scaffold allowed the creation of a stimuli-responsive tree-dimensional device,

61

which was also proved to be biocompatible with HOS cells and adequate for future cell colonization.

Apart from the use of bulky biomolecules to act as molecular gates, other strategies for the creation of smart devices have been developed in the last years. An innovative and helpful method is the one based in the use of aptamers as molecular gates. An aptamer is a sequence of functional oligonucleotides which presents a strong attraction to specific target molecules. For this reason, they have been frequently employed as specific targeting agents for drug delivery and biosensor development.

Arica et al. reported an aptamer-gated nanosystem targeting *Staphylococcus aureus*, which is the most frequent microorganism infecting bone tissues.[174] The system was composed of MSNs loaded with vancomycin and functionalized with a sulfo-linker (SulfoN-succinimidyl 4-maleimidobutyrate sodium salt) for the posterior grafting of the aptamer. The sequence of the aptamer, called SA20, was selected between those found in bibliography upon an interaction experiment which demonstrate that the aptamer had big affinity for the *S. aureus* microorganisms. Thus, SA20 aptamer was modified by the addition of a NH_2 group, and grafted to the sulfo-linker at the entrance to the pores. Under normal conditions, the aptamer blocked the pores and avoided vancomycin release, but in the presence of *S. aureus*, the aptamer was attracted by the bacteria, unblocking the pores and allowing vancomycin release and achieving the consequent bacterial death (see **Figure 1.22**).

---

[174] M. Kavruk, G. Bayramoglu, O. Celikbicak, B. Salih, V. C. Ozalp, M. Y. Arica, B. A. Borsa, F. J. Hernandez, *Chem. Commun.,* **2015**, *51*, 8492.
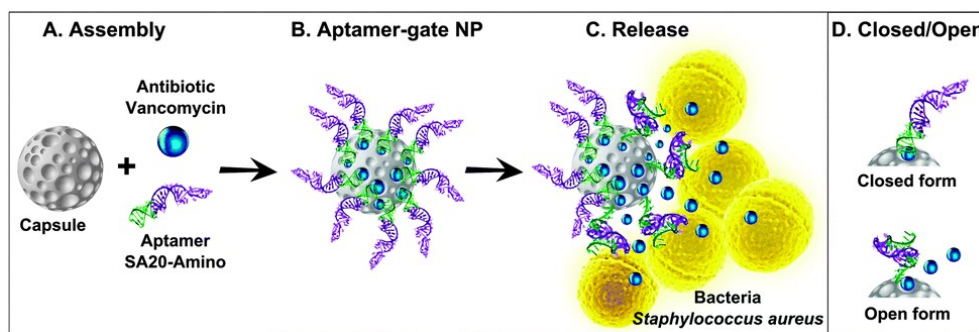
Figure 1.22. Schematic representation of a mesoporous support loaded with vancomycin and capped with the aptamer SA20-amino. Reproduced from *Chem. Commun.*, **2015**, *51*, 8492 with permission from The Royal Society of Chemistry.

The use of oligonucleotides in capped-systems is also interesting in the context of biosensing and microorganism detection. For example, in 2013 Martínez-Máñez and co-workers presented a novel device able to detect the presence of *Mycoplasma*.[175,176,177]

The system consisted of a MSN scaffolding, loaded with a dye and capped with a nucleotide sequence, which was a highly conserved sequence of the 16S ribosomal subunit of in the *Mycoplasma* species genome. When no mycoplasma was present, the oligonucleotide strand stayed at the entrance of the pores and avoided dye release. In the presence of dehybridized genomic DNA of *Mycoplasma fermentants*, the nucleotide sequence attached to the nanoparticle hybridized with complementary free strands of Mycoplasma DNA, unblocking the pores and allowing dye release (see **Figure 1.23**). The monitoring of the

---

[175] E. Climent, L. Mondragón, R. Martínez-Máñez, F. Sancenón, M. D. Marcos, J. R. Murguía, P. Amorós, K. Rurack, E. Pérez-Payá, *Angew. Chem. Int. Ed.* **2013**, *52*, 8938.

[176] L. Pascual, I. Baroja, E. Aznar, F. Sancenón, M. D. Marcos, J. R. Murguía, P. Amorós, K. Rurack, R. Martínez-Máñez, *Chem. Commun.*, **2015**, *51*, 1414-1416.

[177] L. Pla, E. Xifré-Pérez, A. Ribes, E. Aznar, M.D. Marcos, L.F. Marsal, R. Martínez-Máñez, F. Sancenón, *Chem. Plus Chem.*, **2017**, *92*, 337-341.

dye release serves as a specific biosensor, which will only react in the presence of *Mycoplasma* contaminations.
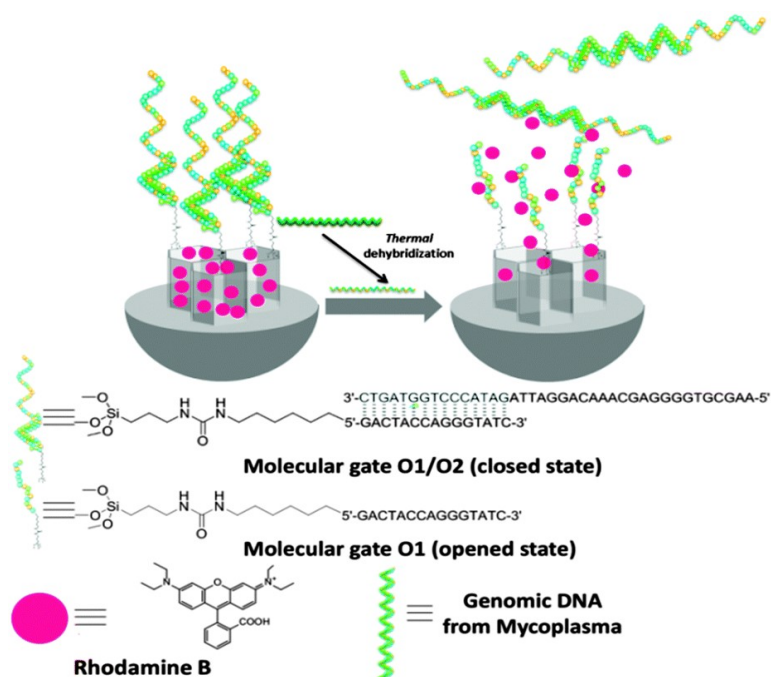

Figure 1.23. Schematic representation of a mesoporous nanoparticle loaded with Rhodamine B and capped with genomic DNA from *Mycoplasma*. Reproduced from *Chem. Commun.*, **2015**, *51*, 1414-1416 with permission from The Royal Society of Chemistry.

To sum up, a wide number of gated systems with far different applications have been designed during the last years. However, the need of developing new materials with biomedical applications is still present. Particularly, more devices which fight bone infection are needed. In this thesis, the design of new gated materials has been explored, and new stimuli-responsive systems have been proposed for specific treatment against infection. For example, new mesoporous materials equipped with molecular gates for the controlled delivery of drugs have been developed for the first time, as we are aware. Specific desings against the infection by *S.aureus* have also been developed.

Moreover, essential oil components (EOCs) have been used in order to take advantage of their antimicrobial activity, and functionalization of calcium phosphates has been carried out in order to combine bone regeneration capabilities with antimicrobial power.

2. Objectives

67

According to the state of the art described in the introduction related to nanochemistry and biogated devices, the general objective or this thesis is to prepare innovative designs able to improve the features of the basic materials. Thus, the specific objectives of this thesis are:

✓ To develop gated mesoporous materials able to release their content in an infection scenario.

✓ To develop smart mesoporous bioactive glasses able to induce a positive response when an infection takes place.

✓ To design and prepare new antibacterial materials base on essential oils combined with calcium phosphate.

3. **Design of gated systems for the prevention and treatment of bone infection**

3.1 Introduction

This chapter is devoted to the design and synthesis of stimuli-responsive systems for the treatment and prevention of infectious processes. Three projects, entitled "Molecular gates in mesoporous bioactive glasses for the treatment of bone tumors and infection", "Mesoporous bioactive glasses equipped with stimuli-responsive molecular gates for the controlled delivery of levofloxacin" and "Gated mesoporous silica materials for the treatment of bone infection by *Staphylococcus aureus*" are reported.

The base of this research was the need to achieve a gated mechanism which would help to the prevention and treatment of infections, particularly in the environment of bone damage. Usually, surgical procedures are necessary for treating bone issues like implanting a prosthesis, refilling a bone-defect or removing a bone tumor. These procedures are not dangerous by themselves, but they may open the door to bacteria, which are able to colonize the damaged tissue or even the implanted device and bring along enormous consequences. Microorganisms-mediated infections are one of the most

frequent problems in hospitals, and hence the need of ideating new devices which are able to fight these kind of pathologies.

In this context, the utility of a gated-system which could respond specifically to an infection marker and release an antibiotic drug was evident. For the design of molecular nanogates which would only react to the presence of a microorganism, two strategies were considered. In the first one, bacterial protease was selected as a marker of an infectious process. The presence of bacteria would mean an increase of secreted proteases, which would act as a stimuli for the opening of enzyme-responsive molecular gates. For this, ε-poly-L-lysine was selected as the gatekeeping entity. According to this design, a mesoporous material was loaded with an antibiotic, and capped with ε-poly-L-lysine molecular gates for enduring a controlled release of the drug only on the presence of bacteria. Experimental results are shown in the publication "Molecular gates in mesoporous bioactive glasses for the treatment of bone tumors and infection".

The second strategy is based on the increase of body markers when a pathologic bone process is happening. Alkaline phosphatase is an enzyme which is present in bone renovation processes, involving as much bone formation as bone resorption. The presence of this enzyme indicates that normal bone regenerative processes are being carried on; however, its abnormal increase means that some pathologic event is occurring. Particularly, high levels of ALP are correlated with the presence of bone metastases. In the publication "Molecular gates in mesoporous bioactive glasses for the treatment of bone tumors and infection", alkaline phosphatase was selected as stimuli for the opening of enzyme-driven molecular systems. ATP gates were then incorporated to a mesoporous material loaded with a cytotoxic drug, since the rise of alkaline phosphatase concentration would trigger the opening of the gate and the cytotoxic drug would be release in order to kill tumor cells.

The same strategy is used in the publication "Mesoporous bioactive glasses equipped with stimuli-responsive molecular gates for the controlled delivery of levofloxacin". While the increase in the concentration of alkaline phosphatase would signal the presence of a bone tumor, the increase of acid phosphatase has been related with the presence of bacterial infection. Thus, ATP molecular gates were implemented again in a mesoporous support loaded with an antibiotic, with the purpose of releasing the drug thanks to the increase to acid phosphatase concentration, which would correlate with the presence of bacterial infection.

Finally, in the case of "Gated mesoporous silica materials for the treatment of bone infection by *Staphylococcus aureus*", the molecular gate is composed by a peptide sequence. *S. aureus* is one of the most frequent microorganisms involved in bone infection, and they secrete a specific protease called V8, which hydrolyses peptide bonds on the carboxyl side of aspartic and glutamic acid residues. For this reason, this V8 protease was selected as a trigger, and the peptide sequence forming the molecular gate was specifically designed to be cleaved by this protease. Thus, this system allows drug delivery in the presence of a *S. aureus* infection.

3.2 Molecular gates in mesoporous bioactive glasses for the treatment of bone tumors and infection

This chapter is derived from the adaptation of the following manuscript: Lorena Polo, Natividad Gómez-Cerezo, Elena Aznar, José-Luis Vivancos, Félix Sancenón, Daniel Arcos, María Vallet-Regí, and Ramón Martínez-Máñez, *Acta Biomaterialia*, **2017**, *50*, 114-126.

3.2.1 Introduction

Mesoporous bioactive glasses (MBGs) are a new generation of bioceramics designed for bone grafting and skeletal regenerative therapies.[178,179] These biomaterials exhibit the bone regenerative properties of non porous bioactive glasses,[180] but significantly increased due to their high surface area and porosity.[181,182] In addition, MBGs possess ordered mesoporous structures similar to those exhibited by pure silica mesoporous materials, which makes them excellent candidates as matrixes in drug delivery applications.[183,184,185] This synergy between osteogenic properties and local drug delivery capabilities is called to play a main role in field of skeletal therapies in near future. Several studies have been carried out to evaluate the behavior of MBGs as drug delivery systems,[186] which have demonstrated that MBGs can release drugs following classical diffusion mechanism.[187]

As stated in the **Introduction** chapter, and in the context of on-command delivery, mesoporous silica has been used as an effective support for the development of controlled-release nanodevices because of their unique characteristics, such as high homogeneous porosity, inertness, robustness, thermal stability, and high loading capacity.[188,189,190,191] Consequently, a number

[178] D. Arcos, M. Vallet-Regí, *Acta Biomater.*, **2010**, *6*, 2874.

[179] C. Wu, J. Chang, *Interface Focus.,* **2012**, *2*, 292.

[180] L.L. Hench, J.M. Polak, *Science*, **2002**, *295*, 1014.

[181] I. Izquierdo-Barba, D. Arcos, Y. Sakamoto, O. Terasaki, A. López-Noriega, M. Vallet-Regí, *Chem. Mater.,* **2008**, *20*, 3191.

[182] X. Yan, C. Yu, X. Zhou, J. Tang, D. Zhao, *Angew. Chemie Int. Ed.*, **2004**, *43*, 5980.

[183] M. Vallet-Regí, F. Balas, D. Arcos, *Angew. Chem. Int. Ed. Engl.*, **2007**, *46*, 7548.

[184] F. Balas, M. Manzano, P. Horcajada, M. Vallet-Regí, *J. Am. Chem. Soc.*, **2006**, *128*, 8116.

[185] D.P. Ferris, Y.L. Zhao, N.M. Khashab, H.A. Khatib, J.F. Stoddart, J.I. Zink, J. *Am. Chem. Soc.*, **2009**, *131*, 1686.

[186] C. Wu, J. Chang, *J. Control. Release*, **2014**, *193*, 282.

[187] A. López-Noriega, D. Arcos, M. Vallet-Regí, *Chem. Eur. J. A*, **2010**, *16*, 10879.

[188] E. Aznar, R. Martínez-Máñez, F. Sancenón, *Expert Opin. Drug Deliv.*, **2009**, *6*, 643.

of nanodevices for on-command delivery that can be triggered by target chemical,[192,193] physical[194,195] or biochemical stimuli[196,197] have been designed recently. However these gated systems have been mainly developed in individual pure silica particles (usually nanometric),[198] and gated functionalities in bioactive compositions for bone regenerative purposes are practically unknown.[199]

In order to explore new bone regeneration strategies, stimuli-responsive 3D macroporous scaffolds have been recently prepared by means of incorporating gated SiO_2 mesoporous nanoparticles within a polymeric matrix.[200] However, as far as we are aware at the time of this PhD project, systems combining bone regenerative properties and on-command drug delivery were not designed. The biological response of MBGs can be partially tailored by controlling the

[189] C. Giménez, C. de la Torre, M. Gorbe, E. Aznar, F. Sancenón, J.R. Murguía, R. Martínez-Máñez, M.D. Marcos, P. Amorós, *Langmuir,* **2015**, *31*, 3753.

[190] E. Aznar, M. Oroval, L. Pascual, J.R. Murguía, R. Martínez-Máñez, F. Sancenón, *Chem. Rev.,* **2016**, *116*, 561.

[191] C. Coll, A. Bernardos, R. Martínez-Máñez, F. Sancenón, *Acc. Chem. Res.*, 2013, *46,* 339.

[192] M. Manzano, M. Vallet-Regí, *J. Mater. Chem.,* **2010***, 20*, 5593.

[193] E. Aznar, R. Villalonga, C. Giménez, F. Sancenón, M.D. Marcos, R. Martínez-Máñez, P. Díez, J.M. Pingarrón, P. Amorós, *Chem. Commun.,* **2013***, 49*, 6391.

[194] J.L. Paris, M.V. Cabanas, M. Manzano, M. Vallet-Regí, *ACS Nano.*, **2015**, *9,* 11023.

[195] N.K. Mal, M. Fujiwara, Y. Tanaka, T. Taguchi, M. Matsukata, *Chem. Mater.*, **2003,** *15*, 3385.

[196] L. Mondragón, N. Mas, V. Ferragud, C. de la Torre, A. Agostini, R. Martínez-Máñez, F. Sancenón, P. Amorós, E. Pérez-Payá, M. Orzáez, *Chem. Eur. J.,* **2014**, *20*, 5271.

[197] Z. Zhang, D. Balogh, F. Wang, I. Willner, *J. Am. Chem. Soc.,* **2013**, *135,* 1934.

[198] B.G. Trewyn, S. Giri, I.I. Slowing, V.S.-Y. Lin, Chem. Commun. (Camb), **2007**, *31*, 3236.

[199] H.M. Lin, W.K. Wang, P.A. Hsiung, S.G. Shyu, *Acta Biomater.*, **2010**, *6*, 3256.

[200] N. Mas, D. Arcos, L. Polo, E. Aznar, S. Sánchez-Salcedo, F. Sancenón, A. García, M.D. Marcos, A. Baeza, M. Vallet-Regí, R. Martínez-Máñez, *Small.*, **2014**, *10*, 4859.

supramolecular mechanisms that rules the synthesis. For instance, the group of professor Vallet-Regí has recently demonstrated that the differentiation of pre-osteoblast toward osteoblast phenotype can be enhanced in contact with MBGs prepared with F68, a $(EO)_{78}$-$(PO)_{30}$-$(EO)_{78}$ triblock copolymer which acts as a structure directing agent.[201] However, the complexity to incorporate the gating mechanisms onto multicomponent SiO_2-CaO-P_2O_5 systems has hindered perhaps the development of stimuli-responsive MBGs up to date. Nonetheless, the design of gated MBGs is highly appealing and might found a number of applications in advanced regenerative therapies.

Based on these concepts, it was the aim of the present work section to demonstrate the possibility to prepare stimuli-responsive MBGs, via the implementation of tailor-made gated ensembles on the surface of bioactive glasses. The final goal was to develop bioactive glasses able to regenerate bone tissue in bone defects while treating the causal pathology of such a defect, for instance bone infection or tumor extirpation. Therefore the mesopores of a selected MBG were capped with two different enzyme-responsive molecular gates based in the use of adenosine triphosphate (ATP) and ε-poly-L-lysine (ε-PL) as caps (*vide infra*), which allowed controlled cargo release in the presence of alkaline phosphatase (ALP) and proteolytic enzymes, respectively. Proteolytic activity can be observed in the presence of different infectious pathogens as *Escherichia coli*,[202,203] whereas high levels of serum ALP have prognostic significance in osteosarcoma scenarios.[204] Such tailor-designed

[201] N. Gómez-Cerezo, I. Izquierdo-Barba, D. Arcos, M. Vallet-Regí, *J. Mater. Chem. B.*, **2015**, *3*, 3810.

[202] M.P. Nandakumar, A. Cheung, M.R. Marten, *J. Proteome Res.*, **2006,** *5*, 1155.

[203] K. Haddadi, F. Moussaoui, I. Hebia, F. Laurent, Y. Le Roux, *Reprod. Nutr. Dev.,* **2005**, *45*, 485.

[204] G. Bacci, A. Longhi, S. Ferrari, S. Lari, M. Manfrini, D. Donati, C. Forni, M. Versari, *Oncol. Rep.,* **2002**, *9*, 171.

systems may have potential applications for the treatment of bone tissue defects commonly associated to osteomyelitis and bone tumors extirpation.

3.2.2 Objectives

The objectives of the present project are:

✓ To design, develop and characterize a hybrid enzyme-responsive system based on a mesoporous bioglass equipped with ε-poly-L-lysine molecular gates for the treatment of bone infections.

✓ To study of the bioactivity of the ε-poly-L-lysine gated solid.

✓ To validate the ε-poly-L-lysine gated system in a bacterial environment.

✓ To design, develop and characterize a hybrid enzyme-responsive system based on a mesoporous support equipped with ATP molecular gates for the treatment of bone tumors.

✓ To study the bioactivity of the ATP gated solid.

✓ To validate the ATP-gated system with a cancer cell line.

3.2.3 Synthesis and characterization

The synthesis strategies developed in this project are aimed to design multifunctional bioceramics with two main features. The first one is the ability of stimulating bone tissue regeneration to repair bone defects. In this sense, the material should exhibit high bioactive behavior, that is, the capability to osteointegrate with the host tissue through the formation of an apatite-like phase on its surface. The second function is to deliver drugs on demand to treat the causal pathology of the bone defect, for instance bone infection or

extirpated bone tumors. In order to reach these goals two different on demand drug delivery systems were designed as depicted in **Scheme 3.2.1**.
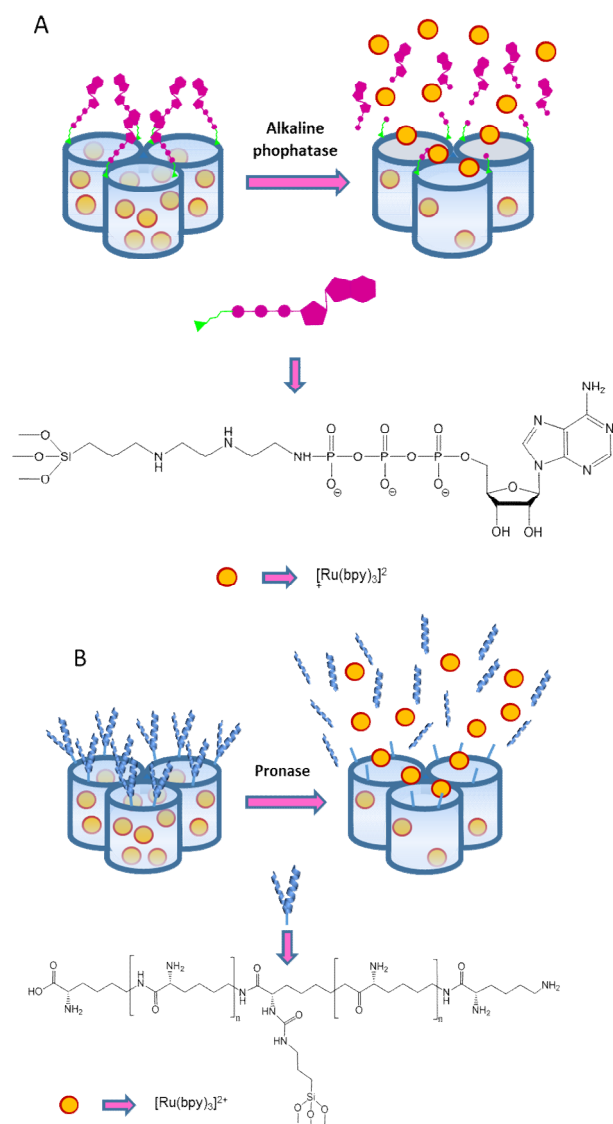
Scheme 3.2.1. Schematic representation of the ATP (A) and e-poly-L-lysine (B) gated materials.

The first one was designed on the basis that ATP molecules can act as capping agents.[23] For this purpose, the mesoporous bioglass was functionalized with 3-[2-(2-aminoethylamino)ethylamino]propyl-trimethoxysilane (**N3**), and then it was treated with ATP. ATP forms a covalent bond with the triamine attached to the external surface of the mesoporous material, capping the pores and inhibiting cargo release. Conveniently, hydrolysis of ATP molecules induced by the over-activity of external ALP would uncap the mesopores, allowing cargo delivery in a controlled and selective way.

The second system was designed by functionalizing the external surface of the MBG with 3-(triethoxysilyl)propyl isocyanate (**NCO**) and treating the solid with ε-poly-L-lysine, to form urea bonds with the isocyanate groups attached to the external surface. ε-poly-L-lysine would cover the surface of the loaded solid, capping the entrance to the pores and inhibiting payload release. Otherwise, the presence of bacterial proteases would induce hydrolysis of the amide bond in ε-poly-L-lysine, allowing cargo release.

In order to study in detail the synthesis and functionality of molecular gates, different solids were prepared. To clarify the composition of each one, a summary of all the prepared solids is shown in **Table 3.2.1**. For this, a mesoporous bioactive glass with a composition of $85\%SiO_2$-$10\%CaO$-$5\%P_2O_5$ (**S1)** was synthetized by the group of prof. Vallet-Regí. The synthesis was carried out by evaporation induced self-assembly (EISA) method, using F68 $(EO)_{78}$-$(PO)_{30}$-$(EO)_{78}$ triblock copolymer as structure directing agent and TEOS, TEP and calcium nitrate $Ca(NO_3)_2 \cdot 4H_2O$ as precursors (see detailed synthesis procedure in **Experimental Section, Chapter 5.1**). Then, a portion of the **S1** solid was functionalized with 3-[2-(2-aminoethylamino)ethylamino] propyltrimethoxysilane in order to yield solid **S2**, and subsequently it was treated with ATP to yield the ATP-gated solid **S3**. Another portion of the initial solid **S1** was functionalized with 3-(triethoxysilyl)propylisocyanate, yielding solid **S4**, and capped with ε-poly-L-lysine, yielding solid **S5**.

In order to check the functionality of the molecular gates, the mesoporous support (**S1**) was loaded with the dye ([Ru(bpy)$_3$]$^{2+}$, and ATP and ε-poly-L-lysine molecular gates were implemented in different portions of the solid, obtaining **S3-Ru** and **S5-Ru**. Stimuli-responsive studies were carried out with this solids in order to demonstrate the controlled-release capabilities. The bioactivity of the materials was also studied in order to check that bioactive properties were not affected by the implementation of the molecular gates. Afterwards, the same procedure was followed with levofloxacin and doxorubicin loaded solids: ATP molecular gate was incorporated to doxorubicin-loaded solid, yielding **S3-Dox**, while ε-poly-L-lysine gate was incorporated to levofloxacin loaded solid, yielding **S5-Levo**. Posterior validation was performed with both solids. For the development of further experiments, **S3-Levo** was also synthesized.

Table 3.2.1. Summary of the synthesized solids.

Name	Support	Cargo	External Functionalization	Cap
S1	MBG	-	-	-
S2	MBG	-	N3	-
S3	MBG	-	N3	ATP
S4	MBG	-	NCO	-
S5	MBG	-	NCO	ε-poly-L-lysine
S3-Ru	MBG	[Ru(bpy)$_3$]$^{2+}$	N3	ATP
S3-Levo	MBG	Levofloxacin	N3	ATP
S3-Dox	MBG	Doxorubicin	N3	ATP
S5-Ru	MBG	[Ru(bpy)$_3$]$^{2+}$	NCO	ε-poly-L-lysine
S5-Levo	MBG	Levofloxacin	NCO	ε-poly-L-lysine

Typical characterization techniques were used to demonstrate that the incorporation of the molecular gates was successful and the structure of the mesoporous materials was not damaged. First, FTIR spectroscopy and solid state NMR were carried out by the group of prof. Vallet-Regí, to confirm the

presence of the corresponding functional groups for solids **S1, S2, S3, S4** and **S5**. **Figure 3.2.1** shows the FTIR spectra obtained for the different stages of the functionalization of **S3** and **S5**. **S1** presents characteristic absorption bands for Si-O at approximately 1040, 800 and 470 cm^{-1} corresponding to ν(Si-O-Si), ϱ(Si-O-Si) and δ(Si-O-Si) vibrations, respectively. Moreover, the characteristic absorption bands for P-O bonds in an amorphous environment can be also observed. **S2** additionally shows bands at 1620 cm^{-1} and 1480 cm^{-1} attributed to δ(C-H) and δ(C-N) ring stretching of bipyridine, indicating the presence of the [Ru(bpy)$_3$]$^{2+}$ in the material. Solid **S3** shows characteristic δ(N-H), δ(C-N) bands at 3250 cm^{-1} and 1550 cm^{-1} and ν(C-H)as, ν(C-H)s and δ(C-H) vibrations at 2900, 2850 and 1650 cm^{-1}. Moreover ν(C-C) and ν(C-N) bands appear at 1469 and 1350 cm^{-1}. Solid **S4** displays typical ν(PO$_4$)$^{3-}$, ν(P-OH) and δ(P-O-P) amorphous bands at 1100 cm^{-1}, 850 cm^{-1} and 550 cm^{-1}, respectively. Finally **S5** shows ν(C-H)as, ν(C-H)s, ν(C=O) and ν(C-N) characteristic vibrations of amide bonds of ε-poly-L-lysine at 2982, 2818, 1635 and 1398 cm^{-1}, respectively.
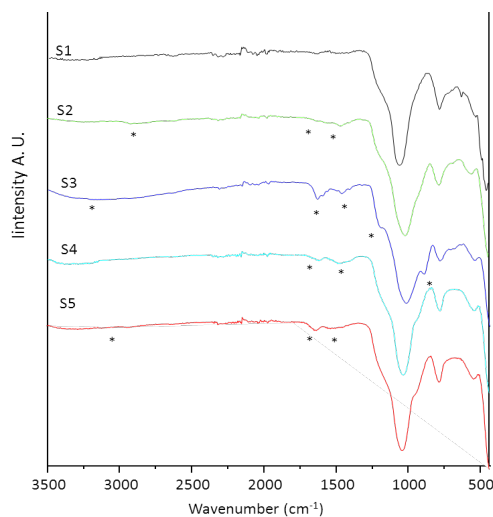

Figure 3.2.1. FTIR spectra for the different synthetized solids. Stars (*) indicate bands assigned to the organic functionalization.

In a second place, the MBG functionalization was followed by solid state NMR to confirm the success of the incorporation of the different components of the gates. Solid-state ^{29}Si single pulse (left) and cross-polarization (right) MAS NMR spectra, solid-state ^{31}P single pulse MAS NMR spectra and solid-state ^{1}H $\rightarrow$ ^{13}C-CP/MAS spectra obtained from solids **S1**, **S3** and **S5** were thoroughly analyzed in order to study the functionalization process. The spectra provide clear evidence that both solids were functionalized with their corresponding gates.

After demonstrating the presence of the molecular gates by solid state NMR studies, the mesoporous structure of the different solids was studied in order to determine if it was damaged upon the functionalization and implementation processes. Thus, powder X-ray diffraction patterns were taken in order to study the order of the mesoporous structure. Powder XRD patterns of solids **S1**, **S3** and **S5** are shown in **Figure 3.2.2**. For **S1**, a sharp peak is shown at 1.29 °, corresponding to the (10) Bragg reflection of a 2D hexagonal p6m structure. **S3** and **S5** show smaller peaks with maximum at 1.39 °, also corresponding to this kind of structure. The displacement of the peaks may be due to the fact that both **S3** and **S5** solids are functionalized and capped, which could slightly modify cell parameters. Moreover, the intensity of the peaks is visibly decreased after functionalizing and capping, possibly due to the contrast loss among these processes. However, despite these small differences, no significant changes are found between the diffractogram of **S1** and the ones of **S3** and **S5**, which could demonstrate that the inner mesoporous structure of the solids remains unchanged after loading and capping procedures.
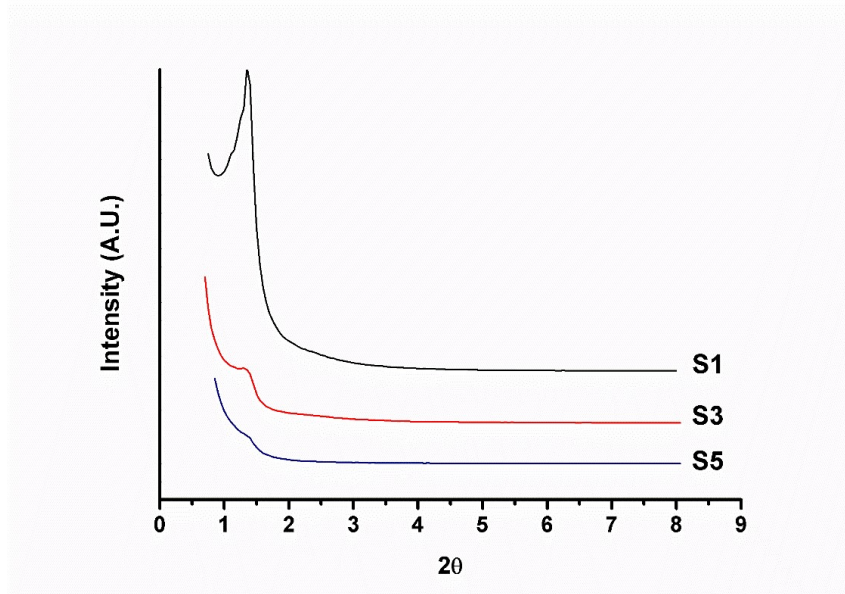
Figure 3.2.2. Powder X-ray diffraction pattern of solids **S1**, **S3** and **S5**.

In order to verify the results obtained by the powder XRD patterns, TEM images were taken. Thus, the mesoporous nanostructure of the solids could be observed (**Figure 3.2.3**). In the case of solid **S1**, the characteristic channels of a mesoporous ordering matrix were observed as alternate black and white stripes, evidencing the 2D hexagonal ordered mesoporous structure (**Figure 1A and B**). The TEM images of solids **S3** and **S5** (**Figure 1C and D**, respectively) also show ordered mesoporous arrangement, confirming that the loading and capping processes undergone by the MBG did not significantly affect the mesoporous structure.
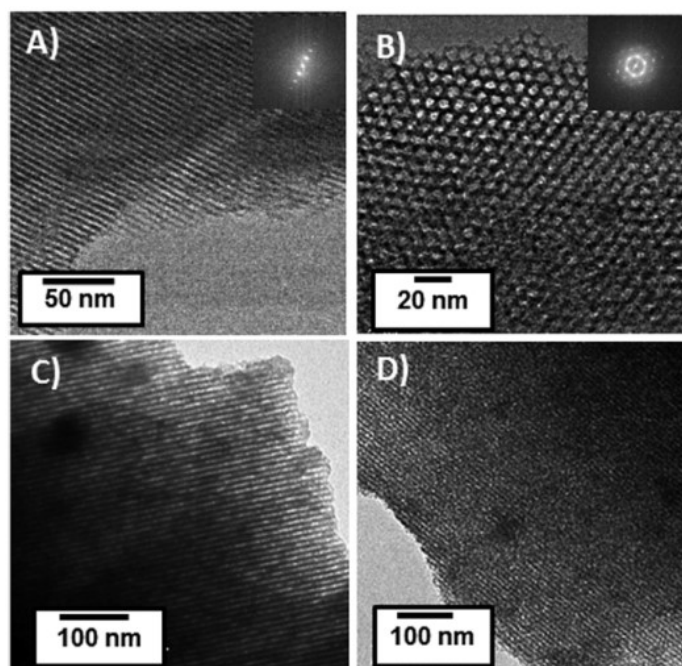
Figure 3.2.3. Representative TEM images of solid **S1** acquired along [10] direction (A), solid **S1** acquired along the [01] direction (B), solid **S3** (C) and solid **S5** (D). The FT diagrams for **S1** solid are included (A and B), evidencing the 2D hexagonal ordering of this sample.

Once verified that the mesoporous structure remained undamaged, thermogravimetric analysis were performed in non-loaded solids in order to study the degree of functionalization and quantify the amount of organic content present in each sample. Thus, thermograms of solids **S2, S3, S4** and **S5** are shown in **Figure 3.2.4**. In each graphic, a modest loss of mass is observed from 0 to 100 °C, corresponding to the mass loss due to evaporation of superficial humidity and possible residues of organic solvents physisorbed on the surface of materials. Then, the loss of mass observed from 100 to 800 °C is due to the combustion of the organic matter attached to the solid (functionalization and capping molecules). Finally, the loss of mass observed between 800 and 1000 °C is due to the condensation of free silanols on the surface of the materials. Thus, the

loss of mass observed for **S2** (16 %) would correspond to the decomposition of 2-(2-aminoethylamino)ethylamino]propyl-trimethoxysilane (N3), which is the only organic compound attached to the surface of **S2**. After the ATP incorporation (solid **S3**) the mass loss increases to 22 %, in agreement with the bonding of this compound. **Table 3.2.2** summarizes the amount of each organic compound related to the amount of inorganic matrix. As happens with **S2**, the loss of mass observed for **S4** (8 %) would correspond to the decomposition of 3-(triethoxysilyl)propylisocyanate (NCO), which is the only organic compound present in this solid. After the ɛ-poly-l-lysine addition (solid **S5**) the mass loss increases to 18 %, in agreement with the incorporation of the peptide. Thus, we can conclude that the functionalization process was more effective in the case of **S2**, since the molar amount of N3 was higher than the molar amount of NCO. However, the incorporation of both ATP and ɛ-poly-L-lysine gates seemed to be successful, since the molar amounts of both compounds were remarkably high.
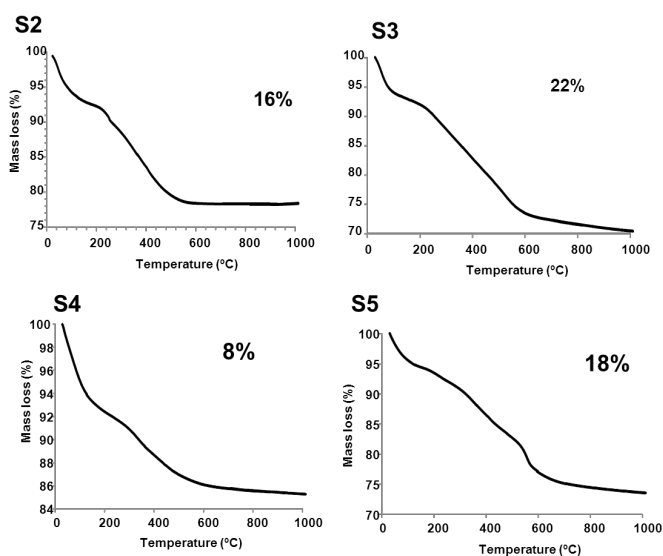

Figure 3.2.4. Thermogravimetric diagrams obtained for samples **S2**, **S3**, **S4** and **S5**.

Table 3.2.2. Organic content in solids **S2, S3, S4 and S5** (α, mmol of N3, ATP or NCO/g of solid, β, g of ε-poly-L-lysine/g of solid).

Solid	α_{N3}	α_{ATP}	α_{NCO}	β_{poly}
S2	0.773	-	-	-
S3	0.773	0.198	-	-
S4	-	-	0.377	-
S5	-	-	0.377	0.143

Apart from the study of non-loaded solids, N_2 adsorption-desorption isotherms of loaded and non-loaded solids were performed in order to study their differences. In this way, isotherms of **S1**, **S3-Ru** and **S5-Ru** were taken. N_2 adsorption-desorption isotherms of **S1** show a type IV curve, characteristic of mesoporous materials (**Figure 3.2.5**). The curve shows a H1 hysteresis loop indicating that mesopores have an opened at both ends cylinder morphology. Solids **S3-Ru** and **S5-Ru** exhibit isotherms corresponding to mesoporous materials with lower surface area and pore volume, as could be expected after loading with $[Ru(bpy)_3]^{2+}$ and subsequent capping with the ATP (solid **S3-Ru**) or ε-poly-L-lysine (solid **S5-Ru**) based gates (see **Table 3.2.3**). Solid **S3-Ru** shows a strong decrease of textural values respect to pristine solid **S1**. In fact, the hysteresis loop changes to type H2 pointing out that the mesopore morphology shifts from open cylinders towards ink-bottle morphology as a consequence of the highly effective capping with the ATP gate. On the other hand, the textural parameters of solid **S5-Ru** underwent a lower decrease than textural parameters of **S3-Ru**, indicating that the loading process was probably not as effective and less cargo was loaded into the pores of **S5-Ru**. This would be consistent with the results obtained from thermogravimetric analysis. As the functionalization process for **S4** was not as effective as the functionalization of **S2**, a higher loss of the dye would happen during the capping step. Thus, the

solid **S5-Ru** would contain less cargo inside the pores, which would result in a smoother decrease of textural parameters compared with **S3-Ru**.
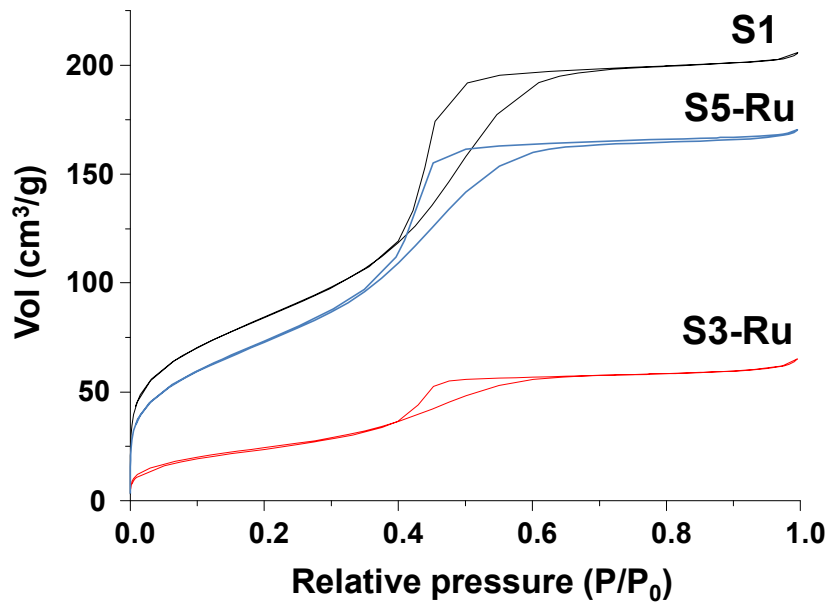

Figure 3.2.5. N$_2$ adsorption-desorption isotherms for solids **S1**, **S3-Ru** and **S5-Ru**.

Table 3.2.3. Textural properties of solids **S1**, **S3-Ru** and **S5-Ru**.

Sample	S$_{BET}$ (m^{2}g^{-1})	Pore volume (cm^{3}g^{-1})	Pore size (nm)
S1	307.10	0.318	4.2
S3-Ru	90.35	0.100	3.7
S5-Ru	268.43	0.263	3.6

3.2.4 Results and discussion

Once the non-loaded solids were correspondingly characterized and the presence of the molecular gates was demonstrated, it was essential to validate that the materials were able to perform a controlled release under selective conditions. For this, the mesoporous support (**S1**) was loaded with ($[Ru(bpy)_3]^{2+}$, and both molecular gates were incorporated to the dye-loaded material. Thus, in order to investigate the gating properties of ATP and ε-poly-L-lysine gates, cargo-release studies were carried out with **S3-Ru** and **S5-Ru**. In a typical experiment, 2 mg of **S3-Ru** were suspended in water at pH 7.6 in the presence and absence of ALP. Suspensions were stirred at 400 rpm at 37 °C for 10 hours, and at given time intervals fractions of both suspensions were taken and filtered to remove the solid. Dye released to the solution was then monitored by measuring the fluorescence of $[Ru(bpy)_3]^{2+}$ at 594 nm (λ_{ex} 454 nm). $[Ru(bpy)_3]^{2+}$ delivery profiles in both, the presence and absence of ALP enzyme, are shown in **Figure 3.2.6A**. A negligible dye release occurs when ALP is not present. Contrarily, the concentration of $[Ru(bpy)_3]^{2+}$ in the solution increased significantly in the presence of the enzyme. This behavior is consistent with a tight pore closure by ATP, which would be hydrolyzed in the presence of ALP, thus unblocking the entrance to the pores and allowing cargo release.

Similar release studies were also performed with the ε-poly-L-lysine-capped solid **S5-Ru** but using pronase enzyme as trigger (**Figure 3.2.6B**). Delivery profiles in both, the presence and absence of pronase enzyme are shown in **Figure 3.2.6B**. A poor $[Ru(bpy)_3]^{2+}$ release was observed in the absence of pronase, while a significant increase of payload delivery occurs when the enzyme is added to the medium. The differences in both release kinetics are due to the fact that two different capping systems and enzymes are being used. ε-poly-L-lysine is a long polymer with a number of amide bonds to be hydrolyzed, yielding L-lysine molecules. The action of the pronase enzyme allows a fast hydrolysis of the molecular gate and a quick leakage of the dye

out of the pores. However, alkaline phosphatase is expected to hydrolyze the phosphate groups of ATP. This anion, in solid **S3-Ru**, is coordinated with positively charged amino moieties located onto a dense network of polyamines grafted onto the outer surface of the loaded support. For this reason, alkaline phosphatase could have some steric hindrance in the hydrolysis of the phosphate groups of ATP and, as a consequence, a slower release of the dye was observed.

These experiments confirm that as much ATP as ɛ-poly-L-lysine are suitable capping systems in MBG supports, which can be hydrolyzed in the presence of ALP or pronase enzymes, thus resulting in cargo release.
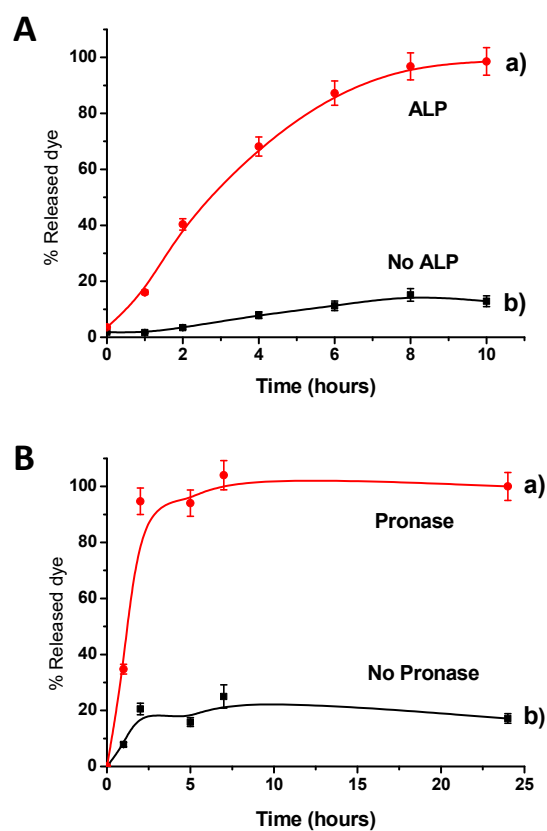

Figure 3.2.6. Dye release studies carried out at 37 °C: A) MBG capped with ATP (**S3-Ru**), B) MBG capped with ɛ-poly-L-lysine (**S5-Ru**).

After demonstrating the controlled release capabilities of solids **S3-Ru** and **S5-Ru**, their bioactive properties were studied. It is known that MBGs are featured by their excellent bioactive properties, which stem from their particular textural characteristics: their high surface area and porosity enhance the ionic exchange with the surrounding media, thus developing an apatite-like phase onto their surface that ensures the integration with the bone under *in vivo* conditions. It is important to mention that a change of the textural properties of a mesoporous bioglass could endure a decrease of their bioactive capabilities and, for this reason, we found it essential to assess the bioactive behavior of gated solids and check that their bioactive power had not been harmed. For this purpose, solids **S3** and **S5** were soaked in simulated body fluid (SBF) at 37 °C to test their capability for nucleating and growing a newly formed apatite-like phase. The tests were carried out in absence and presence of the corresponding enzymatic stimuli. Solid **S3** does not develop any newly formed calcium phosphate layer when soaked in SBF for 1 and 3 days, in absence of stimuli. The SEM micrographs do not evidence significant changes at the MBG surface (**Figure 3.2.7A**, **3.2.7B** and **3.2.7C**). However, in the presence of ALP, i.e. when the gate is open, the MBG recovers the bioactive behavior and develops an apatite-like phase after 1 day in SBF, which further grows after 3 days in contact with this solution (**Figure 3.2.7D** and **3.2.7E**). FTIR spectroscopy agrees with the SEM results in the absence and presence of ALP (**Figure 3.2.7F**). In the absence of ALP, the spectra show the same absorption bands before and after soaking in SBF, *i.e* those corresponding to the vibrations of Si-O bonds and P-O bonds in amorphous environment. On the contrary, in the presence of ALP, the FTIR evidence the splitting of the signal at 590-610 cm^{-1} in the FTIR spectra, pointing out that the newly phase observed by SEM is an apatite-like phase (**Figure 3.2.7F**). On the other hand, solid **S5** exhibits an excellent bioactive behavior. This solid develops a thick newly formed apatite phase in both the presence and absence of enzymatic stimuli, as evidenced by SEM (**Figure 3.2.7H, 3.2.7J, 3.2.7I and 3.2.7K**) and

confirmed by the doublet at 590-610 cm^{-1} appeared in the FTIR spectra (**Figure 3.2.7L**).
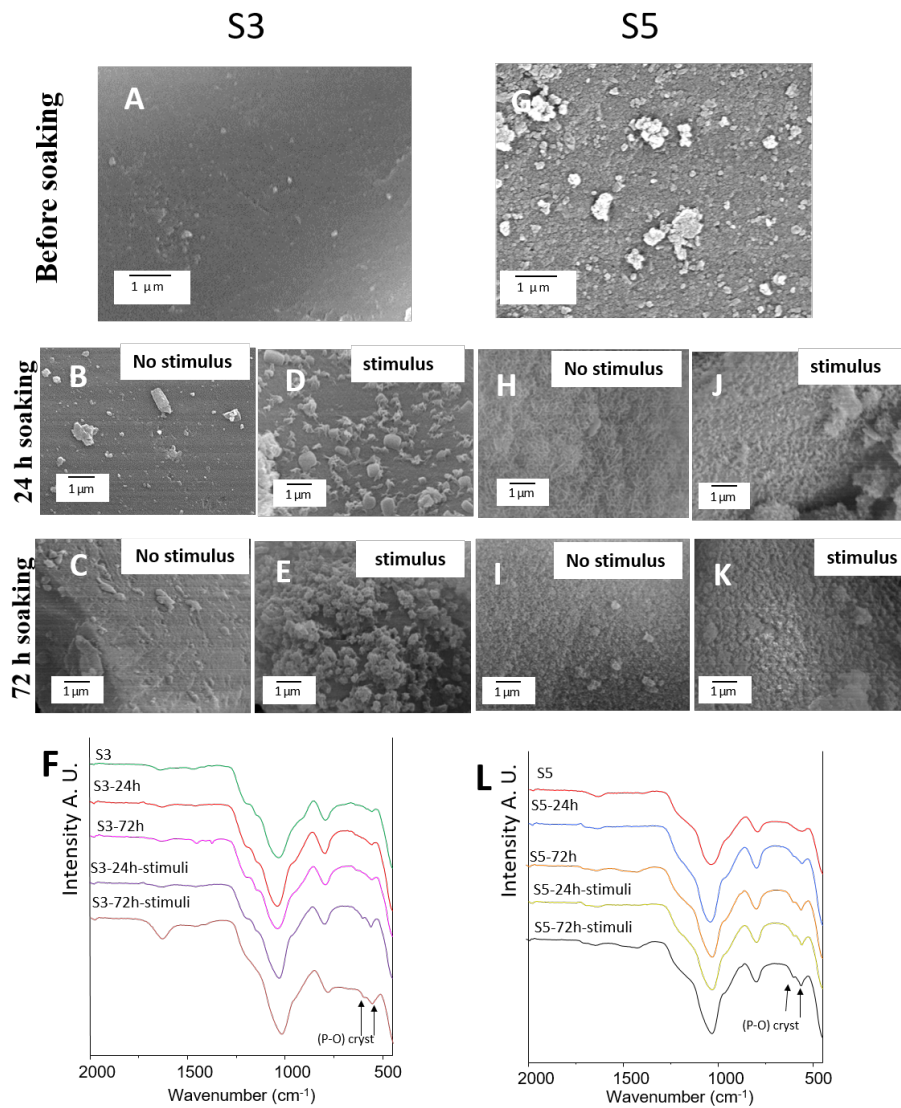

Figure 3.2.7. SEM micrographs of solid **S3** in absence of stimuli, A) before soaking, B) when is soaked in SBF for 24 hours and C) 72 hours. SEM micrographs of solid **S3** in presence of stimuli, D) when is soaked in SBF for 24 hours and E) 72 hours. SEM micrographs of solid **S5**

in absence of stimuli, G) before soaking, H) when is soaked in SBF for 24 hours and I) 72 hours. SEM micrographs of solid **S5** in presence of stimuli, J) when soaked in SBF for 24 hours and K) 72 hours. FTIR spectra for solids F) **S3** and L) **S5**.

The inhibition of the bioactive behavior after the incorporation of the ATP gate in solid **S3** could be related with the significant decrease of textural properties undergone by the MBG. The functionalization strategy used for the preparation of **S3** was very efficient, as could be observed by NMR and porosimetry measurements. The capping of the mesopores would impede the ionic exchange with the surrounding SBF thus avoiding the subsequent nucleation and growth of the newly formed apatite phase. Ca^{2+} release is the first reaction required to initiate the bioactive process.[205,206] The inhibition of this stage seriously hiders the rest of the reactions that lead to the formation of an apatite-like phase similar to the mineral component of the bone. Another possible explanation could be the entrapping of Ca^{2+} by the phosphate groups of the ATP gate. It has been highly demonstrated that the affinity of phosphate groups for Ca^{2+} can inhibit its release (and consequently the bioactivity) by forming CaP nanoclusters that inhibit the Ca^{2+} dissolution. The CaP clusters formation has been widely studied within the walls of the MBGs[207,208,209,210] and we hypothesize that the Ca^{2+} entrapment by phosphates could also occurs at the MBG surface due to the ATP presence. Independently

---

[205] M.R. Filgueiras, G.P. La Torre, L.L. Hench, *J. Biomed. Mater. Res.,* **1993**, *27,* 445.

[206] O.P. Filho, G.P. La Torre, L.L. Hench, *J. Biomed. Mater. Res.*, **1996**, *30*, 509

[207] T. Kokubo, H. Kushitani, S. Sakka, T. Kitsugi, T. Yamamuro, *J. Biomed. Mater. Res.*, **1990**, *24*, 721.

[208] L.L. Hench, *Science*, **1980**, *208*, 826.

[209] C. Turdean-Ionescu, B. Stevensson, I. Izquierdo-Barba, A. García, D. Arcos, M. Vallet-Regí, M. Edén, *J. Phys. Chem. C.*, **2016**, *120*, 4961.

[210] R. Mathew, C. Turdean-Ionescu, B. Stevensson, I. Izquierdo-Barba, A. García, D. Arcos, M. Vallet-Regí, M. Edén, *Chem. Mater.*, **2013**, *25*, 1877.

of the mechanism that inhibits the bioactivity of **S3**, ALP open the ATP based gate and the MBG recovers its bioactivity.

As stated previously, the design of these gated solids responds to the need to perform a double strategy for the treatment of bone diseases. The first aim was the ability to release substances in a controlled way thanks to the implementation of the molecular gates. The previous experiments demonstrated that this goal was successfully achieved. The second aim was to maintain the ability of enhancing bone regenerative processes, which could be harmed by the implementation of the molecular gates. However, the results of the bioactivity studies demonstrated that the bioactive capabilities were not harmed after the gating process. For this reason, once the chemical validation of the materials was completed, we proceeded to the test the loaded materials in cellular and bacterial environments, in order to study their response.

First, the stimuli-responsive properties of the doxorubicin-loaded and ATP-gated solid were studied. The release of doxorubicin from **S3-Dox** solid was analysed in the absence and presence of ALP (**Figure 3.2.8**). A negligible drug release occurs in the absence of ALP, whereas a marked doxorubicin release was observed when ALP is added, pointing out that the enzyme opens the ATP gates.
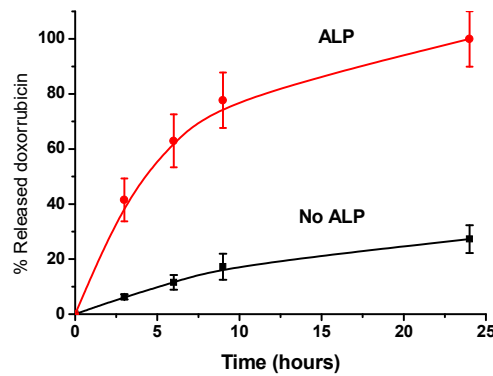

Figure 3.2.8. Doxorubicin release studies carried out at 37 °C with **S3-Dox** in the presence and in the absence of ALP.

In a step forward, the antitumoral activity of **S3-Dox** was studied with HOS cell cultures. HOS cells were cultured in the presence of solid **S3** and **S3-Dox** in the presence and the absence of ALP, and their viability was quantified after 6, 24, 48 and 144 hours. A culture of non-treated HOS cells was used as a control. Thus, HOS viability was measured in the presence of **S3** and **S3-Dox** under absence and presence of ALP (**Figure 3.2.9**). The cells in contact with **S3** show a proliferative behaviour very similar to those cultured on the polystyrene control. However, the cells cultured with **S3-Dox** clearly underwent a cytotoxic effect. In the absence of ALP, the HOS proliferation is significantly hampered after 24 hours respect to the control. This result can be due to the small amount of doxorubicin released, even without the addition of ALP. It must be taken into account that HOS cells produce ALP by themselves and could facilitate the partial opening of the ATP gates. However, 48 hours later HOS proliferate indicating that the doxorubicin released is not enough to inhibit the growth of HOS. On the contrary, in the presence of ALP, HOS cannot proliferate after 48 hours of culture showing a significant viability decrease as a consequence of the released doxorubicin. Finally, the HOS viability was determined for longer exposure times. After 144 hours of test, the HOS viability in the presence of solid **S3** remains unaltered. However, in the case of doxorubicin loaded sample (**S3-Dox**), a significant decrease of HOS viability was observed under both conditions, i.e. ALP presence and absence. This fact can be attributed to the MBG solubility that allows the partial release of the antitumoral drug. However, it must be highlighted that doxorubicin release is still higher in the presence of ALP, pointing out that the stimuli-responsive behaviour is present even after the partial degradation of the MBG matrix associated to the bioactive process.
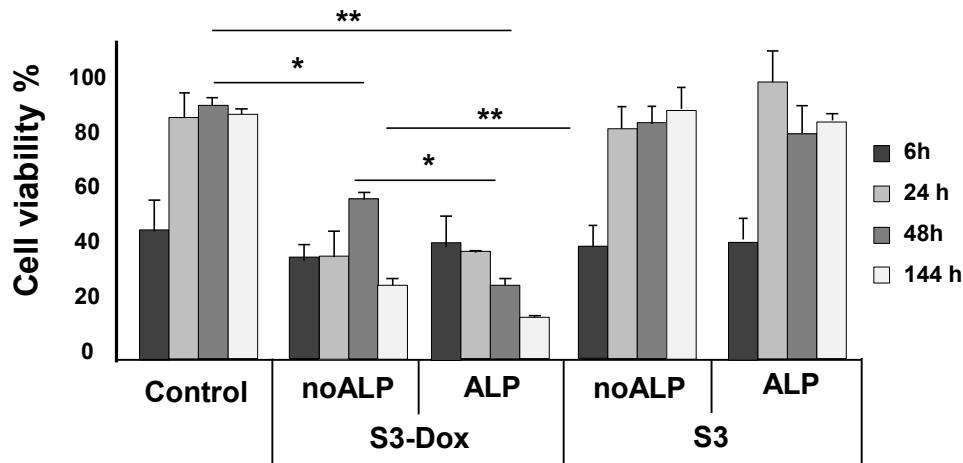
Figure 3.2.9. HOS viability in contact with **S3** and **S3-Dox** solids in the absence and presence of ALP after 6, 24, 48 and 144 hours. Significant differences from 48 and 144 hours: Statistical significance: *p < 0.05, **p < 0.01.

In a second scenario, the MBG solid capped with ε-poly-L-lysine was loaded with the antibiotic levofloxacin (solid **S5-Levo**) and the selective delivery of the antibiotic in the presence of bacteria was evaluated. For this study *Escherichia coli,* DH5α strain, was used as model bacteria. In a first step, the amount of cargo released from **S5-Levo** was determined in the presence and in the absence of bacteria. As shown in **Figure 3.2.10**, a limited payload delivery (less than 20 % after 24 hours) was found in the absence of *E. coli*, whereas a remarkable cargo delivery was found when the bacteria were present. From these studies it was found that maximum amount of levofloxacin released from **S5-Levo** was of 0.322 ng of levofloxacin per mg of solid. Moreover, it was also observed that delivery of antibiotic levofloxacin was concomitant with a reduction of bacteria viability (*vide infra*).
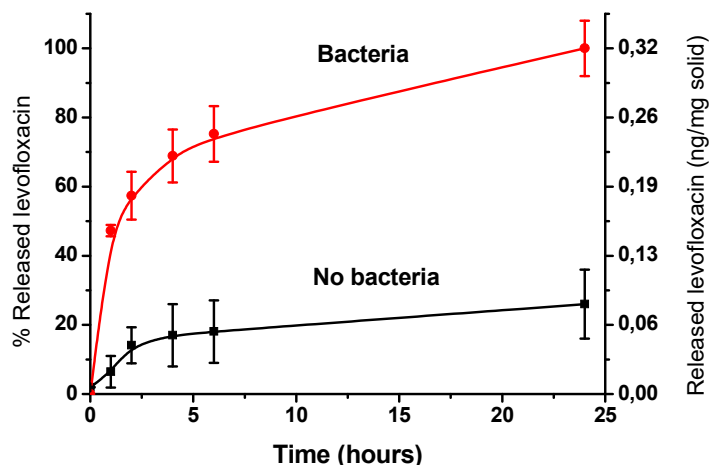
Figure 3.2.10. Levofloxacin release studies carried out at 37 ºC with **S5-Levo** in the presence and in the absence of *E. coli*.

The antimicrobial activity of **S5-Levo** was studied more in detail by carrying clonogenic cell-viability assays in which *E. coli* bacteria were treated with different concentrations of **S5-Levo** at pH 7.6. A negative assay with no bacteria was also carried out and used as control to quantify cell growth. In a typical experiment, bacteria (10^4 cells·mL^{-1}) were incubated for 5 minutes in the presence of **S5-Levo**, and then seeded in petri plates. Seeded plates were incubated at 37 °C for 24 hours and then colony formation units (CFU) were quantified. **Figure 3.2.11** shows the percentage of CFU *versus* the amount of levofloxacin released from **S5-Levo** (i.e. 0.322 ng of levofloxacin per mg of solid, *vide ante*). As seen in the figure, CFU values decrease when the amount of **S5-Levo** added to the bacteria medium increases. **S5-Levo** showed considerable toxicity against *E. coli*, with an EC$_{50}$ value of 22.26 ng·mL^{-1} of levofloxacin. Additionally, to demonstrate that the antibiotic effect found for **S5-Levo** was due to the release of levofloxacin in the presence of *E. coli*, similar experiments were carried out with a MBG support also capped with ε-poly-L-lysine but that did not contain levofloxacin (solid **S5**). This solid showed negligible toxicity against bacteria, strongly suggesting that the delivery

of antibiotic levofloxacin from **S5-Levo** was the responsible for bacterial death. Moreover, in a further experiment the toxicity of solid **S5-Levo** was compared to that of free levofloxacin and free ε-poly-L-lysine. As depicted in **Figure 3.2.11**, levofloxacin and ε-poly-L-lysine showed similar toxicity to *E. coli* with EC_{50} values of 151.99 ng·mL^{-1} and 131.37 ng·mL^{-1}, respectively. This is a remarkable result that indicated that levofloxacin is seven-fold more toxic when entrapped in **S5-Levo** than when free.

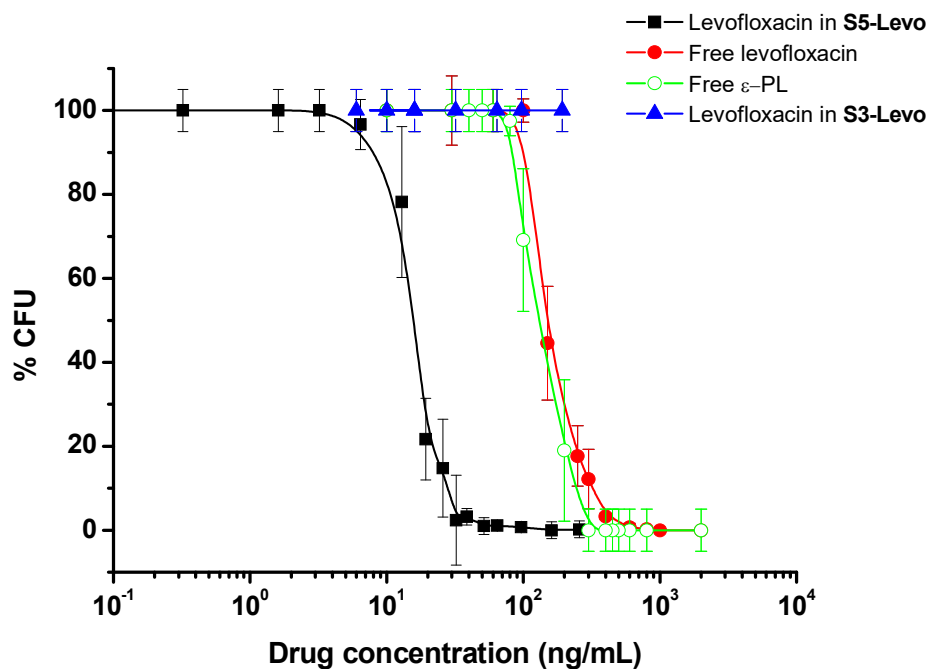**Figure 3.2.11.** Free levofloxacin (solid circles), free ε-poly-L-lysine (open circles), equitoxic concentration of levofloxacin in **S5-Levo** (solid squares) and equitoxic concentration of levofloxacin in **S3-Levo** (solid triangles) versus % CFU.

The toxic effect observed for **S5-Levo** described above against *E. coli* can be understood keeping in mind that ε-poly-L-lysine molecules can be

hydrolyzed by proteolytic enzymes excreted by the bacteria[211] which would result in levofloxacin delivery. In order to demonstrate that protease activity of *E. coli* was the responsible of the release of levofloxacin via degradation of the ε-poly-L-lysine cap, parallel experiments were performed with solid **S3-Levo**. This is a MBG support loaded with the antibiotic levofloxacin and capped with the ATP gate-like ensemble described above. As the ATP gate cannot be degraded by proteases, it was expected that this solid would not be toxic for *E. coli*. The antimicrobial activity of solid **S3-Levo** was studied following a similar protocol to that described above for **S5-Levo**. However, in this case, no remarkable toxicity to *E. coli* was found after treating bacteria with **S3-Levo** and no levofloxacin delivery was observed.

3.2.5 Conclusions

In conclusion, it has been demonstrated that MBGs can be functionalized with tailored molecular gates, allowing a new application as controlled delivery device. Specifically, two different solids were prepared from a MBG selected as an inorganic support. One portion was functionalized with a triamine and capped with ATP, whereas the other portion was functionalized with isocyanates and capped with ε-poly-L-lysine. Solids following each step were correspondingly characterized, finding evidence of their correct functionalization with the tailored molecular gates. Both molecular gated mechanisms were proved to be opened, in the presence of the corresponding enzymes (ALP and pronase, respectively), while they remained closed in the absence of stimuli. Moreover, we have demonstrated the different bioactive behavior in both gated solids. Whereas ε-poly-L-lysine-capped system allows the formation of crystalline hydroxyapatite on their surface under any scenario, the ATP-capped system requires the opening of the molecular gate to initiate the formation of the apatite phase.

---

[211] T. Yoshida, T. Nagasawa, *Appl. Microbiol. Biotechnol.*, **2003**, *62,* 21–26.

Finally, the *in vitro* efficiency of both gated systems was validated. The ATP-capped system responds to the presence of high levels of ALP, opening the gates and releasing doxorubicin. Higher serum ALP levels are found in patients developing osteosarcoma and our ATP-capped system has demonstrated to inhibit HOS cells proliferation under a similar scenario. Regarding the ε-poly-L-lysine-capped system, we demonstrated that the presence of *E.coli* bacteria was also able to hydrolyze the ε-poly-L-lysine gate, allowing levofloxacin release. Therefore, we also tested the cytotoxic effect of the solid, and demonstrated that equitoxic concentration of the levofloxacin contained in the solid was more effective against bacteria than free levofloxacin and free ε-poly-L-lysine. We also proved that the capped solid performed no cellular damage when there was no levofloxacin inside the pores, which evidences that the cytotoxicity is totally caused by the released levofloxacin.

Thus, we have envisioned here a new approach gated MBGs, which is expected to set up innovative pathways to the treatment of bone diseases.

3.2.6 Contribution statement

The presented work is the result of a collaboration between the group of professor Ramón Martínez-Máñez, in Universidad Politècnica de València, and the group of professor María Vallet-Regí, in Universidad Complutense de Madrid. The group of prof. Vallet-Regí performed the synthesis of the mesoporous bioglass, IR, solid state NMR and thermogravimetric analysis, bioactivity and cell viability studies. Specifically, I contributed in preparation of the gated materials from raw MBG, in characterization techniques (TEM, PDRX), in controlled release experiments, and in the validation of **S5-Levo** with bacteria.

3.3 Mesoporous bioactive glasses equipped with stimuli-responsive molecular gates for the controlled delivery of levofloxacin

3.3.1 Introduction

As previously explained, bone diseases have gained importance over the last years due to the ageing of population. Incidence of illnesses like osteoporosis, bone tumors and bone fractures is remarkably higher in elderly patients, due to the age-related loss and weakening of the bone tissue.[212] As stated in the **Introduction**, the treatment of these kind of diseases usually implies the use of implants and bone prosthesis; however, surgical procedures are not always infallible, since they can result in other medical complications.[213,214] Currently, bacterial infection is one of the most recurrent problems related to implant surgery.[215] The creation of a bacterial biofilm on the surface of the implant requires many times its removal and lead to healing difficulties, lowering the life-quality of the patients.[216] Therefore, the need of new therapies and devices for the treatment of these diseases has led to arise the development of innovative biomaterials for bone tissue engineering.[217,218] As it has been seen in the previous section **3.2**, mesoporous bioactive glasses are promising and innovative silica-based bioceramics which have a meaningful significance in bone tissue engineering field due to their excellent properties.[219,220,221] These

---

[212] R. Bernabei, A.M. Martone, E. Ortolani, F. Landi, E. Marzetti, *Clin. Cases Miner. Bone Metab.*, **2014**, *11*, 201.

[213] J. Li, H.-L. Wang, *Implant Dent.*, **2008**, *17*, 389.

[214] A. S. Herford, J. S. Dean, *Oral Maxillofac. Surg. Clin. North Am.*, **2011**, *23*, 433.

[215] C. R. Arciola, L. Visai, F. Testoni, S. Arciola, D. Campoccia, P. Speziale, L. Montanaro, *Int. J. Artif. Organs*, **2011**, *34*, 771.

[216] J. A. Inzana, E. M. Schwarz, S. L. Kates, H. A. Awad, *Bone*, **2015**, *72*, 128.

[217] L.-C. Gerhardt, A. R. Boccaccini, *Materials (Basel),* **2010**, *3*, 3867.

[218] F. Baino, G. Novajra and C. Vitale-Brovarone, *Front. Bioeng. Biotechnol.*, **2015**, *3*, 202.

[219] L. L. Hench, *Science*, **1980**, *208*, 826.

[220] C. Argyo, V. Weiss, C. Bräuchle, T. Bein, *Chem. Mater.*, **2014**, *26*, 435.

materials are biocompatible and resorbable, and are able to integrate living bone in a physiological environment.[222] Moreover, they have an excellent bioactive behaviour, since the contact of the material with physiological fluids can promote the formation of hydroxyapatite on the surface of the implant.

Apart from that, their mesoporous structure gives them special surface features,[223] and converts them suitable to achieve drug delivery of substances.[224,225] Moreover, in the previous section **3.2** it has also been demonstrated that these kind of materials can be equipped with molecular gates, which are usually incorporated in silica matrixes as MCM-41 and mesoporous silica nanoparticles,[226] but very few times have been implemented in mesoporous bioglasses.[227] Despite the relevance of combining the osteoinductive features of mesoporous bioglasses and controlled release characteristics of molecular gates, much effort in the development of this kind of functional biomaterials should be accomplished and applied to a relevant context. In this scenario, the aim of this project is the development of a gated system able to respond specifically to the presence of a stimulus related with bone infection.

For this purpose, a mesoporous bioglass with a different composition of the one studied in the **section 3.2** was used. It had already been demonstrated that

---

[221] X. X. Yan, H. X. Deng, X. H. Huang, G. Q. Lu, S. Z. Qiao, D. Y. Zhao, C. Z. Yu, *J. Non. Cryst. Solids*, **2005**, *351*, 3209.

[222] X. Yan, C. Yu, X. Zhou, J. Tang, D. Zhao, *Angew. Chemie - Int. Ed.*, **2004**, *43*, 5980.

[223] J. R. Jones, *J. Eur. Ceram. Soc.*, **2009**, *29*, 1275.

[224] M. Manzano, M. Vallet-Regí, *J. Mater. Chem.*, **2010**, *20*, 5593.

[225] M. Vallet-Regí, D. Arcos, *Acta Mater.,* **2013**, *61*, 890.

[226] S. Alberti, G. J. A. A. Soler-Illia, O. Azzaroni, *Chem. Commun.*, **2015**, *51*, 6050.

[227] L. Polo, N. Gómez-Cerezo, E. Aznar, J.-L. Vivancos, F. Sancenón, D. Arcos, M. Vallet-Regí, R. Martínez-Máñez, *Acta Biomater.*, **2017**, *50*, 114.

mesoporous bioglasses with a composition of $85\%SiO_2$-$10\%CaO$-$5\%P_2O_5$ could be equipped with molecular gates, but the studies presented in this section demonstrate that also mesoporous bioglasses with other compositions are susceptible to act as controlled release systems.

Thus, $80\%SiO_2$-$15\%CaO$-$5\%P_2O_5$ (% mol) mesoporous bioglass was selected as inorganic support (**S1**). This solid was loaded with levofloxacin and functionalized with 3-[2-(2-aminoethylamino)ethylamino]propyl-trimethoxysilane (N3). The resulting solid (**S2**) was treated with ATP and EDC, achieving the coordination of the ATP phosphates with the polyamines of N3. In this way, ATP molecules were grafted to the surface of the solid, blocking the entrance to the mesopores and keeping the cargo in the pore voids from being released. As occurred in **section 3.2**, ATP molecules would remain intact in a non-pathological scenario, and levofloxacin would continue stored inside the pores of the mesoporous bioglass. However, in the presence of a stimulus as acid phosphatase, ATP molecules would be hydrolyzed, unblocking the surface of the pores and allowing the release of the drug. Acid phosphatase (APase) was selected as stimulus since its concentration significantly increases with osteoclast activity.[228,229] Both osteoblast deposition and osteoclast resorption are two balanced processes which are fundamental for bone regeneration,[230] but the presence of infectious microorganisms as *S.aureus* can enhance osteoclast resorption and lead into bone damage with the subsequent increase of acid phosphatase levels.[231] The action mechanism of phosphatase enzymes consists in the cleavage of phosphate bonds. Thus, in a bone infection scenario ATP molecules would be cleaved, unblocking the entrance to the mesopores of the MBG and allowing the release of the drug to the media (**Scheme 3.3.1**).

---

[228] H. Bull, P. G. Murray, D. Thomas, A. M. Fraser, P. N. Nelson, *Mol. Pathol.*, **2002**, *55*, 65.

[229] C. P. Price, A. Kirwan, C. Vader, *Calcif. Tissue Int.*, **1982**, *34*, 285.

[230] L. J. Raggatt, N. C. Partridge, J. Biol. Chem., **2010**, *285*, 25103.

[231] J. A. Wright, S. P. Nair, *Int. J. Med. Microbiol.*, **2010**, *300*, 193.
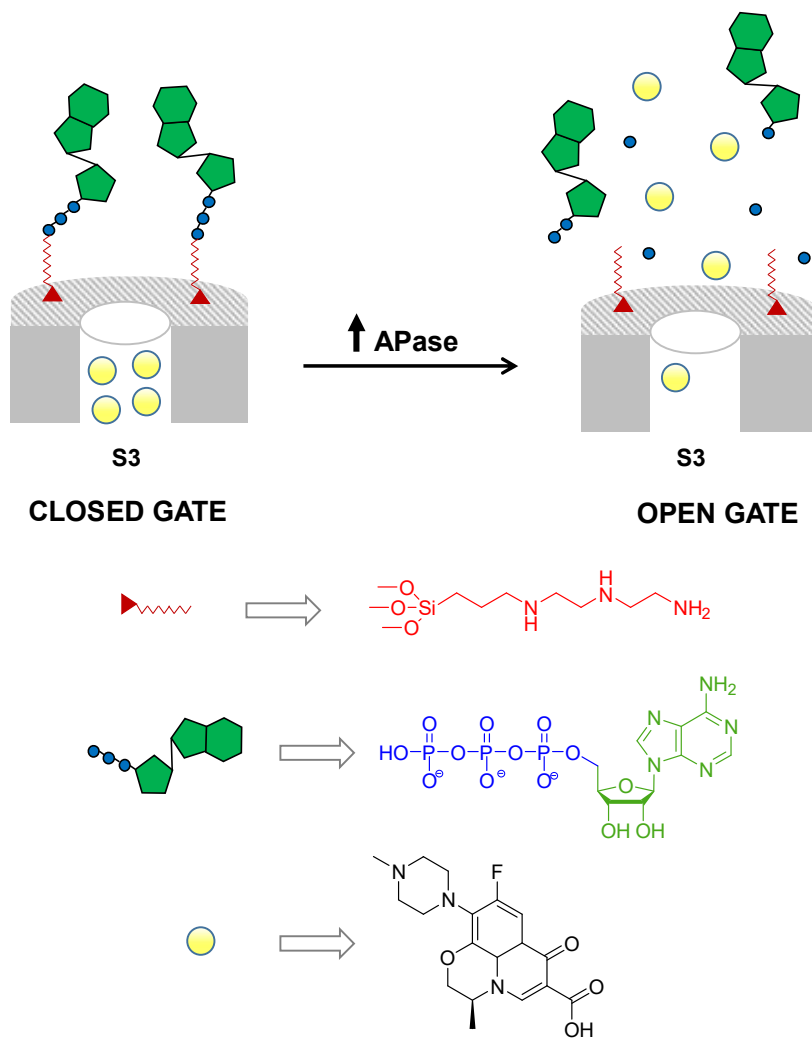
Scheme 3.3.1. Schematic representation of solid **S3** capped with the ATP molecular gates.

3.3.2 Objectives

With these precedents, the objectives of the present project are:

✓ To design, develop and characterize a hybrid enzyme-responsive system based on a MBG with composition of $80\%SiO_2$-$15\%CaO$-$5\%P_2O_5$ (% mol)

109

loaded with an antibiotic and equipped with ATP molecular gates for the treatment of bone infections.

✓ To study the bioactivity of the ATP gated solid.

✓ To validate the ATP-gated system in a bacterial environment.

3.3.3 Synthesis and characterization

As commented previously, the aim of this project was the development of an innovative solid able to encourage bone formation and deliver substances which would treat bone diseases like bacterial infection. For this, the mesoporous bioglass (solid **S1**) was prepared using P123 surfactant (see **Experimental Section**, **5.2** for futher details) by evaporation induced self-assembly method, using SiO_2, $Ca(NO_3)_2 \cdot 4H_2O$ and P_2O_5 as silicon, calcium and phosphorus precursors. After the calcination and the grind of the resultant solid **S1**, it was loaded with levofloxacin and then functionalized with N3 and ATP to yield solids **S2** and **S3**, respectively. Then, the synthesized solids were correspondingly characterized in order to study the presence of the ATP molecular gates, and to demonstrate that the features of the final solid **S3** had not been damaged upon the functionalization and capping processes. A summary of the prepared solids is shown in **Table 3.3.1**.

Table 3.3.1. Summary of the synthesized solids.

Name	Support	Cargo	External Functionalization	Cap
S1	MBG		-	-
S2	MBG	Levofloxacin	N3	-
S3	MBG	Levofloxacin	N3	ATP

In this way, chemical, structural and textural characterization techniques were performed in solids **S1**, **S2** and **S3**. On the first place, it was our aim to

demonstrate that the mesoporous structure of the solids remained unchanged after all the synthesis steps. For this, powder X-ray diffraction patterns were taken. In **Figure 3.3.1**, it can be observed that the powder XRD pattern for **S1** shows a single peak at 1.71 °, that corresponds to a (10) Bragg reflection of a 2D hexagonal p6m structure and is typical of these kind of solids with ordered mesopores. **S2** and **S3** show similar peaks with maximum at 1.71 too, which means that the hexagonal mesoporous structure is maintained. Peaks intensity decreases among loading and capping steps, due to contrast loss in these processes, but the presence of the peak indicates that the mesoporous structure has not been damaged.

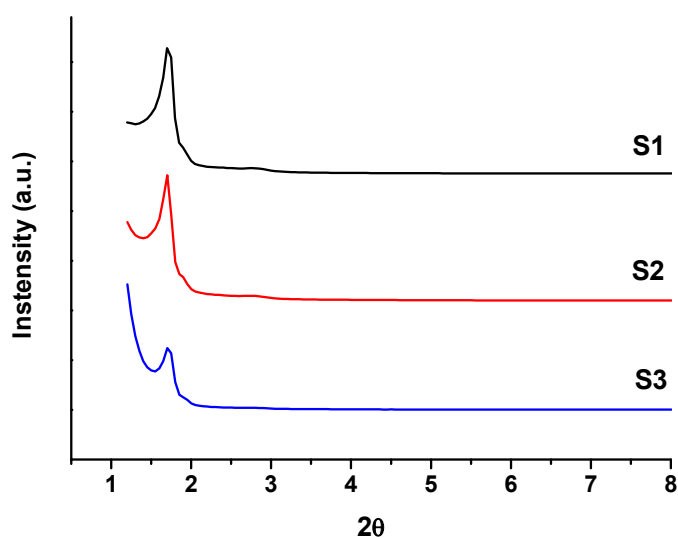**Figure 3.3.1.** Powder X-ray diffraction pattern of solids **S1**, **S2** and **S3**.

In order to support these results and confirm that effectively the pore arrangement in the inorganic matrix does not change during the synthesis of solids **S2** and **S3**, transmission electronic microscopy images of these solids were taken and then compared with those of solid **S1**. Thus, TEM image of **S1**

evidence hexagonal mesoporous structure, showing alternate black and white stripes typical of p6m hexagonal pore symmetry (**Figure 3.3.2**). TEM images of **S2** and **S3** show similar pore arrangement with easily visible mesoporous channels, which effectively demonstrates that the nanoporous structure of the solids was not affected during loading and capping processes.
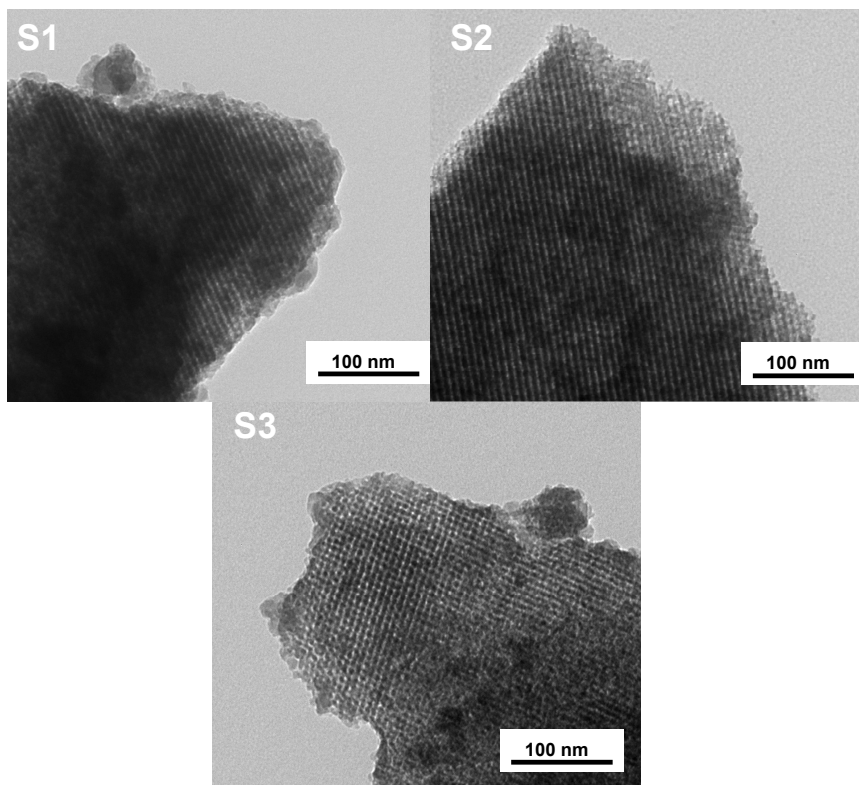

Figure 3.3.2. Transmission electron microscope images of solids **S1**, **S2** and **S3**.

Textural properties of the prepared solids were characterized by N_2 adsorption-desorption studies. In this way, N_2 adsorption-desorption isotherm of non-loaded solid **S1** shows a curve of type IV, typical of mesoporous solids (**Figure 3.3.3**).
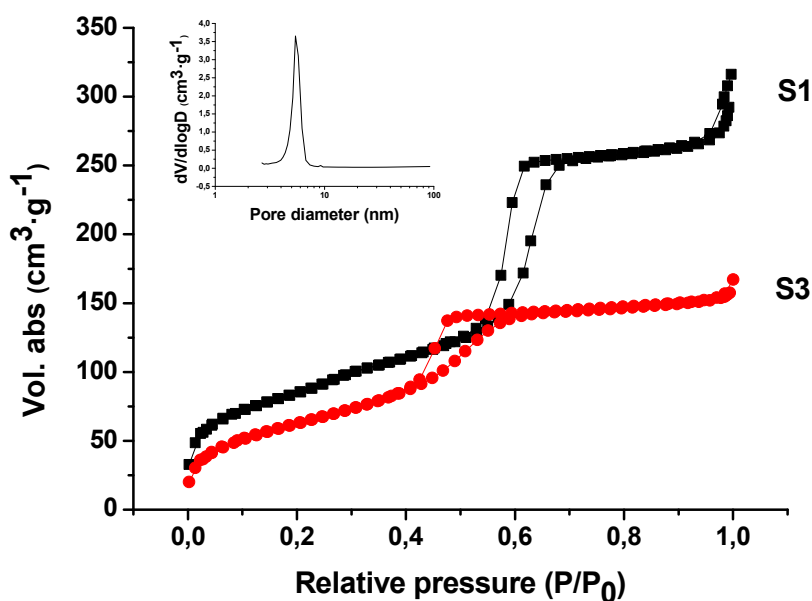
Figure 3.3.3. N_2 adsorption-desorption isotherms for solids **S1** and **S3**.

The curve shows an adsorption step between P/P_0 0.4 and 0.6, due to N_2 condensation inside the empty pores. Moreover, the curve has a H1 hysteresis loop also typical of mesoporous materials, which indicates that mesopores have an opened cylinder morphology. N_2 adsorption-desorption isotherm of **S3** shows a decrease of textural values compared to solid **S1**, which demonstrates that pore volume has decreased due to the loading of the material. Hysteresis loop of the curve changes to type H2, which means that the morphology of the pore has also changed among the loading process, showing an ink-bottle shape according to the capping of the material. Finally, the surface area was determined using the Brunauer-Emmett-Teller (BET)[232]

---

[232] S. Brunauer, P.H. Emmett and E. Teller, *J. Am. Chem. Soc.*, **1938***, 60*, 309.

method, and pore size distribution was determined from the adsorption branch of the isotherm by means of the Barret-Joyner-Halenda (BJH)[233] method. Textural parameters values of **S1** and **S3** are summarized in **Table 3.3.2**. As observed, non-loaded solid **S1** shows BET surface and pore volume compared with loaded-solid **S3**. BET surface and pore volume and size values decrease when loading the material with levofloxacin, which is consistent with the proposed design.

Table 3.3.2. Textural parameters of solids **S1** and **S3**.

Solid	BET surface $(m^2 \cdot g^{-1})$	Pore Volume $(cm^3 \cdot g^{-1})$	Pore size (nm)
S1	305.50	0.386	5.5
S3	233.98	0.210	3.9

Apart from that, thermogravimetric analysis was performed in solid **S3** in order to determine the amount of N3 and ATP attached to the surface of the material. Results are shown in **Table 3.3.3**. Moreover, the amount of levofloxacin into the pores was determined by fluorescence with a calibration curve. For this, different dilutions of levofloxacin in water at pH 7.6 were measured by fluorescence spectroscopy (λ_{ex} 292 nm, λ_{em} 494 nm) to construct the calibration curve. Then, 10 mg of solid **S3** were treated with APase and the solid allows to release the cargo for 24 hours. From the fluorescence calibration curve it was determined that the amount of levofloxacin was 2.53 mg per gram of **S3**.

Table 3.3.3. Organic content (α, mmol/g of solid) in solid **S3**.

Solid	α_{levo}	α_{N3}	α_{ATP}
S3	0.007	0.677	0.045

[233] E.P. Barrett, L.G. Joyner, P.P. Halenda, *J. Am. Chem. Soc.*, **1951**, *73*, 373.

3.3.4 Results and discussion

As previously stated, the designed nanodevice is based on the combination of a biocompatible material and a gating mechanism to induce apatite-like formation and controlled drug release at the same time. For this reason, both bioactivity and drug delivery assays have been carried out with solid **S3**. In order to demonstrate that the ATP-capped solid is capable to release payload only in specific scenarios, drug delivery studies have been undertaken in the presence and the absence of acid phosphatase. In a typical experiment, 2 mg of **S3** were suspended in water at pH 7.6 and stirred for 24 hours in the presence and the absence of the stimuli. At given time intervals, fractions of both suspensions were taken and filtrated to remove the solid. Then, drug released from the pore voids was monitored by fluorescence spectroscopy (λ_{ex} 292 nm, λ_{em} 494 nm). Moreover, in order to demonstrate that the opening of the gate was caused by the presence of APase, controlled release experiments were carried out in the presence of other enzymes as amylase and lipase. Drug delivery kinetics of these experiments are shown in **Figure 3.3.4**.
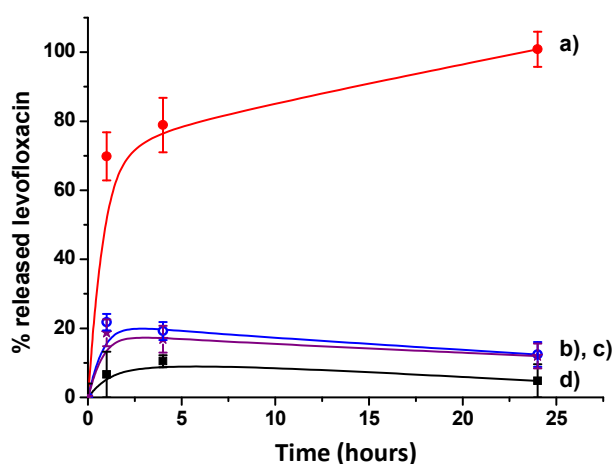

Figure 3.3.4. Delivery kinetics of solid **S3** in the presence of (a) acid phosphatase, (b) amylase, (c) lipase, and in the absence (d) of acid phosphatase.

In the absence of any stimuli, the solid showed negligible release, lower than 20 % of the cargo (d). Contrarily, in the presence of acid phosphatase, remarkable payload of the drug is achieved, reaching 100 % at 24 hours (a). Moreover, in the presence of other enzymes as lipase and amylase, the release of levofloxacin is also negiglible (b, c). These results are consistent with the design of the nanodevice. In the absence of APase, the ATP gates remain closed, blocking the entrance to the pores and avoiding levofloxacin leakage. When acid phosphatase is added to the solid, phosphate bonds of ATP molecules are hydrolysed and pore entrances are unblocked and allow levofloxacin release to the solution. Upon 24 hours, the total hydrolysis of ATP gates is completed and 100 % of the cargo is released from pore voids to the acqueous solution. These results also demonstrate that the presence of other enzymes do not affect the stability of the gate.

These results open up a new approach in the treatment of bone diseases concerning bacterial infection. Acid phosphatase is produced by the organism under non-pathologic conditions, but an abrupt increase of this enzyme is found in situations of bone damage. The high levels of acid phosphatase lead to the opening of the molecular gate and the subsequent release of the therapeutic drug against bacteria only in specific scenarios.

As we have seen in **Section 3.2,** molecular gates provide to mesoporous bioglass the ability to perform controlled drug release, but also imply a certain modification of its textural properties. As bioactivity of MBGs stems from their microstructure, we found that it was also important to check that molecular gates did not harm bioactive capability of the material. Thus, bioactive behaviour of solid **S3** was studied by soaking the material in simulated body fluid (SBF) at 37 °C. As solid **S3** was meant to be useful in the presence of acid phosphatase, the bioactivity test with **S3** was carried on in the absence and the presence of the enzyme in order to study the system with both open and closed gates. Bioactivity of solids was studied by FTIR spectroscopy

to identify the signals corresponding to the presence of phosphate bonds. In addition, field emission scanning microscopy images were taken with the purpose of confirming FTIR results, and EDX analysis was performed in order to study the components of the solids surface before and after the soaking in SBF.

FTIR spectra of **S3** in the presence and the absence of APase at 0 and 72 hours are shown in **Figure 3.3.5**. Non-soaked solid **S3** shows typical Si-O signal at 900-1250 cm^{-1}, and signal in 520-610 cm^{-1} corresponding to the presence of amorphous phosphate bonds. Spectra of **S3** after being soaked for 72 hours in the absence of APase remains unchanged, which could mean that the solid loses its bioactivity when grafted with molecular gates. However, FTIR spectra of solid **S3** in the presence of acid phosphatase shows typical MBG signals, but the splitting of the signal at 560 and 600 cm^{-1} is also clearly observed after 24 and 72 hours of soaking. This splitting demonstrates the presence of P-O bonds corresponding to a crystalline phase, which could be consistent with the formation of apatite.
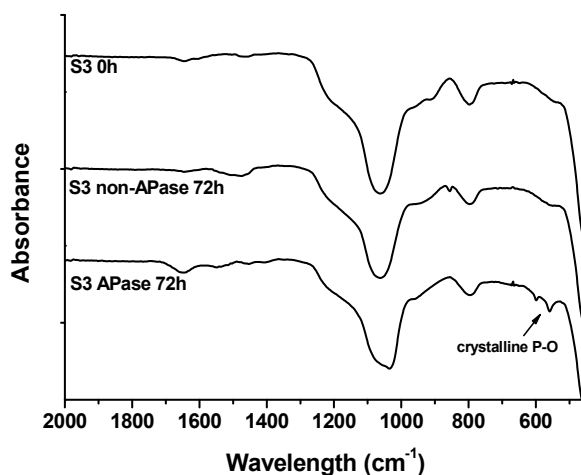

Figure 3.3.5. FTIR spectra of non-soaked **S3**, 72 hours soaked **S3** with no APase, and 72 hours soaked **S3** with APase.

In order to confirm the results given by FTIR spectroscopy, FESEM images of the different treated solids were taken, and EDX analysis of the solids surface was performed. Si, Ca and P percentages are shown in **Table 3.3.3**. Non-soaked solid **S3** showed a neat surface with no apatite (**Figure 3.3.6A**), and **S3** soaked for 72 hours in the absence of APase also presents the same neat surface, with low calcium and phosphor percentages (**Figure 3.3.6B**). Actually, the amount of calcium decreases due to the release of Ca^{2+} ions typical of mesoporous bioglasses. Ca^{2+} release from the material also causes the rise of silicon percentage, while phosphorous amount slightly rises too. These results are consistent with FTIR spectra, which show no crystalline P-O presence and therefore no bioactive behaviour of the solid after the grafting of ATP molecular gates.

However, when **S3** is soaked for 72 hours in the presence of acid phosphatase, a new thick phase is rapidly formed on the surface of the solid (**Figure 3.3.6C**). EDX analysis confirms the high amounts of calcium and phosphorus. Ratio Ca/P was found to be 1.46, which demonstrates the presence of the apatite-like phase. Again, these results are consistent with FTIR spectra, demonstrating that the solid with "open gates" recovers its bioactive properties.
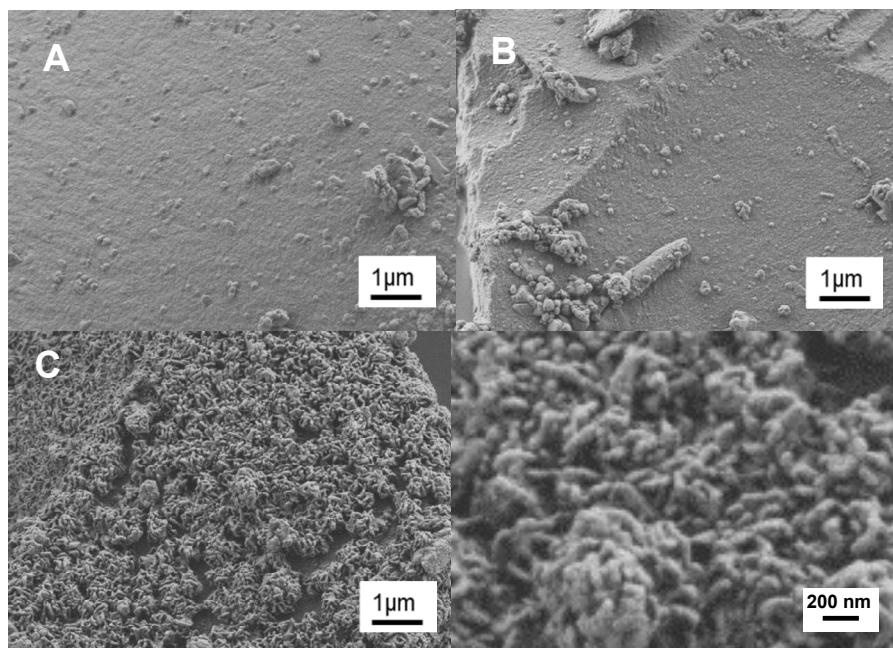
Figure 3.3.6. SEM images of non-soaked **S3** (A), 72 hours soaked **S3** with no APase (B), and 72 hours soaked **S3** with APase (C and D).

Table 3.3.3. EDX results of Si, Ca and P percentages in non-soaked **S3**, 72 hours soaked **S3** with no APase, and 72 hours soaked **S3** with APase.

%	S3 0h	S3 72h	S3-APase 72h
Si	85.37	90.03	75.66
Ca	11.13	6.01	14.46
P	3.50	3.96	9.88

The loss of bioactivity after the incorporation of ATP molecular gates has not been deeply studied in this work. As it was commented in the previous **Section 3.2**, a hypothetical explanation to the non-bioactive behaviour of solid **S3** in the absence of acid phosphatase could be related to the ability of mesoporous bioglasses of releasing Ca^{2+} ions to the media. As stated in

literature,[234] bioactive processes start with the Ca^{2+} leaking from the silica net and undergoing an exchange with H^+ ions. In a physiological media, calcium ions are capable of react with phosphates and form a crystalline apatite layer. Also, it has also been studied that phosphate groups have a high affinity for Ca^{2+} ions.[235] In this context, it is possible that the phosphate net formed by the ATP molecules entraps the Ca^{2+} ions, avoiding the leakage to the media and therefore inhibiting bioactive behaviour. Moreover, the breaking of the phosphate net would allow the entrapped calcium release and would get back bioactive features, which is consistent with results of **S3** in the presence of acid phosphatase. Actually, the release of ATP molecules would rise phosphates concentration in the media, which could also favour the apatite phase formation.

Thus, we found that solid **S3** was not bioactive when capped with the ATP molecular gates. However, once mimicked bacterial infection conditions (with the subsequent increase of acid phosphatase in the media), we found that **S3** bioactivity was restored.

After these two experiments of validation, it is important to remind that the objective of the material was to fight bacteria in a scenario of bone infection. For this, once demonstrated that the controlled-release capabilities were effective and that the bioactive behaviour had not been harmed, bacterial viability assays were carried out with the purpose of demonstrating the bactericide effect of the nanomaterial. Thus, the solid was stirred at 37 °C in the absence and the presence of acid phosphatase for 24 hours. The amount of released levofloxacin was measured in both cases, finding that in the presence of acid phosphatase, the amount of released levofloxacin was maximum, while in the absence of the enzyme, the amount of released levofloxacin was negligible. These results were consistent with prior experiments. Then, two

---

[234] L. L. Hench, *J. Am. Ceram. Soc.,* **1991**, *74*, 1487.

[235] R. Mathew, C. Turdean-Ionescu, B. Stevensson, I. Izquierdo-Barba, A. García, D. Arcos, M. Vallet-Regí, M. Edén, *Chem. Mater.*, **2013**, *25*, 1877.

different *E.coli* suspensions were treated with 50 µL of each sample. Bacteria were stirred for 20 minutes and afterwards 100 µL of each suspension was seeded in an agar plate and incubated at 37 °C. After 24 hours, cell viability was quantified by counting the colonies. As seen in **Figure 3.3.7**, bacteria treated with non-APase suspension showed a viability of 80.41 %, which is remarkably higher than 18.75 % of viability of bacteria when treated with APase suspension. Decreased viability compared with control (100 %) can be due to the residual release of levofloxacin in the absence of acid phosphatase. Moreover, bacteria were also treated with only APase and no significant bacterial death was observed, showing that the bacterial death was due to the presence of released levofloxacin. These results are consistent with the design of the gated support **S3**. In the presence of acid phosphatase, the gated support delivers levofloxacin in a much higher amount that that in the absence of the stimulus. The higher concentration of drug in APase supernatant undertakes higher cell toxicity, demonstrating that the bactericide effect of the solid is only achievable in the presence of an infection marker as acid phosphatase.
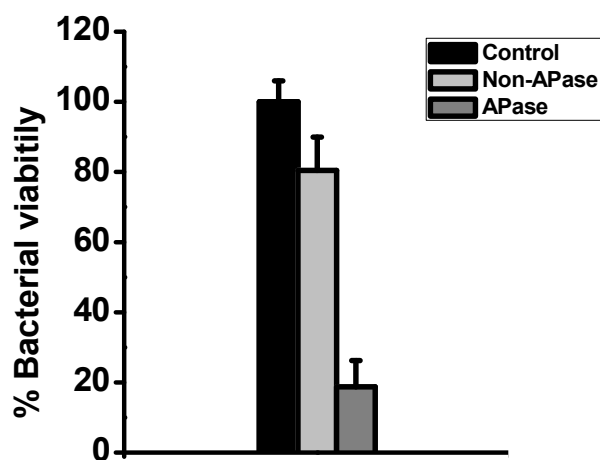

Figure 3.3.7. Bacterial viability of *E.coli* when treated with 50 µL of a suspension of **S3** in the presence and the absence of APase.

Finally, cytotoxicity studies were carried out in order to check that the prepared material was compatible with human cells. For this purpose, U-2 OS human osteosarcoma cells were placed with different amounts (25, 50, 100 and 200 $\mu g \cdot mL^{-1}$) of **S3** during 24 and 48 hours, and mitochondrial activity (WST-1 assays) was measured after these intervals. As depicted in **Figure 3.3.8**, **S3** solid was well-tolerated by U-2 OS cells at concentrations up to 200 $\mu g \cdot mL^{-1}$ after 24 and 48 hours of exposure, which means that the prepared solid does not present a cytotoxic effect. Thus, it has been demonstrated that ATP-gated mesoporous bioglasses are totally biocompatible with human cells, and they are a good strategy for treating bone infection and enhancing bone regeneration without causing any harm to the organism.

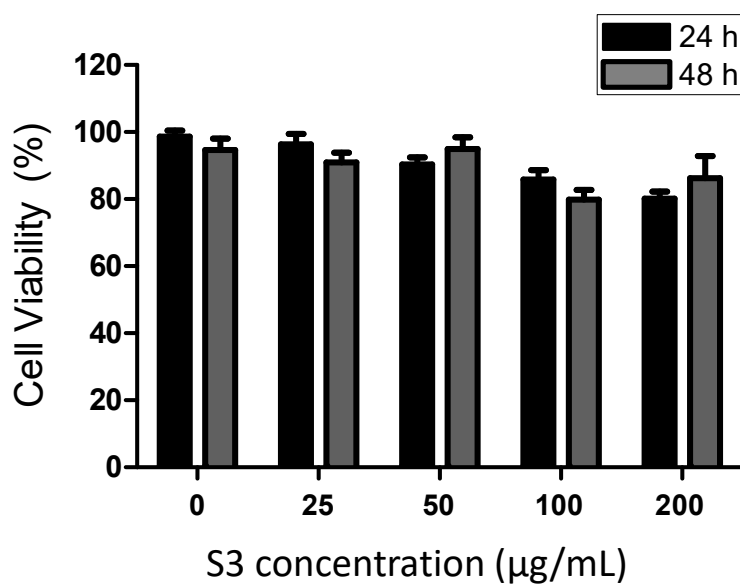**Figure 3.3.8.** Cell viability results in the presence of **S3** (0, 25, 50, 100 and 200 $\mu g \cdot mL^{-1}$) after 24 hours (black) and 48 hours (gray) of incubation. Three independent experiments containing triplicates were carried out. Data are expressed as mean $\pm$ s.e.

3.3.5 Conclusions

In summary, we have developed a double-strategy device which is able to enhance bone regeneration and achieve controlled drug release against bacteria. A mesoporous bioactive glass was loaded with levofloxacin, functionalized with a polyamine, and capped with ATP molecules. The structure of the resulting solids was characterized by standard techniques, demonstrating that the incorporation of molecular gates into MBG did not imply any changes in its textural properties. Then, both drug release capability and bioactive behaviour were tested. Drug release experiments were carried out with the final solid in the presence and the absence of acid phosphatase, and also in the presence of other enzymes as amylase and lipase, observing only a complete release of the drug when acid phosphatase was present. This demonstrates that controlled release is achieved only in the presence of a specific stimulus typical of a bone infection environment. On the other hand, bioactivity studies were carried out with S3 in the presence and the absence of acid phosphatase. Our studies proved that the solid did not have bioactive capabilities when capped with ATP gates, however, it was found that the solid recovered its bioactive behaviour in the presence of the acid phosphatase stimulus. Antibacterial effect of S3 was also studied, and it was demonstrated that solid treated with acid phosphatase was much more effective killing bacteria than the untreated solid. Finally, cytotoxicity studies were carried out with S3, showing that the prepared material was not toxic for U-2 OS human cells upon 24 and 48 hours.

In this way, our double-strategy design has been proved to be successful as a drug delivery system and bone regeneration enhancer. This kind of double-edged nanodispositives opens up a new approach in tissue engineering field, particularly in the treatment of osseous diseases as bone infection.

3.4 Gated mesoporous silica materials for the treatment of bone infection by *Staphylococcus aureus*.

3.4.1 Introduction

Bone complications are one of the most common pathologies nowadays. The prevalence of diseases like osteogenesis imperfecta, osteomyelitis, osteoporosis, osteosarcoma and traumatic injuries has been increased due to the poor healing capability of the bones associated with an advanced age.[236] Various strategies for the treatment of these pathologies have been studied, but these procedures often provoke complications like donor site morbidity, inflammation and long recovery times.[237] To avoid these problems, synthetic materials which could be used as bone replacers were developed during the last century, becoming a goal for researchers who wanted to improve life conditions of patients with bone diseases.[238,239] Today, the implantation of a bone substitutive material like a metallic prosthesis, the use of an orthopedic implant or the refilling of a bone defect with bone cement are common practices which allow the patient recovery without excessive trouble, but there are still some complications which are difficult to deal with.[240]

As it has been stated in the previous sections, one of the most common problems related to the use of bone prosthesis is the relative easiness for developing an infectious process.[241] The presence of bacteria is very common in clinical environments, and they have the ability to remain on the surface of implanted material and infect surgery-derived injuries, leading to a worsening of the patient's life quality and complications in their recovery. Bacteria like *Pseudomonas aeruginosa* and *Staphylococcus epidermidis* are examples of bacteria able to infect bone injuries, but the most frequent microorganism which develops

[236] W. Zimmerli, A. Trampuz, P. E. Ochsner, *N. Engl. J. Med.*, **2004**, *351*, 1645.

[237] J. R. Porter, T. T. Ruckh, K. C. Popat, *Biotechnol. Prog.*, **2009**, *25*, 1539.

[63] N. Eliaz, N. Metoki, *Materials*, **2017**, *10*, 334.

[239] A. K. Nayak, *Int. J. ChemTech Res.*, **2010**, *2*, 903.

[240] J. Li, H.-L. Wang, *Implant Dent.*, **2008**, *17*, 389.

[241] M. Bassetti, F. Ginocchio, M. Mikulska, *Crit. Care*, **2001**, *15*, 215.

bone infection is *Staphylococcus aureus*.[242] As other infectious microorganisms, *S. aureus* is known by its high virulence and easiness to colonize human tissues.[243,244] In order to harm body tissues and enhance their own proliferation, bacteria are able to secrete virulence factors which are able to abolish human defenses and allow the spreading of the infection along the tissues. Particularly, *Staphylococci* are able to secrete up to eight different serine proteases, two cysteine proteases, and one metalloprotease with important roles in the infection process. Thus, staphylococcal proteases are able to inactivate the host's protease inhibitors and antimicrobial peptides,[245,246] degrade immunoglobulins and complement cascade proteins,[247] and, in short, disrupt the body's immunological strategies in order to proliferate and colonize the organism.[248] Moreover, Staphylococci are also able to create a biofilm,[249] which is a thin layer composed by microorganisms that is "constructed" on the surface of materials. This way, bacteria infecting implants and bone substitutes are protected by the biofilm matrix, which also improves their adhesion and proliferation, and even make them resistant to

[242] C. R. Arciola, L. Visai, F. Testoni, S. Arciola, D. Campoccia, P. Speziale, L. Montanaro, *Int. J. Artif. Organs*, **2011**, *34*, 771.

[243] A. Abdelnour, S. Arvidson, T. Bremell, C. Ryden, A. Tarkowski, *Infect. Immun.*, **1993**, *61*, 3879.

[244] L. Shaw, E. Golonka, J. Potempa, S. J. Foster, *Microbiology*, **2004**, *150*, 217.

[245] J. Potempa, W. Watorek, J. Travis, *J. Biol. Chem.*, **1986**, *261*, 14330.

[246] M. Sieprawska-Lupa, P. Mydel, K. Krawczyk, K. Wójcik, M. Puklo, B. Lupa, P. Suder, J. Silberring, M. Reed, J. Pohl, W. Shafer, F. McAleese, T. Foster, J. Travis, J. Potempa, *Antimicrob. Agents Chemother.*, **2004**, *48*, 4673.

[247] F. M. McAleese, E. J. Walsh, M. Sieprawska, J. Potempa, T. J. Foster, *J. Biol. Chem.*, **2001**, *276*, 29969.

[248] G. Dubin, J. Koziel, K. Pyrc, B. Wladyka, J. Potempa, *Curr. Pharm. Des.*, **2013**, *19*, 1090.

[249] N. K. Archer, M. J. Mazaitis, J. W. Costerton, J. G. Leid, M. E. Powers, M. E. Shirtliff, *Virulence*, **2011**, *2*, 445.

several antibiotics.[250] The treatment against bacterial infection and biofilm formation often includes continuous drug administration or even prosthesis replacement, but these remedies are usually expensive and insufficient and may affect the patient's health in the long term.

Apart from that, as stated in the **Introduction Chapter**, ceramic materials have been proved to present meaningful applications in biotechnology and biomedicine. The use of porous materials as substance carriers has been increased in the last years, since the possibility of releasing different cargos as antibiotics, antitumor drugs or growth factors has showed great effectiveness in the treatment of bone diseases.[251] Particularly, MCM-41 type mesoporous silica nanoparticles have been used as an inorganic support for creating controlled release devices showing promising results.[252] Up to now, a number of molecular gates have been designed in order to respond to specific stimuli.

In this project, a new gated-system which specifically recognizes the presence of an infection by *S. aureus* has been designed. MSNs were used as inorganic scaffold, and its pores were loaded with a dye, yielding solid **S1**. Then, the external surface of the loaded solid was functionalized with 3-(azidopropyl)triethoxysilane (solid **S2**) and capped with a designed peptide with the following peptidic sequence: SEEDKGGDESEEDKGGDESEEDKK-pentinoic acid. This sequence was designed in order to be cleaved by the specific activity of *S. aureus* endoproteinase V8,[253] since this protease cleaves specifically peptide bonds on the carboxyl side of aspartic and glutamic acid residues.[254] Finally, the final capped solid was called **S3**. The solid would

---

[250] S. Chihara, J. Segreti, *Disease-a-Month*, **2010**, *56*, 6.

[251] S. Bagherifard, *Mater. Sci. Eng. C*, **2017**, *71*, 1241.

[252] M. Vallet-Regí, A. Rámila, R. P. Del Real, J. Pérez-Pariente, *Chem. Mater.*, **2001**, *13*, 308.

[253] C. Burlak, C. H. Hammer, M. A. Robinson, A. R. Whitney, M. J. Mcgavin, B. N. Kreiswirth, F. R. Deleo, *Cell. Microbiol.*, **2007**, *9*, 1172.

[254] S. Valisena, P. E. Veraldo, G. Satta, *J. Bacteriol.*, **1982**, *151*, 636.

remain capped under normal circumstances, while in the presence of V8 protease, the peptidic sequence would be hydrolyzed and would allow the dye to be released in a local and specific way (**Scheme 3.4.1**). Thus, in this system, the molecular gate remains closed in the absence of infection, while the presence of *S. aureus* and the subsequent secretion of V8 causes the opening of the gate.
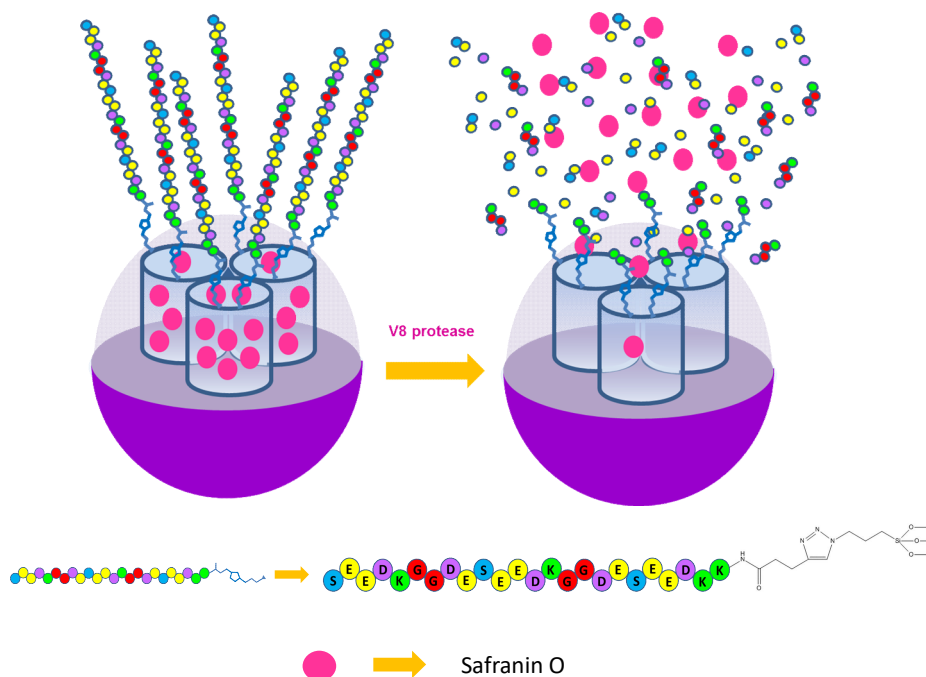
Scheme 3.4.1. Schematic representation of the gated solid **S3**.

3.4.2 Objectives

The objectives of the present project are:

✓ To design of a hybrid enzyme-responsive system based on a mesoporous support equipped with designed peptidic gates for the detection and treatment of bone infections.

✓ To characterize the prepared solids.

✓ To validate *in vitro* the dye-loaded device in the presence and the absence of V8 endoproteinase.

3.4.3 Synthesis and characterization

As stated previously, different solids were prepared in order to study in detail the synthesis and functionality of molecular gates (see **Experimental Section, 5.3** for further explanation). First, MSN were prepared using CTABr as a surfactant and TEOS as a silicon precursor. Then, the mesoporous silica nanoparticles (MSN) were calcined in order to remove the organic surfactant, yielding **S0**, and they were loaded with Safranin O in order to yield solid **S1**. This solid was filtered and dried, and then functionalized with 3-(azidopropyl)triethoxysilane (solid **S2**). Finally, the peptidic sequence was incorporated as a molecular gate by means of Click Chemistry reaction. This procedure is based on the reaction between the azide of 3-(azidopropyl)triethoxysilane and the terminal alkine attached to one of the ends of the peptidic sequence. Thus, the peptide was anchored to the surface of the MSNs yielding final solid **S3**. An explicative scheme of the synthesized solids is showed in **Table 3.4.1**.

Table 3.4.1. Summary of the synthesized solids.

Name	Support	Cargo	External Functionalization	Cap
S0	MCM-41	-	-	-
S1	MCM-41	Safranin O	-	-
S2	MCM-41	Safranin O	Azide	-
S3	MCM-41	Safranin O	Azide	Peptidic sequence

On the first place, our aim was to demonstrate that the mesoporous structure of the original solid was not damaged upon the dye loading, functionalization, and gating processes. For this, different techniques were used for the study of the synthesized solids.

Thus, structure of as-synthesized MSN, calcined nanoparticles (**S0**) and peptide-capped nanoparticles (**S3**) was studied by powder X-ray diffraction and transmission electron microscopy techniques. **Figure 3.4.1** shows the diffraction pattern of as synthesized MSN, calcined nanoparticles (**S0**) and peptide-capped MSN (**S3**). The powder XRD pattern displays typical features of hexagonal ordered mesopores, with characteristic peaks of hexagonal arrangement which can be indexed as (100), (110), (200) and (210) Bragg peaks. A slight displacement of the (100) peak in the XRD pattern of the calcined material is appreciated, which corresponds with cell contraction due to the calcination process. The presence of the mesoporous structure was also confirmed by transmission electronic microscopy (TEM) analysis. In **Figure 3.4.2A** and **3.4.2B**, the typical mesoporous channels as alternate black and white stripes of calcined MSN (**S1**) and peptide-capped MSN (**S3**) can be observed. The images also confirm that the mesoporous structure is not damaged upon the implementation of the molecular gates.
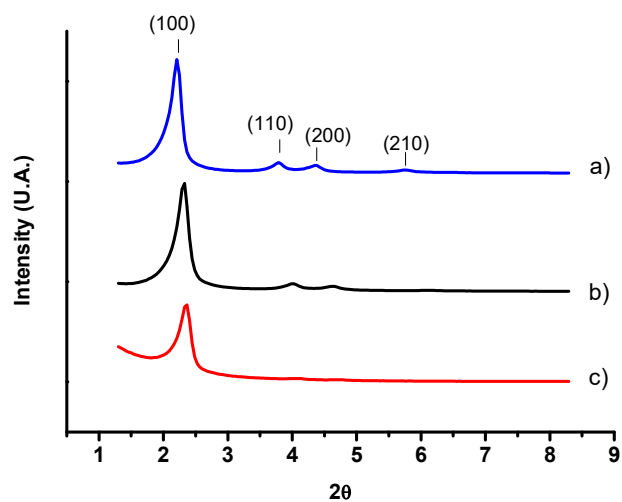
Figure 3.4.1. Powder X-Ray diffraction pattern of as synthesized MSN (a), calcined MSN (b) and peptide-gated MSN (c).
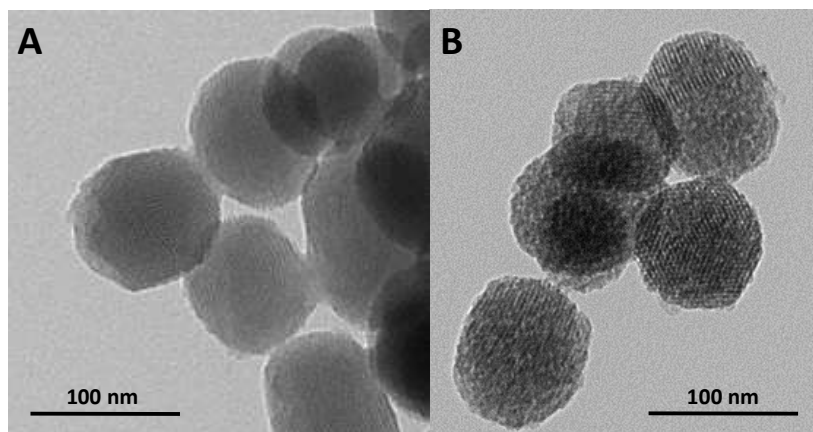

Figure 3.4.2. Representative TEM images of calcined MCM-41 nanoparticles (A) and peptide-capped nanoparticles (B).

Once it was demonstrated that the mesoporous structure did not suffer any changes after the synthesis processes, a further characterization of the loaded and non-loaded solids was needed, in order to compare their textural

parameters as specific surface area, pore volume and pore size. For this, N_2 adsorption-desorption porosimetry was performed on the empty mesoporous support (**S0**) and the dye-loaded and functionalized mesoporous solid (**S3**). The analysis could not be performed on the peptide-gated mesoporous material because of the small amount of synthesized material **S3**.

The N_2 adsorption-desorption isotherms of the empty solid **S0** showed a type IV curve, typical of materials with regular mesoporous channels (**Figure 3.4.3**). In the adsorption curve, it can be observed that the volume of adsorbed N_2 increases from 0 to 0.4 P/P_0, which corresponds to the nitrogen condensation in the mesopore inlets. The desorption process follows the same path in the opposite way, thanks to the uniformity in the pore distribution of the material. The absence of an hysteresis loop indicates the cylindrical uniformity of the mesopores. Contrarily, the N_2 adsorption-desorption isotherm of the loaded solid **S3** shows a very different behavior, showing a negligible increase of adsorbed volume of N2 between 0 and 0.6 P/P_0 due to the nanoparticles loading.
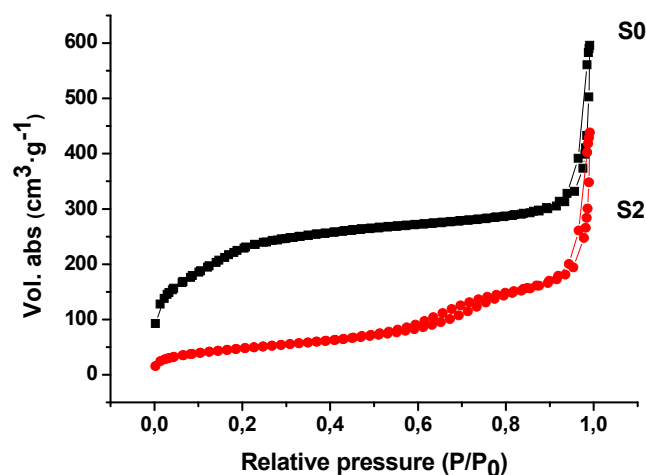

Figure 3.4.3. N_2 adsorption-desorption isotherms for solids **S1** and **S3**.

Furthermore, surface area of both solids were determined using the Brunauer-Emmett-Teller (BET) method,[255] and pore size distribution between 0.5 and 40 nm was determined from the adsorption branch of the isotherm by means of the Barret-Joyner-Halenda (BJH) method.[256] These results are consistent with the designed system: the non-loaded solid has empty pores and thus a bigger specific surface for the nitrogen adsorption, as well as big pore volume and size. On the other hand, the loaded solid presents full pores and lower values of the textural parameters, due to the presence of the dye inside the mesopores (**Table 3.4.2**).

Table 3.4.2. Textural properties of solids **S0 and S1.**

Sample	S_{BET} (m^{2}g^{-1})	Pore volume (cm^{3}g^{-1})	Pore size (nm)
S0	863.08	0.539	2.3
S1	176.48	0.122	-

In a third place, thermogravimetric analysis were performed with solids **S1** and **S2** for the determination of the organic matter contained in each solid, and the quantification of the loading and functionalizing molecules used in each step. Results are shown in **Table 3.4.3**. Data from **S3** could not be evaluated due to the small amount of synthesized solid **S3**.

Table 3.4.3. Organic content (α, mmol/g of SiO$_2$) in solids **S1** and **S2**.

Solid	$\alpha_{safranin}$	α_{azide}
S1	0.292	-
S2	0.292	0.2527

[255] S. Brunauer, P. H. Emmett, E. Teller, *J. Am. Chem. Soc.*, **1938**, *60*, 309.

[256] E. P. Barrett, L. G. Joyner, P. P. Halenda, *J. Am. Chem. Soc.*, **1951**, *73*, 373.

Once the synthesized materials were correspondingly characterized from a structural, textural and chemical point of view, demonstrating the integrity of the solids and the correct implementation of the molecular gates, it was our aim to demonstrate that the designed system was able to perform controlled release of substances.

3.4.4 Results and discussion

Thus, in order to investigate the gating properties of **S3** material, cargo-release studies were carried out in the absence and the presence of endoproteinase V8. For this, a small amount of **S3** was suspended in 200 μL of PBS at pH 7.5 in the absence and the presence of V8 protease. Dye release was measured at given time intervals. Moreover, in order to demonstrate that the gate responded specifically upon proteolytic enzymes, the same experiment was performed in the presence of amylase and lipase enzymes.

Release profiles of these experiments are shown in **Figure 3.4.4**. As observed, a negligible release of safranin O is performed in the absence of V8 protease (curve d), whereas a significant release of the dye is achieved in the presence of the enzyme (curve a). Moreover, in the presence of other enzymes as lipase (b) and amylase (c), the payload remains under the 50 % at both cases. These results are consistent with the designed mechanism: as expected, the entrance of the pores remains blocked by the peptidic sequence under normal conditions, avoiding the leakage of the dye to the solution. However, in the presence of infection by *S. aureus* and its subsequent secretion of V8 protease, the peptide is cleaved and the dye is released. Regarding the other enzymes as amilase and lipase, their presence may have a minimal effect on the peptidic gate, but they are not able to cleave it completely, since the payload of the cargo in the presence of this enzymes is not high.
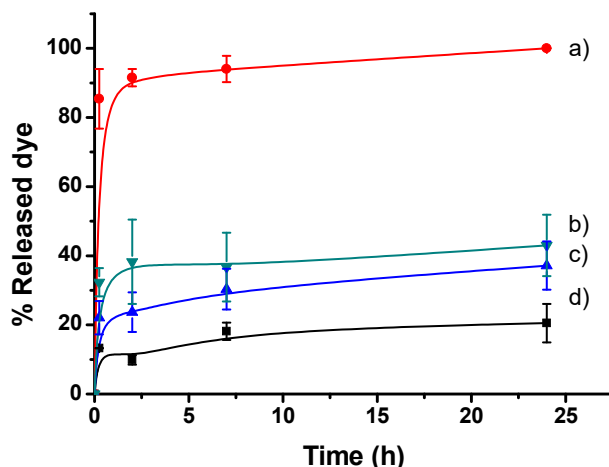
Figure 3.4.4. Dye release studies carried out at 37 ºC in the presence of V8 protease (a), lipase (b), amylase (c), and in the absence of stimuli (d).

Apart from that, our future aims are to validate the system in the presence of the bacteria *S. aureus*, demonstrating the efficacy and selectivity of this molecular-gated device. The next step would be to load the mesoporous support with an antibiotic able to kill *S.aureus*, and then demonstrate that the loaded solid could achieve specific killing in the presence of these bacteria. Thus, this resulting material would be able to perform specific and controlled release of substances in the presence of *S.aureus*-mediated infection, helping to the prevention and treatment of bone infection processes. The preliminary results showed in this chapter show encouraging results regarding the treatment of bone diseases, demonstrating that this kind of gated systems will open up to new approaches for bone infection treatments.

3.4.5 Conclusions

As seen previously, *Staphylococcus aureus* is one of the most common microorganisms present in bone infections. Thus, there was the need of designing a device able to respond specifically to the presence of these

bacteria. As a result, we have synthesized a new enzymatic-responsive gated material for the controlled release of substances in an infection environment. The system is composed of a mesoporous support loaded with a dye and functionalized with 3-(azidopropyl)triethoxysilane. Then, a specific peptide sequence has been attached to the surface of the material, in order to cap the pores and avoid the release of the cargo under normal conditions. The peptidic sequence, SEEDKGGDESEEDKGGDESEEDKK-pentinoic acid, is designed specifically to be cleaved on the carboxyl side of aspartic and glutamic acid residues by the action of V8 protease. For this reason, the gated system is expected to open only in the presence of this specific protease.

Moreover, this system has been correspondingly characterized from a structural point of view, demonstrating that the inner structure and properties of the raw materials were not modified upon the loading, functionalization and gating processes. Textural analysis has also been performed in order to study the textural parameters of the solids, and thermogravimetric analysis was performed in order to determine the degree of loading and characterization. Finally, it has been demonstrated that, effectively, the designed material was able to perform the controlled release of the dye only in the presence of V8 protease.

4. Functionalization of calcium phosphates for the prevention of bone infection

4.1 Introduction

This chapter is devoted to the design of new-functionalized calcium phosphates for the treatment and prevention of infection in bone. The results are reported in the publication entitled "Antimicrobial activity of commercial calcium phosphate functionalized with vanillin". Herein, a calcium phosphate material is treated with an essential oil component derivative in order to achieve antimicrobial properties. Then, biological validation of the material is performed.

The interest of this work resides in the double strategy to perform both antibacterial and regenerative activities. The fact of being coated with an antimicrobial molecule provided the material with antibiotic properties, but it was also important to determine if those materials were still compatible with human body and effective for bone regenerative processes. For this, *in vitro* experiments with two different cells lines were carried out, in order to check cell cytotoxicity in the presence of the materials, and in order to study the ability of cells to attach to the surface of the material and perform regenerative processes.

4.2 Antimicrobial activity of commercial calcium phosphate based materials functionalized with vanillin

This chapter is derived from the adaptation of the following manuscript: Lorena Polo, Borja Díaz de Greñu, Elena Della Bella, Stefania Pagani, Paola Torricelli, José Luis Vivancos, María Ruiz-Rico, José M. Barat, Félix Sancenón, Ramón Martínez-Máñez, Milena Fini, and Elena Aznar, *Acta Biomaterialia*, submitted.

4.2.1 Introduction

Over the last years the use of regenerative medicine to recover bulk and functionality of damaged tissues in trauma, large resections following primitive tumors or metastases, congenital defects, malformations or infections is increased. In particular, as it has been seen along this PhD thesis, bioceramics have been extensively studied and a great number of ceramic-based devices have been commercialized due to their suitability as bone substitutes or prosthesis coating.[257,258] Among these ceramic-based devices, calcium phosphates (CaP) have become essential in fields as orthopaedics and dentistry, and have been used in developing different types of prosthesis surfaces and bone cements for bone defects filling. The main reason for their suitability as bone grafts is their huge similarity to bone matrix, which is formed in a 60% by calcium phosphate.[259,260] Several different CaP compositions can be found in the surgery market nowadays; however, this project is centred in the use of composites of β-tricalcium phosphate (β-$Ca_3(PO_4)_2$) and hydroxyapatite ($Ca_{10}(PO_4)_6(OH)_2$). These materials have been proved to show good biocompatibility, bioactivity, and biodegradability.[261,262,263] Biocompatibility is a fundamental characteristic in surgical materials, since it is the ability to be implanted without eliciting a negative response from the host body. Lack of toxicity of calcium phosphates has been extensively tested.[264]

[257] S. Oh, N. Oh, M. Appleford, J. L. Ong, *Am. J. Biochem. Biotechnol.*, **2006**, *2*, 49–56.

[258] L. L. Hench, I. Thompson, *J. R. Soc. Interface*, **2010**, *7*, 379-91.

[259] J. Ferguson, M. Diefenbeck, M. McNally, *J. Bone Jt. Infect.*, **2017**, *2*, 38–51.

[260] F. Baino, G. Novajra, C. Vitale-Brovarone, *Front. Bioeng. Biotechnol.*, **2015**, *3*.

[261] V. Uskoković, V. M. Wu, *Materials (Basel)*, **2016**, *9*, 434.

[63] N. Eliaz, N. Metoki, Materials (Basel), **2017**, *10*, 334.

[263] V. S. Kattimani, S. Kondaka, K. P. Lingamaneni, *Bone Tissue Regen. Insights*, **2016**, *7*, 9–19.

[264] A.H. Choi, B. Ben-Nissan, R.C. Conway, I.J. Macha, in: Besim Ben-Nissan (Eds.) Advances in Calcium Phosphate Biomaterials. Springer Series in Biomaterials Science and Engineering, vol 2. Springer, Berlin, Heidelberg, **2014**, pp. 489-509.

Moreover, these materials have proved to perform high bioactivity, which means that are able to participate in specific biological reactions which help the bone to regenerate.[265] CaP supports are also able to release ionic products, when implanted into the body, that reacted with the phosphates present in a physiological environment allowing the formation of an apatite-like phase on the surface of the implant.[266,267]

The real potential of CaP materials arise from their osteoconductive, osteointegrative and osteoinductive capabilities.[268] Moreover, biodegradability of surgical devices is also important, since the progressive solution of these materials avoids the necessity of performing a second intervention to remove the graft.[269] However, as well as all types of implant, even CaP shows some drawbacks. The surgery needed for the collocation of bone graft or prosthesis can lead to site morbidity and excessive inflammation, but often the major problem of these type of surgical interventions is the apparition of bone infections caused by pathogenic microorganisms found on the surface of the implants.[270] Actually, septic failure is the second most frequent cause of prosthetic failure *(18.4%).*[271] As seen previously, bacteria are able to replicate and create a biofilm on the material's surface, which makes them resistant to

---

[265] K. de Groot, J. G. C. Wolke, J. A. Jansen, *Proc. Inst. Mech. Eng. Part H J. Eng. Med.*, **1998**, *212*, 137–147.

[266] Q. Liu, S. Huang, J. P. Matinlinna, Z. Chen, H. Pan, *Biomed Res. Int.*, **2013**, 2013.

[267] R. Z. LeGeros, *Clin. Mater.*, **1993**, *14*, 65–88.

[268] H. Yuan, Z. Yang, Y. Li, X. Zhang, J. D. De Bruijn, K. De Groot, *J. Mater. Sci. Mater. Med.*, **1998**, *9*, 723–726.

[269] F. C. J. van de Watering, J. J. J. P. van den Beucken, R. P. F. Lanao, J. G. C. Wolke, J. A. Jansen, in ed. N. Eliaz, Springer New York, New York, **2012**, pp. 139–172.

[270] J. Esteban, J. Cordero-Ampuero, *Expert Opin. Pharmacother.*, **2011**, *12*, 899–912.

[271] W. Healy, C. Della, R. Iorio, K. Berend, F. Cushner, D. Dalury, J. Lonner, *Clin. Orthop. Relat. Res.,* **2013***, 471*, 215-220.

diverse antibiotics and hinders healing during the post-operative process.[272] For this reason, during the last years, the development of new bioceramics with antimicrobial properties against the development of bone infection processes has increased in interest.[273,274]

In the context of antibacterial substances, numerous antibiotic drugs have been developed and tested. Though oral administration may be a good solution for antibacterial treatment, high doses of drug are required and this can lead to antibiotic resistance or renal and liver complications.[275] For this reason, both drug delivery devices and antibacterial surfaces are being largely developed, with the purpose of achieve a local action of the drugs.[276] Apart from antibiotics, other substances are being studied as antimicrobial strategies in order to avoid secondary effects of some drugs. In this context, essential oil components (EOCs) have been found to present antimicrobial activity.[277] These products are naturally synthesized by plants, are fragrant and volatile, and have been demonstrated to possess antimicrobial, antifungal, antiviral, insecticidal and antioxidant activity.[278,279,280] Particularly, it has been studied that

[272] C. R. Arciola, L. Visai, F. Testoni, S. Arciola, D. Campoccia, P. Speziale, L. Montanaro, *Int. J. Artif. Organs*, **2011**, *34*, 771–780.

[273] N. Mas, I. Galiana, S. Hurtado, L. Mondragón, A. Bernardos, F. Sancenón, M. D. Marcos, P. Amorós, N. Abril-Utrillas, R. Martínez-Máñez and J. R. Murguía, *Int. J. Nanomedicine*, **2014**, *9*, 2597–2606.

[274] L. Polo, N. Gómez-Cerezo, E. Aznar, J.-L. Vivancos, F. Sancenón, D. Arcos, M. Vallet-Regí, R. Martínez-Máñez, *Acta Biomater.*, **2017**, *50*, 114–126.

[275] S. Bagherifard, *Mater. Sci. Eng. C*, **2017**, *71*, 1241–1252.

[276] N. Mas, D. Arcos, L. Polo, E. Aznar, S. Sánchez-Salcedo, F. Sancenón, A. García, M. D. Marcos, A. Baeza, M. Vallet-Regí, R. Martínez-Máñez, *Small*, **2014**, *10*, 4859–4864.

[277] I. A. Freires, C. Denny, B. Benso, S. M. De Alencar, P. L. Rosalen, *Molecules*, **2015**, *20*, 7329–7358.

[278] I. H. N. Bassolé, H. R. Juliani, Molecules, **2012**, *17*, 3989–4006.

[279] S. Burt, *Int. J. Food Microbiol.*, **2004**, *94*, 223–253.

their antimicrobial activity is due to the presence of hydroxyl moieties, which can interact with cellular membrane and augments its permeability, causing pH destabilization and membrane disruption.[281,282] Thanks to these properties, EOCs (as carvacrol, eugenol, thymol, vanillin or cinnamaldehyde) have been widely used in food and pharmacologic industry. However, their high volatility and strong odor makes them difficult to apply in therapeutic fields.[283] For this reason, several studies have been carried out in order to attach essential oils to specific surfaces and to enhance and prolong their antimicrobial effect.[284,285]

Taking into account the above mentioned facts, in this project, a commercial bone-regenerative material was coated with an essential-oil derivative molecule in order to combine its original bone regeneration properties with antimicrobial action of EOCs. For this purpose, commercially available (Surgibone©) CaP microparticles in powder (**Pw**) and blocks with the form of scaffolds (**Sc**) were used as supports. Then, vanillin was used as antimicrobial compound and grafted onto the surface of the selected scaffolds (see **Scheme 4.2.1**). Functionalized materials were characterized by field emission scanning electronic microscopy (FESEM) and thermogravimetric analysis. Also, the antimicrobial behavior of the prepared materials was assessed using clonogenic viability tests against *E.coli DH5a* bacteria. Finally,

[280] Z. E. Suntres, J. Coccimiglio, M. Alipour, *Crit. Rev. Food Sci. Nutr.*, **2015**, *55*, 304–318.

[281] A. Rao, Y. Zhang, S. Muend, R. Rao, *Antimicrob. Agents Chemother.*, **2010**, *54*, 5062–5069.

[282] A. Ahmad, A. Khan, F. Akhtar, S. Yousuf, I. Xess, L. A. Khan, N. Manzoor, *Eur. J. Clin. Microbiol. Infect. Dis.*, **2011**, *30*, 41–50.

[283] D. J. Fitzgerald, M. Stratford, M. J. Gasson, J. Ueckert, A. Bos, A. Narbad, *J. Appl. Microbiol.*, **2004**, *97*, 104–113.

[284] M. Ruiz-Rico, É. Pérez-Esteve, A. Bernardos, F. Sancenón, R. Martínez-Máñez, M. D. Marcos, J. M. Barat, *Food Chem.*, **2017**, *233*, 228–236.

[285] S. Ribes, M. Ruiz-Rico, É. Pérez-Esteve, A. Fuentes, P. Talens, R. Martínez-Máñez, J. M. Barat, *Food Control*, **2017**, *81*, 181–188.

biocompatibility assays were carried out for checking that the original bioactive properties of the material were not damaged upon the functionalization process.
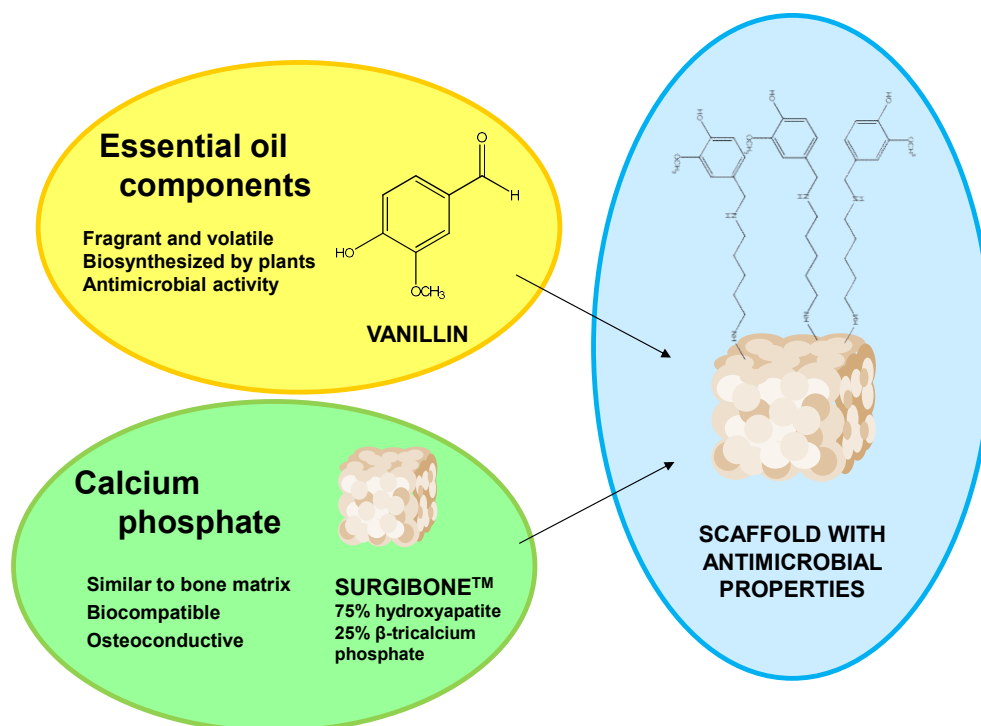
Scheme 4.2.1. Schematic representation of the functionalized scaffold.

4.2.2 Objectives

With these precedents, the objectives of the present project are:

✓ To synthesize and characterize a vanillin-derivated molecule with antimicrobial properties.
✓ To functionalize and characterize the calcium phosphate materials.
✓ To validate the antimicrobial activity of the new materials.
✓ To validate the citocompatibility and bioactivity of the new materials.

4.2.3 Synthesis and characterization

In this project, two different commercially available CaP materials (as powder **Pw** or as scaffold **Sc**) were functionalized with an EOC derived molecule with the purpose to combine bone regenerative capabilities of calcium phosphates with antimicrobial activity of essential oil components. For this, vanillin (**1**) was selected as an EOC due to its well-known antimicrobial activity, and then was properly derivatized with a diamine (**2**) to yield the modified-vanillin product (**3**) in order to achieve its grafting onto the external surface of the materials to obtain **Pw-3** and **Sc-3**. Moreover, diamine-functionalized scaffolds (**Sc-2**) were also synthesized for comparative purposes.

Thus, vanillin (**1** in **Scheme 4.2.2**) was derivatized using a two-step protocol shown in **Scheme 4.2.2** (see **Experimental Section**, **5.4** for more details). In a first step, vanillin was reacted with 1,5-pentanediamine (**2**) yielding the corresponding Schiff base. [286,287] As it is known, Schiff bases are not stable in an aqueous environment due to their imine bond, so that a reduction reaction was needed. Thus, in a second step, the imine bond of the Schiff base was reduced with sodium borohydride, and vanillin derivative 4-{[(3-aminopentyl)amino]methyl}-2-methoxyphenol (compound **3**) was yielded. As it can be observed, one of the two primary amines of the 1, 5-pentanediamine has become a secondary amine, but there is still one primary amine moiety that allows the grafting of this compound onto the CaP supports.

---

[286] E. H. Cordes, W. P. Jencks, *J. Am. Chem. Soc.*, **1962**, *84*, 832–837.

[287] J. Billman, A. Diesing, *J. Org. Chem.*, **1957**, *22*, 1068–1070.
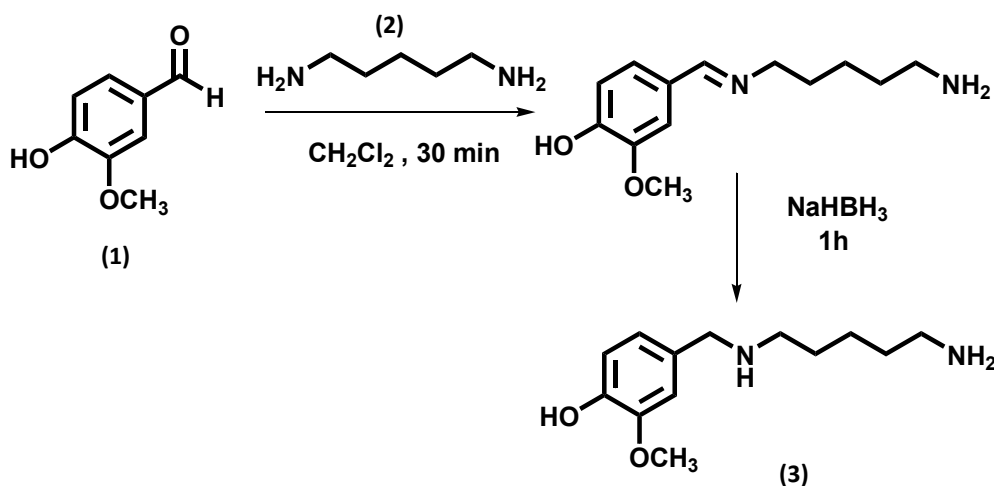
Scheme 4.2.2. Synthetic protocol used to prepare vanillin derivative **3**.

In order to check the suitability of compound **3** to be grafted onto the surface of the CaP materials, this compound was fully characterized using ^{1}H, ^{13}C-NMR and HRMS, and the following data were obtained:

^{1}H-NMR (MeOD): δ = 6.8 (1H, s); 6.62 (2H, s); 3.72 (3H, s); 3.52 (2H, m); 2.63-2.35 (4H, m); 1.46-1,30 (4H, m), 1.28-1.18 (2H, m).

^{13}C-NMR (MeOD): δ = 149.11 (1C); 147.14 (1C), 131.59; 122.41; 116.10; 113.29; 65.33; 56.33, 54.27; 42.16; 32.89; 30.05; 25.66.

HRMS, calculated for $C_{13}H_{22}N_2O_2$ was 238.1681, and found 239.1754 (M+H$^+$).

These results are consistent with the structure and molecular weight of **3**, which evidences that the reaction was successfully performed and the desired component was obtained.

Once characterization techniques were performed on vanillin derivative **3** in order to verify its composition and structure, CaP powder microparticles (**Pw**) and scaffolds (**Sc**) were finally functionalized with this compound through

phosphoramidate formation using N'-ethylcarbodiimide hydrochloride (EDC) as coupling agent. This procedure yielded solids **Pw-3** and **Sc-3**. Besides, **Sc** support was also functionalized, using EDC, with 1,5-pentanodiamine (compound **2**) for comparative purposes (**Sc-2** material). **Table 4.2.1** shows the five materials used in this project.

Table 4.2.1. Summary of the solids used in this project.

Name	Inorganic support	Organic attachment
Pw	CaP powder	-
Pw-3	CaP powder	**3**[a]
Sc	CaP scaffold	-
Sc-2	CaP scaffold	**2**[b]
Sc-3	CaP scaffold	**3**[a]

[a] Derivatized vanillin.
[b] 1, 5 pentanediamine.

The prepared materials were fully characterized using typical techniques for smart materials characterization[288,289,290] such as thermogravimetric analysis (TGA) and field emission scanning electronic microscopy (FESEM). TGA analysis of solids **Pw-3**, **Sc-2** and **Sc-3** were carried out in order to assess the organic matter anchored onto their surface (see **Table 4.2.2**). The obtained thermogravimetric curves presented three different steps. The first step, from 0

[288] A. Agostini, L. Mondragõn, A. Bernardos, R. Martínez-Máñez, M. Dolores Marcos, F. Sancenón, J. Soto, A. Costero, C. Manguan-García, R. Perona, M. Moreno-Torres, R. Aparicio-Sanchis and J. R. Murguía, *Angew. Chemie - Int. Ed.*, **2012**, *51*, 10556–10560.

[289] C. De La Torre, I. Casanova, G. Acosta, C. Coll, M. J. Moreno, F. Albericio, E. Aznar, R. Mangues, M. Royo, F. Sancenón, R. Martínez-Máñez, *Adv. Funct. Mater.*, **2015**, *25*, 687–695.

[290] À. Ribes, E. Xifré-Pérez, E. Aznar, F. Sancenón, T. Pardo, L. F. Marsal, R. Martínez-Máñez, Sci. Rep., **2016**, *6*.

to 100 °C, corresponds to the loss of adsorbed water or organic solvents. The second step, from 100 °C to 700 °C, quantifies the combustion of organic matter attached to the CaP scaffolds. The last step, from 800 °C to 1000 °C, could be ascribed to a mass loss associated with the hydroxyapatite decomposition into tetracalcium phosphate (TTCP) and α-tricalcium phosphate (αTCP). The higher degree of functionalization was observed for **Pw-3** material (6.86 mg·mg^{-1} of solid) whereas those obtained for **Sc-3** and **Sc-2** were lower and quite similar between them (3.46 and 3.14 mg·mg^{-1} solid respectively). The larger organic matter content of **Pw-3**, when compared to that for **Sc-2** and **Sc-3**, was clearly related with its higher specific surface area due to its microparticulated nature. Also, thermogravimetric studies with raw **Pw** and **Sc** materials were carried out. As expected, thermogravimetric curves of **Pw** and **Sc** only showed the last step related with hydroxyapatite decomposition.

Table 4.2.2. Amount of organic matter before and after the functionalization of different solids.

Material	Pw	Pw-3	Sc	Sc-2	Sc-3
mg·g solid^{-1}	0.078	6.861	1.055	3.136	3.463

Moreover, in order to demonstrate that the surface of the materials did not undergo substantial changes during the functionalization process, FESEM studies were taken. At this respect, FESEM images of **Sc, Sc-2** and **Sc-3** are shown in **Figure 4.2.1**. As observed, all solids present a uniform porous structure typical of CaP materials. Besides, the surface of the materials before and after functionalization with vanillin derivative **3** was quite similar. This fact indicated that functionalization process did not change the structure of the initial raw material.
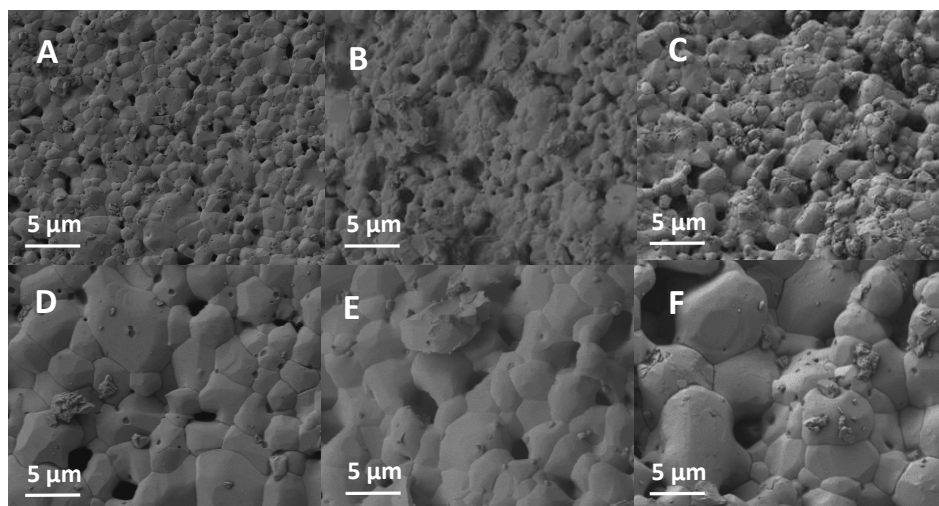
Figure 4.2.1. FESEM images of **Sc**, **Sc-2** and **Sc-3** surfaces.

4.2.4 Results and discussion

After the characterization of the prepared materials, their antimicrobial behaviour against *E.coli* bacteria was tested. For this purpose, solid **Pw-3** was selected and used for the quantification of its dose dependent antibacterial activity. Thus, suspensions of bacteria (10^3 CFU·mL^{-1}) were stirred in the presence of different amounts of **Pw-3**. The suspensions were diluted and seeded and, after 24 hours of incubation, CFU were quantified. The same experiments were carried out with equitoxic concentrations of vanillin derivative **3**, 1,5-pentanediamine (**2**) and free vanillin (**1**), in order to compare the antibacterial activity of each compound. Moreover, bacteria were also treated with different concentrations of non-functionalized microparticles (**Pw**) as a control. The obtained results are shown in **Figure 4.2.2** which shows the decrease on bacterial viability upon the treatment with increasing concentrations of **Pw-3**, **3**, **2** and **1**.

As could be seen in **Figure 4.2.2**, equitoxic concentrations of vanillin derivative **3** attached onto the microparticles surface (solid **Pw-3**) were more

effective in killing *E.coli* bacteria than free vanillin (**1**), free 1,5-pentanediamine (**2**) and free **3**. **Table 4.2.3** showed the EC_{50} (half maximal effective concentration, which represents the amount of drug necessary to achieve 50% of bacterial death) values measured for **1, 2, 3** and **Pw-3**. The less effective compound was vanillin (EC_{50} of 6.33 mg·mL^{-1}) probably due to its volatility. The antibacterial activity of **2** and **3** were quite similar with EC_{50} values of 0.092 and 0.083 mg·mL^{-1} respectively. However, the EC_{50} value measured for **Pw-3** material (0.015 mg·mL^{-1}) was approximately one order or magnitude lower than that measured for free vanillin derivative **3**. This enhanced antibacterial activity of **Pw-3** could be ascribed to a marked reduction in the volatility of derivative **3** upon its grafting onto the surface of the microparticles. Besides, in order to check that the antibacterial activity measured for **Pw-3** was due to the grafted vanillin derivative **3** and not to the solid itself, the same antimicrobial experiments were carried out with **Pw**. These experiments indicated the non-toxicity nature of **Pw** with negligible changes in bacterial viability.
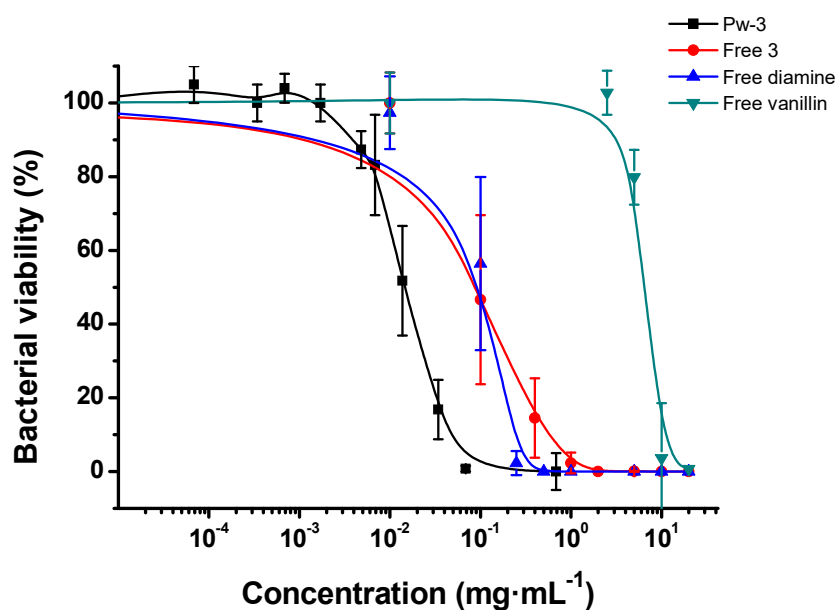
Figure 4.2.2. Cell viability after treating bacteria with different concentrations of
functionalized microspheres Pw-3 (squares), free diamine (circles), free vanillin-derivative
(triangles) and free vanillin (inverted triangles).

Table 4.2.3. EC$_{50}$ of raw powder CaP material (**Pw**), functionalized CaP material (**Pw-3**), free
vanillin, free diamine and free **3**.

Material	Pw	Pw-3	1	2	3
EC$_{50}$ (mg·mL^{-1})	-	0.015	6.330	0.092	0.083

After testing of the antibacterial effect of the **Pw-3** microspheres, *E.coli*
bacteria were treated with the functionalized scaffolds in order to verify that
the tridimensional materials also performed an antimicrobial activity. For this
experiment, different suspensions of 10^3, 10^4 and 10^5 CFU·mL^{-1} were treated
with **Sc-3**, and a control was carried out by incubating bacteria with the non-
functionalized scaffold (**Sc**). In addition, diamine-functionalized scaffolds (**Sc-
2**) were also tested in order to study the effect of the diamine in bacteria and
compare it with the effect of vanillin. Also, equitoxic concentration of vanillin
derivative **3** and free vanillin (**1**) were tested. Finally, untreated suspensions of
bacteria 10^3, 10^4 and 10^5 CFU·mL^{-1} were used as a control. The obtained
results, in terms of bacterial viability, are shown in **Figure 4.2.3**. As it could be
seen, raw scaffolds (**Sc**) did not affect significantly bacterial viability. On the
other hand, as expected, **Sc-3** solid induced a marked reduction in *E. coli*
viability (*ca.* 90% for 10^3 CFU·mL^{-1}). Besides, toxicity of **Sc-3** scaffold
decreased at higher bacteria concentration (*ca.* 60 % for 10^5 CFU·mL^{-1}). These
results clearly indicated that antibacterial activity of **Sc-3** solid was due by the
grafted vanillin derivative **3**. Similar results were obtained when using **Sc-2**
solid (CaP scaffold functionalized with 1,5-pentanediamine). On the other
hand, vanillin derivative **3** showed high toxicity for the three bacterial
concentrations tested while free vanillin (**1**) showed a poor antibacterial activity.

Also, **Sc-3** solid was able to induce more marked bacterial viability reduction than equitoxic concentrations of free vanillin (**1**) demonstrating that grafting of EOCs onto the surface of CaP scaffolds increased their antibacterial features (most probably because the immobilization process prevents volatilization).
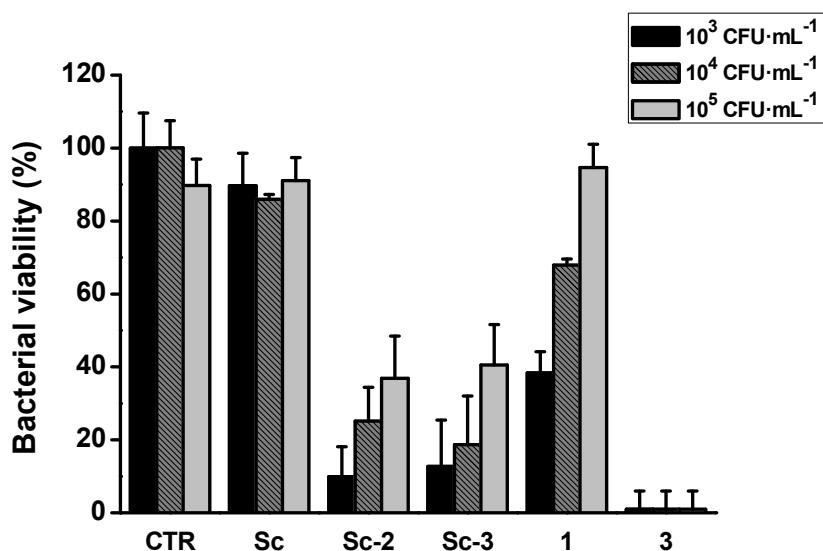

Figure 4.2.3. Cell viability after treating bacteria with 3-functionalized scaffolds (**Sc-3**), diamine-functionalized scaffolds (**Sc-2**), raw scaffolds (**Sc**), vanillin (**1**) and modified vanillin (**3**) compared to a control (**CTR**)

In order to study the effect of **Sc** and **Sc-3** on *E. coli* morphology, FESEM images were taken (see **Figure 4.2.4**). As could be seen, the morphology of *E. coli* bacteria treated with the raw non-functionalized scaffold (**Sc**) did not present any structural damage (**Figure 4.2.4A**). However, when bacteria were treated with **Sc-3** scaffold, the external membrane was damaged (**Figure 4.2.4B**), followed by shrinking (**Figure 4.2.4C**) and, finally, bacterial death (**Figure 4.2.4D**). The bacterial death observed with **Sc-3** supported the

mechanism described in bibliography, according to which the antimicrobial power of EOCs comes from their ability of disrupting cell membrane by damaging the ion exchange channels. This makes the cell membrane more permeable and allows the leaking of cytoplasmatic components, leading to the shrinking of the cell wall and consequent cell death as seen in the images of different bacteria photographed during the different stages.
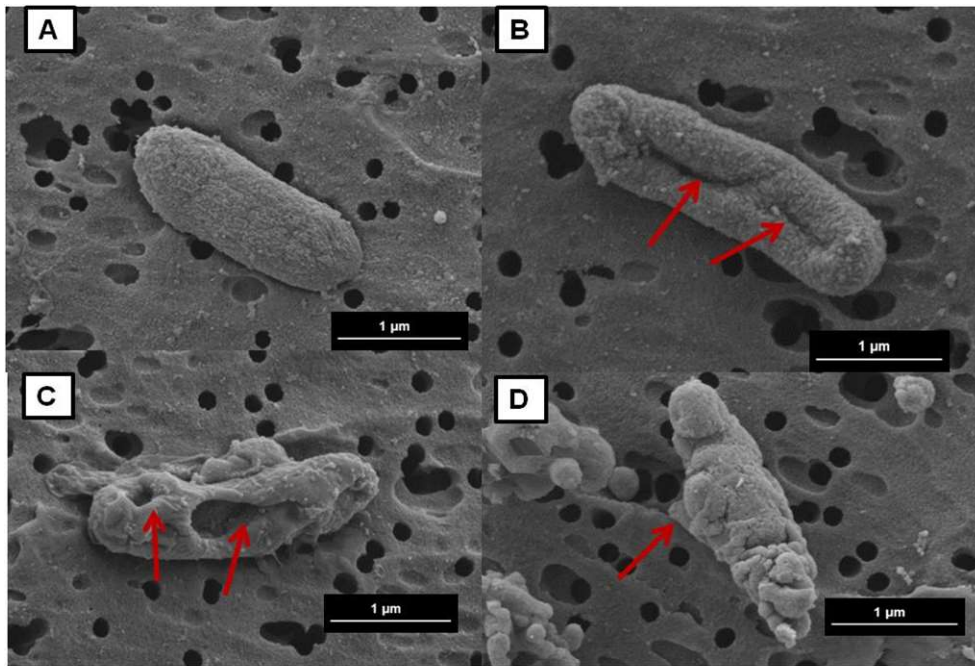
Figure 4.2.4. FESEM images of bacteria treated with the non-functionalized scaffold (A) and with the functionalized scaffold **Sc-3** (B, C, D).

After assessing the antimicrobial activity of the prepared scaffold-based materials (**Sc-2** and **Sc-3**), cytotoxicity experiments were carried out. To perform these experiments, L929 fibroblast-like cells were cultured in the presence of **Sc**, **Sc-2** and **Sc-3** scaffolds. Besides, positive (CTR+, addition of

0.5 % phenol solution to the growth medium) and negative (CTR-, cell culture in DMEM) controls were also performed. Cell viability was quantified by Alamar Blue assay, and the obtained results after 24 and 48 hours are shown in **Figure 4.2.5A**. As could be seen in **Figure 4.2.5A**, the percentage of viability, compared with negative control (considered as 100 %), for samples treated with **Sc**, **Sc-2** and **Sc-3** was ca. 100 %, which means that no cytotoxic effect was triggered by the bare and functionalized scaffolds.

Levels of lactate dehydrogenase (LDH) in the cell culture supernatant were also measured in order to assess the effect of **Sc**, **Sc-2** and **Sc-3** scaffolds in the cell viability. As LDH is an intracellular enzyme, high concentrations in the culture supernatant would mean cellular membrane damage. The obtained results are shown in **Figure 4.2.5B**. As could be seen, negligible amounts of LDH (similar to that presented by negative control) were observed in the culture supernatants of L929 cells treated with **Sc**, **Sc-2** and **Sc-3** materials after 24 hours. Besides, after 48 hours, the amounts of LDH released are lower than 20 % (materials were classified as toxic when extracellular LDH levels are higher than 30 %).
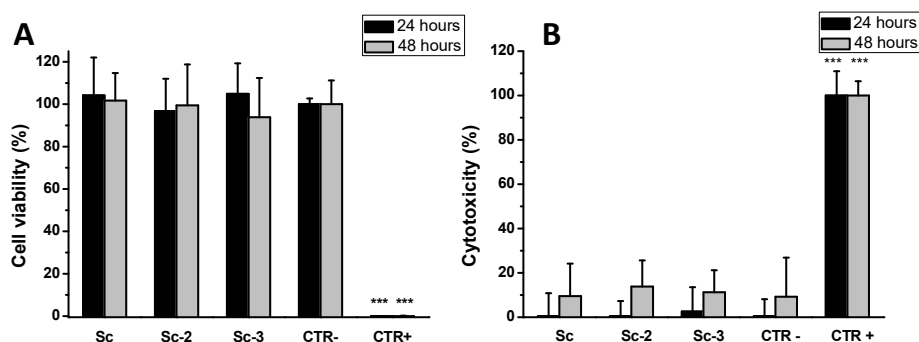

Figure 4.2.5. Alamar blue assay (a), and LDH release (b) evaluated on L929 cells after 24 and 48 hours of culture in presence of **Sc**, **Sc-2**, **Sc-3** and CTRs. Values are reported as mean ±SD (***:$p<0.0005$).

a) *** CTR+ vs **Sc**, **Sc-2**, **Sc-3** and CTR- (24 and 48 hours);
b) *** CTR+ vs **Sc**, **Sc-2**, **Sc-3** and CTR- (24 and 48 hours).

Furthermore, to confirm cell viability quantified by Alamar Blue and to appreciate cell morphology, also the Neutral Red staining was performed. Images of L929 cells cultured in the presence of **Sc**, **Sc-2** and **Sc-3** were taken and compared to those obtained from negative and positive controls (**Figure 4.2.6**). All cultures in presence of the scaffolds (**Sc**, **Sc-2** and **Sc-3**) showed a noticeable cell red staining, similar to that appreciable in the negative control (CTR-) condition, after 24 and 48 hours of incubation. This red staining indicated a high L929 cell viability as only living cells are able to uptake Neutral Red. Besides, as could be seen in **Figure 6**, L929 cell morphology did not show any significant changes supporting the previous results. On the other hand, L929 cells in positive control (CTR+) conditions showed no red staining and its morphology clearly indicated cell death.
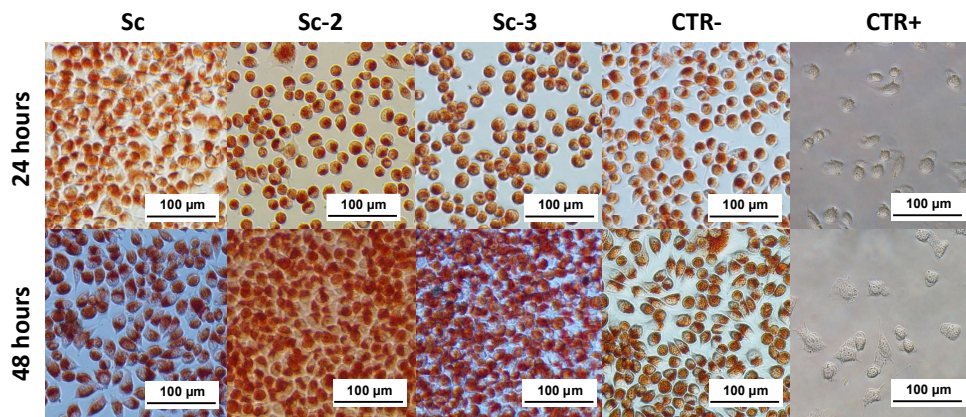

Figure 4.2.6. Neutral Red staining of cells cultured in the presence of **Sc**, **Sc-2**, **Sc-3**, and CTR- and CTR+ after 24 and 48 hours (Magn 4x).

In conclusion, it can be said that no significant cytotoxic effect on L929 cells was observed in the presence of the three scaffolds (**Sc**, **Sc-2** and **Sc-3**).

Once assesed the antimicrobial behaviour and the cytotoxicity of the functionalized scaffolds, bioactivity assays to test if the prepared supports were suitable for enhancing bone regeneration were performed. For this purpose, MG-63 human osteoblast-like cells were directly seeded on the surface of the scaffolds (**Sc, Sc-2** and **Sc-3**) and the samples were studied for 3 weeks.

In a first step, cell viabililty in **Sc, Sc-2** and **Sc-3** treated groups was studied using Alamar Blue dye test after 24 hours, 1, 2 and 3 weeks. The obtained results are shown in **Figure 4.2.7**. As could be seen in **Figure 4.2.7**, a very similar trend of the cell viability for the three scaffolds tested (i.e. **Sc, Sc-2** and **Sc-3**) was observed with a regular increase until 2 weeks. After this time viabililty remained constant, probably due to the possible cell confluence achieved that could have slown its growth. On the other hand, the cell viability of the control was higher than that observed with **Sc, Sc-2** and **Sc-3** (data not shown) probably due to the difference of the seeding areas. The seeded area corresponded to 0.5 cm^2 in the case of the scaffods, while the bottom well area was 2 cm^2 in the case of the controls. Neverthless, the control group represent an "internal control" for checking the cell culture conditions; the smooth and flat surface of the culture well, in contrast with the rough, irregular and partially porously structure of the CaP-based scaffolds, makes the **Sc** the correct control for the others materials. Statistical analysis showed the same difference among controls and all experimental materials at each timepoints (*** p < 0.0005).
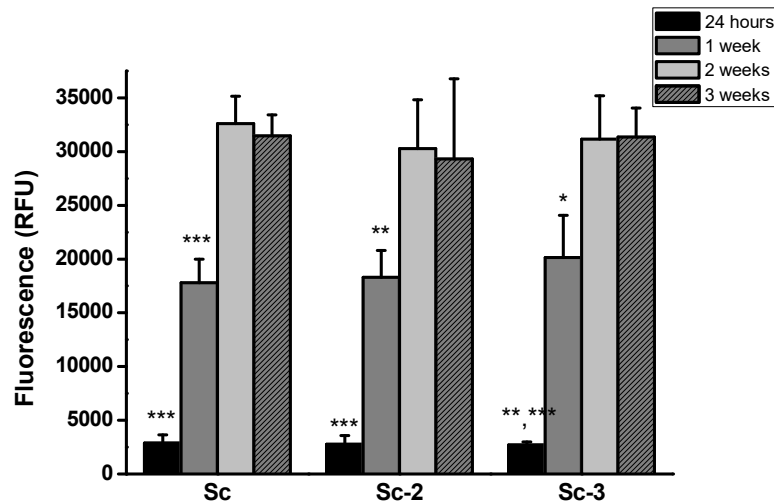
160

Figure 4.2.7. Cell viability by Alamar blue on **Sc**, **Sc-2**, **Sc-3** after 24 hours, 1 week, 2 weeks and 3 weeks of culture (* $p<0.05$; ** $p<0.005$; *** $p<0.0005$).
Sc: ***24 hours vs 1, 2, 3 weeks; ***1week vs 2, 3 weeks; **Sc-3**: ***24 hours vs 1, 2, 3 weeks; **1week vs 2, 3 weeks; **Sc-2**: **24 hours vs 1 week; ***24 hours vs 2, 3 weeks; *1week vs 2, 3 weeks.

In order to confirm the viability findings obtained by Alamar test, MG-63 human osteoblast-like cells morphology and sample colonization were also observed. For this purpose, three samples of **Sc**, **Sc-2** and **Sc-3** were stained using the LIVE/DEAD® kit. **Figure 4.2.8** shows cell colonization of the scaffolds surface, displaying living and dead cells in green and red colour, respectively. The porous architecture of the scaffolds can be observed in the images and, after 24 hours, only a small number of cells adhered to the inner surface of the macropores. After 1 and 2 weeks of culture, cells progressively covered the surface of the scaffolds in all replicates. At this respect, no dead cells were observed in the presence of **Sc** or **Sc-3** scaffolds after 1 and 3 weeks. However, some dead cells were observed only on **Sc-2** scaffold, possibly due to slight toxicity of the amine derivatives after a long-time exposure. At the end of the experimental time, the scaffold surfaces were observed to be totally

covered by cells, which indicated that scaffold colonization is possible after surface functionalization. Dead cells are also observed, probably due to the long cell exposure to a confluence environment in a static system. However, as confirmed by Alamar Blue results, the quantity of dead cells was minimum and did not affect total cell viability.
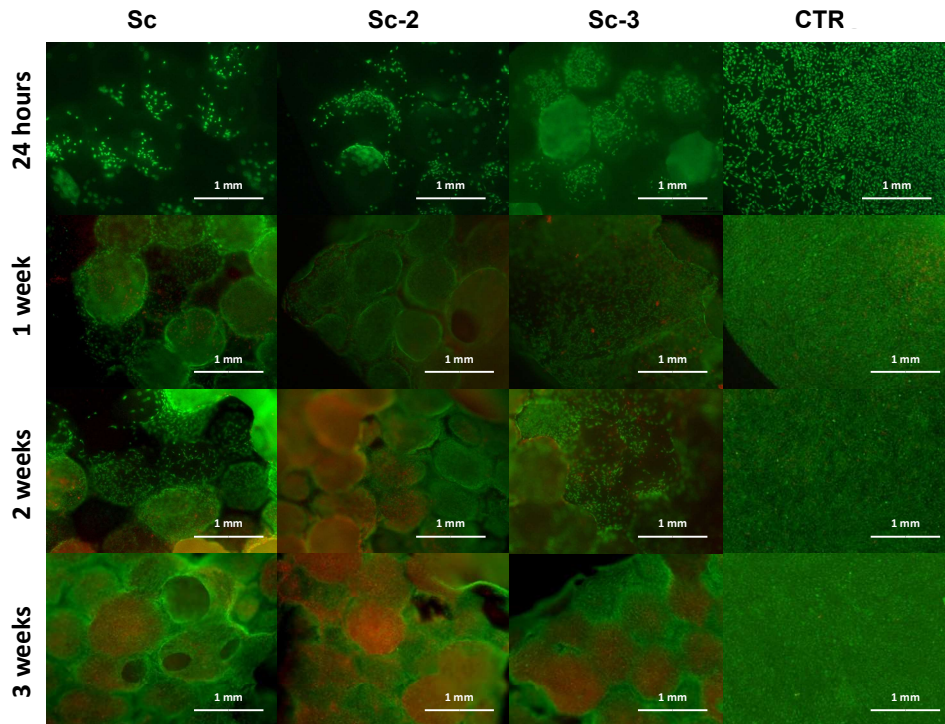
Figure 4.2.8. Cell viability by LIVE/DEAD assay on the surface of **Sc**, **Sc-2**, **Sc-3** and a control well upon 24 hours, 1 week, 2 weeks and 3 weeks.

Finally, in order to broaden the knowledge about these new functionalized scaffolds in terms of osteoinductivity, the expression of *ALPL*, *COL1a1* and *BGLAP* genes (typically expressed by osteoblasts) was evaluated. The levels of gene expression are shown in **Figure 4.2.9**. As could be observed there was no significant differences in gene expression for the three scaffolds tested (**Sc**, **Sc-**

2 and **Sc-3**). In particular, **Sc-3** scaffold induced a slightly enhancement in gene expression over time compared with the corresponding controls. This overall behavior allowed to state that the chemical modifications of the hydroxyapatite-based scaffold did not affect its ability to stimulate the bone matrix synthesis.
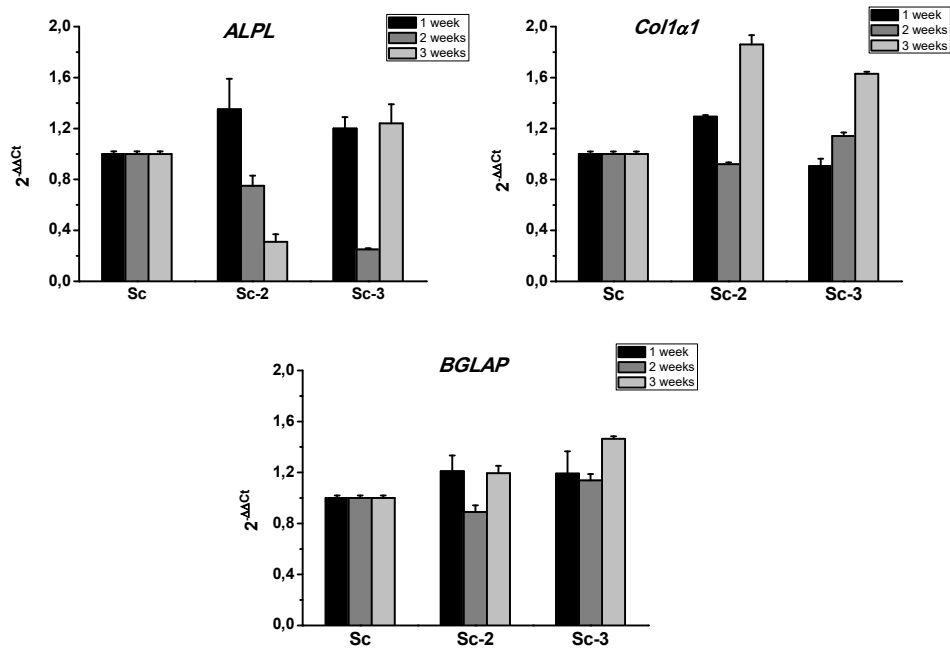
Figure 4.2.9. Expression of typical osteoblast related genes during the *in vitro* culture: *ALPL* (a)*, COL1a1* (b)*, BGLAP* (c). No significant differences were evidenced.

4.2.5 Conclusions

In conclusion, new vanillin-functionalized microspheres (**Pw-3**) or scaffolds (**Sc-3**) with antimicrobial features have been developed. The synthetic vanillin derivative **3** or diamine **2** were covalently anchored onto the CaP microparticles

and scaffolds. No substantial changes in the materials were observed during the functionalization processes according to TGA and FESEM studies. Moreover, their antibacterial activity was tested against E. coli bacteria. Treatment with 10 mg·mL-1 of solid **Pw-3** resulted in 100% bacterial death, whereas scaffolds **Sc-2** and **Sc-3** also caused bacterial death. In addition, **Sc**, **Sc-2** and **Sc-3** scaffolds were no cytotoxic and highly biocompatible, yet they did not display any toxic effect over non-bacterial cells, because they preserve the ability to express the genes *ALPL*, *COL1A1* and *BGLAP*. In short, these results demonstrate that commercially available scaffolds can be easily functionalized with EOCs, achieving outrageous antimicrobial activity and opening up a new approach for the treatment and prevention of infections. This study represents the first step to identify new antibacterial strategy based on the use of EOCs; even if the findings are encouraging in all the investigated aspects, other insights are mandatory before the clinical use of the materials, such as an in vivo phase to confirm their efficacy and the absence of toxicity.

5. Experimental section

5.1 Molecular gates in mesoporous bioactive glasses for the treatment of bone tumors and infection

5.1.1 Chemicals

The chemicals tetraethyl orthosilicate (TEOS), triethyl phosphate (TEP), calcium nitrate $Ca(NO_3)_2 \cdot 4H_2O$, F68 $(EO)_{78}$-$(PO)_{30}$-$(EO)_{78}$ triblock copolymer, tris(2,2'-bipyridyl)ruthenium(II) chloride hexahydrate ($[Ru(bpy)_3]^{2+}$), 3-[2-(2-aminoethylamino) ethylamino]propyl-trimethoxysilane (**N3**), adenosine 5'-triphosphate disodium salt hydrate (ATP), N-(3-Dimethylaminopropyl)-N'-ethylcarbodiimide hydrochloride (EDC), alkaline phosphatase (ALP) from bovine intestinal mucosa(buffered aqueous glycerol solution, $\geq$ 6,500 DEA units/mg protein), 3-(triethoxysilyl)propyl isocyanate, acetonitrile anhydrous, hydrochloric acid, levofloxacin, Dulbecco's Modified Eagle's Medium and pronase enzyme from *S. griseus* were purchased from Sigma–Aldrich Química S.A. Triethylamine (TEA) was purchased from J.T. Baker Chemicals. ε-Poly-L-lysine was purchased from Chengdu Jinkai Biology Engineering Co., Ltd. Fetal Bovine Serum (FBS) was obtained from Gibco, BRL. LB medium was provided from Laboratorios Conda. L-glutamine, penicillin and streptomycin were purchased from BioWhittaker-VWR Europe. Doxorubicin used was obtained from the European Pharmacopoeia Reference Standard (Council of Europe EDQM).

5.1.2 General Techniques

FTIR spectroscopy was carried out with a Nicolet Magma IR 550 spectrometer. TEM images were obtained with a 100 kV Jeol JEM-1010 microscope. SEM images were obtained with a 20kV JEOL F-6335 microscope. Differential thermal analysis was done in a TG/DTA Seiko SSC/5200 thermobalance between 50 °C and 1000 °C at a heating rate of 10°C·min^{-1}. The textural properties of the calcined materials were determined by nitrogen adsorption porosimetry by using a Micromeritics ASAP 2020

porosimeter. To perform the N_2 adsorption measurements, the samples were previously degassed under vacuum for 15 hours, at 150 °C. The surface area was determined using the Brunauer-Emmett-Teller (BET) method. The pore size distribution between 0.5 and 40 nm was determined from the adsorption branch of the isotherm by means of the Barret-Joyner-Halenda (BJH) method. ^1H-^{29}Si and ^1H-^{31}P CP (cross-polarization)/MAS (magic-angle-spinning) and single-pulse (SP) solid-state nuclear magnetic resonance (NMR) measurements were performed to evaluate the different silicon and phosphorus environments in the synthesized samples. The NMR spectra were recorded on a Bruker Model Avance 400 spectrometer. Samples were spun at 10 kHz for ^{29}Si and 6 kHz in the case of ^{31}P. Spectrometer frequencies were set to 79.49 and 161.97 MHz for ^{29}Si and ^{31}P, respectively. Chemical shift values were referenced to tetramethylsilane (TMS) and H_3PO_4 for ^{29}Si and ^{31}P, respectively. The CP spectra were obtained using a proton enhanced CP method, at a contact time of 1 millisecond. The time period between successive accumulations was 5 and 4 seconds for ^{29}Si and ^{31}P, respectively, and the number of scans was 10000 for all spectra. Solid-state ^{13}C spectra were obtained with a Bruker Model Avance 400 spectrometer 75.46 MHz. For the cell proliferation test, the absorbance was measured using a Helios Zeta UV-VIS spectrophotometer.

5.1.3 Synthesis of solids

5.1.3.1 Synthesis of the mesoporous bioactive glass (S1)

$85\%SiO_2$-$10\%CaO$-$5\%P_2O_5$ (% mol) mesoporous glass (**S1**) was synthetized by evaporation induced self-assembly (EISA) method, using F68 $(EO)_{78}$-$(PO)_{30}$-$(EO)_{78}$ triblock copolymer as structure directing agent. TEOS, TEP and calcium nitrate $Ca(NO_3)_2 \cdot 4H_2O$ were used as SiO_2, P_2O_5 and CaO sources, respectively. In a typical synthesis, 2 g of F68 were dissolved in 30 g of ethanol with 0.5 ml of HCl 0.5 M solution at room temperature. Afterward, 3.70 g of TEOS, 0.34 g of TEP and 0.49 g of $Ca(NO_3)_2 \cdot 4H_2O$ were added under stirring in 3 hours intervals. The resulting solution was stirred during 12 hours

and casted into Petri dishes (9 cm in diameter). The colorless solution was evaporated at 30 °C during 11 days. Eventually, the dried gels were removed as homogeneous and transparent membranes, and heated at 700 °C for 3 hours under air atmosphere. Finally the MBG powder was gently milled and sieved, collecting the particle size fraction below 40 μm.

5.1.3.2 Synthesis of S2

1 g of **S1** was suspended in 30 mL of anhydrous acetonitrile under inert atmosphere. Then, 1 mL (3.88 mmol) of 3-[2-(2-aminoethylamino)ethylamino] propyl-trimethoxysilane (**N3**) was added and the mixture was stirred for 5.5 hours. Finally, the solid was filtered, washed with H_2O repeatedly and dried under vacuum for 12 hours.

5.1.3.4 Synthesis of S3

200 mg of solid **S2** were suspended in a solution of EDC 0.1 M and ATP 1.8 M, previously adjusted to pH 7 with NaOH. The suspension was stirred for 6 hours at room temperature. The resulting solid was filtered and dried under vacuum for 12 hours.

5.1.3.5 Synthesis of S4

In a typical synthesis, 1 g of **S1** was suspended in 50 mL of methanol, inside a round-bottom flask under inert atmosphere. Then, an excess of 3-(triethoxysilyl)propylisocyanate (isocyanate) (1 mL, 4 mmol) was added and the final mixture was stirred for 5.5 hours at room temperature. The solid was filtered, washed with H_2O repeatedly, and dried under vacuum for 12 hours.

5.1.3.6 Synthesis of S5

A solution of 1 g of ε-poly-L-lysine (0.2 mmol) and TEA (1.6 mL, 11.5 mmol) in 20 mL of methanol was added onto the solid **S4**, and the mixture was stirred for 2 hours. Finally, the solid was filtered off and dried under vacuum.

169

5.1.3.7 Synthesis of S3-Ru and S5-Ru

In order to carry out the proof of concept about the functioning of ATP and ε-poly-l-lysine based gates, both systems were loaded with a fluorescence dye. For this purpose 2 g of **S1** were suspended in a solution of 1.6 g tris(2,2'-bipyridil)ruthenium(II) chloride hexahydrate ([Ru(bpy)$_3$]$^{2+}$ dye in 70 mL of anhydrous acetonitrile in a round-bottomed flask. Then, 10 mL of acetonitrile were distilled with a dean-stark, in order to remove the possible water present in the pores of the solid. Afterwards, the mixture was stirred at room temperature during 24 hours, in order to achieve maximum loading in the pores of the MBG scaffolding. The resulting solid was then filtered and dried under vacuum for 12 hours. Subsequently, the solid was functionalized and capped as **S3** and **S5** respectively, as described above. Once dried, the solids were suspended in 5 mL of water and stirred in short washing, in order to remove the excess of dye remaining on the surface of the materials. The solids were filtered again and dried under vacuum for 12 hours.

5.1.3.8 Synthesis of S3-Levo and S5-Levo

In order to test the functioning of ATP and ε-poly-L-lysine based gates as on command antibiotic delivery devices, both systems were loaded with levofloxacin. For this purpose 800 mg of **S1** were suspended in a solution of 400 mg (1.11 mmol) of levofloxacin in 20 mL of methanol inside a round-bottom flask under inert atmosphere. The mixture was stirred at room temperature during 24 hours to achieve maximum loading in the pores of the MBG. Subsequently, the solution was split in two and each part was functionalized in a similar way to **S3** and **S5** respectively. Finally **S3-Levo** and **S5-Levo** were washed in water to remove the excess of antibiotic remaining on the surface.

5.1.3.9. Synthesis of S3-Dox

In order to test the functioning of the ATP based gate as on command antitumoral delivery devices, 30 mg of solid **S2** and 6 mg of doxorubicin were suspended in 5mL of methanol and stirred for 50 hours. Then, the solid was centrifuged and dried under vacuum for 1 hour. Finally the solid was introduced in a solution of EDC 0.1 M and ATP 1.8 M previously adjusted to pH 7 with NaOH. The suspension was stirred for 6 hours at room temperature. The resulting solid was centrifuged, washed several times with water and methanol and dried under vacuum for 12 hours.

5.1.4 Stimuli-responsive studies

5.1.4.1 Stimuli-responsive studies with S3-Ru and S5-Ru

4 mg of the **S3-Ru** and **S5-Ru** were suspended in 10 mL of water, and the pH was adjusted to 7.6 with NaOH. Both suspensions were split in two in order to study the dye release in the absence or presence of the corresponding stimuli, i.e. ALP and pronase for **S3-Ru** and **S5-Ru**, respectively. The two samples were stirred at 400 rpm and 37°C, and then several 250 μL aliquots were taken for each sample at different times. These aliquots were filtered with PFTE filters (0.22 μm) to monitor the $[Ru(bpy)_3]^{2+}$ release (λ_{ex} 454 nm, λ_{em} 593 nm) by fluorescence spectroscopy

5.1.4.2 Stimuli-responsive studies with S5-Levo

4 mg of **S5-Levo** were suspended in 10 mL of water, and the pH was adjusted to 7.6 with NaOH. The suspension was split in two in order to study the levofloxacin release in the absence and the presence of *E.coli* (final concentration 10^5 cells mL^{-1}). The two samples were stirred at 400 rpm and 37 °C, and then several 250 μL aliquots were taken for each sample at different times. These aliquots were filtered with PFTE filters (0.22 μm) to monitor the levofloxacin release (λ_{ex} 292 nm, λ_{em} 494 nm) by fluorescence spectroscopy.

5.1.4.3 Stimuli-responsive studies with S3-Dox

4.6 mg of **S3-Dox** were suspended in 2 mL of H_2O pH 7.6. Then, 0.5 mL of this suspension was placed on a Transwell permeable support with polycarbonate membrane (0.4 μm). The well was filled with 1.5 mL of H_2O pH 7.6 and the suspension was stirred at 37 °C and 100 rpm during all the experiment. To study the enzymatic responsiveness of the solid, the suspension was in contact with ALP on a Transwell. The amount of cargo released was determined by fluorescence spectrometry λ_{exc} 490, λ_{em} 514 nm, and the solution outside the Transwell insert was replaced with fresh medium, with or without ALP.

5.1.5 Bioactivity assays with solids S3 and S5

Assessments of in vitro bioactivity were carried out on **S3** and **S5** solids. For this purpose, 40 mg of the solids were soaked into 6 mL of filtered simulated body fluid (SBF)[46] in polyethylene containers at 37 °C under sterile conditions.[38] The evolution of the solids surfaces were analysed by Fourier transform infrared (FTIR) spectroscopy and scanning electron microscopy (SEM).

5.1.6 Biological assessment of the gated materials

5.1.6.1 E. coli DH5α culture conditions

For viability studies, bacteria *Escherichia coli (E. coli)*, cell culture DH5α was used. Bacteria cells were maintained in glycerol 15 % at -80 °C. For the assays, cells were grown for 24 hours at 37 °C and under constant stirring with 5 mL of LB medium. Cells from 1 mL culture were collected by centrifugation for 30 seconds at 13000 rpm and resuspended in 1 mL of milliQ water at pH 7.6. Then a dilution of $2 \cdot 10^4$ cells·mL^{-1} was prepared, in order to achieve a final concentration of 10^4 cells·mL^{-1}. The same procedure was carried out for both kinetic and viability assays.

5.1.6.2 Clonogenic cell viability assay with S5-Levo, levofloxacin and ε-poly-L-lysine

For the clonogenic cell viability assay with **S5-Levo**, different suspensions of **S5-Levo** containing bacteria (final concentration 10^4 cells·mL^{-1}) were prepared, achieving the final solid concentrations of 800, 500, 300, 200, 160, 120, 80, 60, 40, 20, 10, 5, 1 and 0 µg solid·mL^{-1}. The samples were stirred at 180 rpm (37 °C) during 10 minutes. Then, the suspensions were suitably diluted with milliQ water (pH 7.6) in order to obtain a cell growth easy to quantify. Finally, 100 µL of the new dilutions were seeded in LB plates (3 % agar) and incubated at 37°C for 24 hours. Then, Colony Formation Units (CFU) were quantified.

To test the cytotoxicity of the non-loaded ε-poly-L-lysine capped solid (**S5**), the same experiment was carried out with final solid concentratons of 600, 300, 200, 100, 50, 30, 20, 5 and 0 µg solid·mL^{-1}.

To determine the cytotoxicity of free levofloxacin and free ε-poly-L-lysine, final concentrations of 2000, 1000, 800, 600, 400, 300, 250, 200, 150, 100, 60, 30, 10 and 0 ng·mL^{-1} (levofloxacin) and 600, 400, 200, 100, 80, 50, 40, 30, 10 and 0 ng·mL^{-1} (ε-poly-L-lysine) were achieved. In order to test the specificity of the gates, solid **S3-Levo** (capped with ATP) was submitted to the same procedure.

5.1.6.3 Human Osteosarcoma (HOS) cells culture test

HOS cells were seeded on well culture plates (CULTEK), at a density of 40000 cell per mL in Dulbecco's Modified Eagle's Medium with 10 % foetal bovine serum, 1 mM L-glutamine, penicillin (200 mg·mL^{-1}), and streptomycin (200 mg·mL^{-1}), under a CO_2 (5 %) atmosphere at 37 °C, 24 hours to reach the confluence in each cell plate. Thereafter, **S3-Dox** solid was added on the seed cells at half confluence at 200 µg·mL^{-1}concentration. In order to study the stimuli-responsive behaviour of the ATP gate, ALP was added to the culture wells to simulate a scenario of ALP activity excess.

5.1.6.4 Cell proliferation test

Cell proliferation in contact with **S3** and **S3-Dox** was determined by the MTT method. Samples were incubated for 4 hours at 37 °C and 5 % CO_2 under dark conditions. Then, the medium was removed and 0.5 mL of isopropanol–HCl solution were added. Finally, the absorbance was measured at 460 nm.

5.1.7 Statistics

Statistics Data are expressed as means-standard deviations of experiments. Statistical analysis was performed using the Statistical Package for the Social Sciences (SPSS) version 22 software (IBM). Statistical comparisons were made by analysis of variance (ANOVA). Subsequently, post hoc analyses were carried out to correct for multiple comparisons. In all of the statistical evaluations, $P<0.01$ was considered as statistically significant.

5.2 Mesoporous bioactive glasses equipped with stimuli-responsive molecular gates for the controlled delivery of levofloxacin

5.2.1 Chemicals

Chemicals poly(ethylene glycol)-*block*-poly(propylene glycol)-*block*-poly(ethylene glycol) (P123), tetraethyl orthosilicate (TEOS), triethyl phosphate (TEP), calcium nitrate $Ca(NO_3)_2 \cdot 4H_2O$, 3-[2-(2-aminoethylamino)ethylamino]propyl-trimethoxysilane (N3), adenosine 5'-triphosphate disodium salt hydrate (ATP), N-(3-dimethylaminopropyl)-N'-ethylcarbodiimide hydrochloride (EDC), acid phosphatase, acetonitrile anhydrous, hydrochloric acid, levofloxacin, Dulbecco's Modified Eagle's Medium (DMEM), fetal bovine serum (FBS) and Dulbecco's phosphate-buffered saline (PBS) were purchased from Sigma–Aldrich Química S.A. LB medium was provided from Laboratorios Conda. Cell proliferation reagent WST-1 was obtained from Roche Applied Science.

5.2.2 General Techniques

FTIR spectroscopy was carried out with a Tensor 27 FT-IR spectrometer (Bruker). TEM images were obtained with a 100 kV Jeol JEM-1010 microscope. FESEM images were obtained with a ZEISS ULTRA 55. Powder X-ray diffraction measurements were performed on a Philips D8 Advance diffractometer using Cu Kα radiation. The textural properties of the calcined materials were determined by nitrogen adsorption porosimetry by using a Micromeritics TriStar II PLUS porosimeter. To perform the N_2 adsorption measurements, the samples were previously degassed under vacuum for 24 hours, at 90 °C. The surface area was determined using the Brunauer-Emmett-Teller (BET) method. The pore size distribution between 0.5 and 40 nm was determined from the adsorption branch of the isotherm by means of the

Barret-Joyner-Halenda (BJH) method. For the cell proliferation test, cell viability measurements were taken in a Wallac 1420 workstation.

5.2.3 Synthesis of materials

5.2.3.1 Synthesis of mesoporous bioactive glass (S1)

80%SiO_2-15%CaO-5%P_2O_5 (% mol) mesoporous glass (**S1)** was synthetized by evaporation induced self-assembly (EISA) method, using P123 triblock copolymer as structure directing agent. TEOS, TEP and calcium nitrate $Ca(NO_3)_2 \cdot 4H_2O$ were used as SiO_2, P_2O_5 and CaO sources respectively. In a typical synthesis, 4 g of P123 were dissolved in 60 g of ethanol with 1 mL of HCl 0.5 M solution at room temperature. Afterwards, 7.18 mL of TEOS, 0.73 mL of TEP and 1.29 g of $Ca(NO_3)_2 \cdot 4H_2O$ were added under stirring in 3 hours intervals. The resulting solution was stirred during 12 hours and casted into Petri dishes (9 cm in diameter). The colorless solution was evaporated at 37 °C during 1 day. Eventually, the dried gels were removed as homogeneous and transparent membranes, and heated at 700 °C for 3 hours under air atmosphere. Finally the MBG powder was gently milled and sieved, collecting the particle size fraction below 20 μm.

5.2.3.2 Synthesis of S2

500 mg of **S1** were suspended in a solution of 145 mg of levofloxacin in 20 mL of anhydrous acetonitrile under inert atmosphere. After stirring for 24 hours in order to achieve the maximum load of the pores, 0.5 mL of 3-[2-(2 aminoethylamino)ethylamino] propyl-trimethoxysilane (**N3**) was added, and the mixture was stirred for 5.5 hours. Finally, the solid was filtered and dried under vacuum for 12 hours.

5.2.3.3 Synthesis of S3

400 mg of solid **S2** were suspended in a solution of EDC 0.6 M and ATP 0.5 M and an excess of levofloxacin, previously adjusted to pH 7.6 with NaOH. The suspension was stirred for 6 hours at room temperature. The resulting solid was filtered and dried under vacuum for 12 hours.

5.2.4 Stimuli-responsive studies with S3

4 mg of **S3** were suspended in 10 mL of water at pH 7.6 adjusted with NaOH. The suspension was divided in two and acid phosphatase (2.5 mg, 1.25 enzymatic units) was added to one of the samples. The two samples were stirred at 400 rpm and 37 °C, and then several 250 μL aliquots were taken for each sample at different times (0, 1, 2, 4, 7 and 24 hours). These aliquots were filtered with PTFE filters (0.22 μm) to monitor the levofloxacin release by fluorescence spectroscopy (λ_{ex} 292 nm, λ_{em} 494 nm). Moreover, the same experiment was performed in the presence of other enzymes as amylase and lipase. For this, 10 mg of **S3** were suspended in 25 mL of water at pH 7.6 and the suspension was divided in four samples. APase, lipase and amylase (7.5 enzymatic units) were added to respective samples. The samples were stirred at 400 rpm and 37 °C, and then several 250 μL aliquots were taken for each sample at different times. These aliquots were filtered with PTFE filters (0.22 μm) to monitor the levofloxacin release by fluorescence spectroscopy (λ_{ex} 292 nm, λ_{em} 494 nm).

5.2.5 Bioactivity assays with S1 and S3.

In vitro bioactivity assays were carried out on **S1** and **S3** solids. 10 mg of each solid were soaked into 2 mL of filtered simulated body fluid (SBF)[291] at 37 °C under sterile conditions. The evolution of the solids surfaces were analysed

---

[291] T. Kokubo, H. Kushitani, S. Sakka, T. Kitsugi, T. Yamamuro, *J. Biomed. Mater. Res.*, **1990**, *24*, 721.

by Fourier transform infrared (FTIR) spectroscopy and field emission scanning electron microscopy (FESEM).

5.2.6 Bacterial viability assay

5.2.6.1 E. coli DH5α culture conditions

For bacterial viability studies, *Escherichia coli (E.coli)* DH5α cell culture was used. Bacteria cells were maintained in glycerol 15 % at -80 °C. For the assays, cells were grown for 24 hours at 37 °C and under constant stirring with 5 mL of LB medium. Cells from 1 mL culture were collected by centrifugation for 30 seconds at 13000 rpm and resuspended in 1 mL of milliQ water at pH 7.6.

5.2.6.2 Bacterial viability assay

In order to determine the antibacterial effect of **S3**, 5 mg of the solid were stirred in water at pH 7.6 in the absence and the presence of acid phosphatase for 24 hours. Then, two suspensions of 10^4 cells·mL^{-1} were prepared and treated with 50 μL of each sample. A control experiment with no solid was also carried out. The suspensions were stirred at 180 rpm (37 °C) during 10 minutes. Then, they were suitably diluted with milliQ water (pH 7.6) in order to obtain a cell growth easy to quantify. Finally, 100 μL of the new dilutions were seeded in LB plates (3 % agar) and incubated at 37 °C for 24 hours. Then, Colony Formation Units (CFU) were quantified.

5.2.7 Citotoxicity assay

5.2.7.1 Cell culture conditions

U-2-OS human osteosarcoma cells were purchased from the ATCC and were grown in DMEM supplemented with 10 % of FBS. Cells were incubated at 37 °C in an atmosphere of 5 % carbon dioxide and 95 % air, and underwent passage twice a week.

5.2.7.2 Cell toxicity assay

In order to study viability of cells in contact with **S3**, U-2-OS cells were seeded in a 96-well plate in a density of 10.000 cells·well^{-1} and treated with 25, 50, 100 and 200 µg·mL^{-1} of **S3** in PBS. A control assay with no solid was also carried out. After 24 and 48 hours of incubation, WST-1 was added in order to determine cell viability. The cells were incubated for 60 minutes, and then absorbance was measured at 595 nm.

5.2.8 Statistics

Statistics Data are expressed as means-standard deviations of experiments. Statistical analysis was performed using the Statistical Package for the Social Sciences (SPSS) version 22 software (IBM). Statistical comparisons were made by analysis of variance (ANOVA). In all of the statistical evaluations, P<0.01 was considered as statistically significant.

5.3 Gated mesoporous silica materials for the treatment of bone infection by *Staphylococcus aureus*.

5.3.1 Chemicals

The chemicals tetraethyl orthosilicate (TEOS), *n*-cetyltrimethylammonium bromide (CTABr), sodium hydroxide (NaOH), endoproteinase Glu-C V8 from *Staphylococcus aureus* **and** Safranin O were acquired from Sigma-Aldrich and were used without further purification. 3-(azidopropyl)triethoxysilane was provided by SelectLab Chemicals. Copper (II) sulphate pentahydrate ($CuSO_4 \cdot 5H_2O$) and sodium ascorbate were purchased from Scharlab. The designed peptide sequence (SEEDKGGDESEEDKGGDESEEDKK-Pentynoic Acid) was purchased from ChinaPeptides CO. LTD.

5.3.2 General Techniques

Powder X-ray measurements were performed in a Seifert 3000TT diffractometer using CuKα radiation. TEM images were obtained with a 100 kV Jeol JEM-1010 microscope. Differential thermal analysis was done in a TG/DTA Seiko SSC/5200 thermobalance between 50 °C and 1000 °C at a heating rate of $10°C \cdot min^{-1}$. The textural properties of the calcined materials were determined by nitrogen adsorption porosimetry by using a Micromeritics ASAP 2020 porosimeter. To perform the N_2 adsorption measurements, the samples were previously degassed under vacuum for 15 hours, at 150 °C. The surface area was determined using the Brunauer-Emmett-Teller (BET) method. The pore size distribution between 0.5 and 40 nm was determined from the adsorption branch of the isotherm by means of the Barret-Joyner-Halenda (BJH) method.

5.3.3 Synthesis of the mesoporous silica support (S0)

The MCM-41 mesoporous nanoparticles were synthesized by the following procedure: n-cetyltrimethylammoniumbromide (CTABr, 1 g, 2.74 mmol) was first dissolved in 480 mL of deionized water. Then, a 3.5 mL of NaOH 2.00 M in deionized water was added to the CTABr solution, followed by adjusting the solution temperature to 80 ºC. TEOS (5.00 mL, $2.57 \cdot 10^{-2}$ mol) was then added dropwise to the surfactant solution. The mixture was allowed stirred for 2 hours to give a white precipitate. Finally, the solid product was centrifuged, washed with deionized water and ethanol, and was dried at 60 ºC (MCM-41 as-synthesized). To prepare the final porous material (MCM-41), the as-synthesized solid was calcined at 550 ºC for 5 hours using an oxidant atmosphere in order to remove the template phase.

5.3.4 Synthesis of solid S1

500 mg of calcined MCM-41 and 33.2 mg (0.09 mmol) of Safranin O dye were suspended in 40 mL of PBS. Then, the mixture was stirred during 24 hours at room temperature with the aim of achieving maximum loading in the pores of the MCM-41 scaffolding. Afterwards, the solid was filtered and dried under vacuum for 12 hours.

5.3.5 Synthesis of solid S2

500 mg of the resulting solid **S1** were suspended in anhydrous acetonitrile in the presence of an excess of Safranin O, in order to avoid dye leakage. Then, an excess of 3-azidopropyl)triethoxysilane (0.918 g, 3.71 mmol) was added, and the suspension was stirred for 5.5 hours. Finally, the dark-purple solid was filtered off and dried at 37 ºC for 12 hours.

5.3.6 Synthesis of solid S3

For the preparation of the solid **S3**, azide-functionalized nanoparticles S2 (56 mg) and the peptide (95 mg) were suspended in a 50:50 v/v DMF-PBS

mixture (50 ml) in the presence of an excess of safranine O (50 mg, 0.2 mmol) in order to avoid the delivery of the dye from the pores to the bulk solution during the synthesis of the final solid. Then, a solution of 167 μL of CuSO$_4$·5H$_2$O 10^{-3} M and 167 μL of sodium ascorbate 10^{-2} M was prepared separately, and added to the reaction mixture. The reaction mixture was stirred at 90 °C for 3 days. Then, the nanoparticles were centrifuged and washed thoroughly with water to remove unreacted and absorbed molecules. One last washed was carried out with PBS. The resulting purple solid was finally dried under vacuum during 12 hours.

5.3.7 Stimuli-responsive studies with S3

In order to investigate the gating properties of **S3** material, cargo-release studies were carried out. In a typical experiment, 0.1 mg of **S3** were suspended in 200 μL of PBS at pH 7.5 in the absence and the presence of V8 protease (293 enzymatic units). Suspensions were stirred at 1000 rpm and 37 °C during 24 hours, and at given time intervals they were centrifuged in order to measure the supernatant fluorescence (λ_{ex} 520 nm, λ_{em} 571 nm). In order to determine the specificity of the system, the same stimuli-responsive experiments were performed in the presence of the same enzymatic units of amylase and lipase.

5.4 Antimicrobial activity of commercial calcium phosphate based materials functionalized with vanillin

5.4.1 Chemicals

Commercial Surgibone© material was purchased in the form of microspheres (Pw) and tridimensional blocks (Sc) composed by 75 % hydroxyapatite and 25 % β-tricalcium phosphate (βTCP). CaP powder microspheres presented a diameter of ca. 100 μm, whereas CaP scaffolds sized 10 x 10 x 5 mm were thoroughly cut in order to obtain pieces of 5 x 5 x 5 mm.

The chemicals vanillin, 1,5-pentanediamine, imidazole, N-(3-dimethylaminopropyl)-N'-ethylcarbodiimide hydrochloride (EDC), sodium borohydride (NaBH4) and glutaraldehyde were purchased from Sigma–Aldrich Química S.A. Ethylendiaminetetraacetic acid (EDTA) was purchased from Scharlab S.L. ɛ-Poly-L-lysine was purchased from Chengdu Jinkai Biology Engineering Co. Luria-Bertani agar medium used in bacterial experiments was provided from Laboratorios Conda. For cell experiments, Dulbecco's minimum essential medium (DMEM), β-glicerophosphate, ascorbic acid, Neutral Red dye and Erythrosyn B were purchased from Sigma-Aldrich, UK. Fetal bovine serum (FBS) was obtained from Euroclone, (Pero, Milan, Italy). Penicillin and streptomycin were obtained from Gibco, (Life Technologies, USA). Alamar blue dye was purchased from Serotec, (Oxford, UK). Lactate dehydrogenase (LDH) cytotoxicity detection kit was obtained from Roche Diagnostics GmbH, (Manheim, Germany). LIVE/DEAD® assay kit was purchased from Molecular Probes, (Eugene, OR, USA). RNeasy Mini Kit, SYBR green PCR kit and primers set were obtained from Qiagen SRL, (Milan,

Italy), and Superscript Vilo cDNA synthesis kit was obtained from Life Technologies, (Carlsbad, CA, USA).

5.4.2 General Techniques

FESEM images were obtained with a ZEISS ULTRA 55. Thermogravimetric analysis were carried out on a TGA/SDTA 851e Mettler Toledo balance, using an oxidant atmosphere (air, 80 mL·min-1) with a heating program consisting on a heating ramp of 10 °C per minute from 393 to 1273 K and an isothermal heating step at this temperature during 30 minutes.

1H and 13C-NMR spectra were acquired in a BRUKER ADVANCE III (400 MHZ). The NMR samples were dissolved in deuterated solvents purchased from Sigma-Aldrich, and TMS or the residual solvent were used as internal standard. Electron impact ionization mass spectrometry (MS-EI) was performed on a Thermo Finnigan MAT SSQ710 single stage quadropole instrument and high resolution mass spectra (HRMS) were carried out in a TRIPLETOF T5600 (ABSciex, USA) spectrometer. Matrix-assisted laser-desorption/ionization mass spectrometry was performed on a Bruker Autoflex III Smartbeam mass spectrometer, utilizing a 2,5-dihydroxybenzoic acid (DHB) matrix.

For cell experiments, Alamar Blue fluorescence was read at 590 nm (excitation at 530 nm) using a Micro Plate reader (VICTOR X2030, Perkin Elmer, Milan, Italy). LDH test was measured by an iMark microplate reader, BIORAD, Milan, Italy at 490 nm against 655 nm as reference. Cell images after Neutral Red staining were taken with a standard light microscope (Nikon Eclipse, Ti-U, Nikon Italia Srl, Italy) equipped with a digital camera, at 4x and 10x magnification. Cell images after LIVE/DEAD fluorescent labelling were taken using the same microscope equipped with an epifluorescence set-up (Eclipse TiU, NIKON Europe BV, NITAL SpA, Milan, Italy): excitation/emission setting of 488/530 nm to detect green fluorescence (live cells) and 530/580 nm to detect red fluorescence (dead cells). Gene expression

was evaluated by qPCR in a Light Cycler 2.0 Instrument (Roche Diagnostics, GmbH, Manheim, Germany), following a protocol which included 3 main steps: denaturation, amplification and melting curve analysis.

5.4.3 Synthesis of solids and compounds

5.4.3.1 Synthesis of 3

A two-step synthetic procedure was used to prepare the vanillin-derivative (**3**). In a first step, vanillin (**1**, 0.76 g, 5 mmol) was dissolved in dichloromethane (15 mL) and added dropwise over a solution of 1,5-pentanediamine (2, 0.616 mL, 5 mmol) in dichloromethane (25 mL) under vigorous stirring. After 30 minutes of reaction, diethyl ether (40 mL) was added over the suspension and the pale yellow solid was filtered-off. In a second step, a portion of the resulting solid (0.7 g, 2.97 mmol) was dissolved in ethanol (30 mL) and $NaBH_4$ (123 mg, 3.26 mmol) was slowly added in small portions. The solution was stirred for 1 hour and then ethanol was evaporated. The product was washed with ethyl acetate (3×5 mL). Finally, acetone was added to the crude and the suspension was filtered to remove the boron salts. Evaporation of the solvent under vacuum afforded the final product (3, 522.83 mg, 2.21 mmol, 74 % yield) as a yellow solid.

5.4.3.2 Preparation of Pw-3, Sc-3 and Sc-2

For the functionalization of the CaP materials (**Pw** and **Sc**), vanillin derivative **3** (523 mg, 2.21 mmol) or 1,5-pentanediamine (**2**, 257 mg, 2.51 mmol) was dissolved in a solution of imidazole in water (10 mL, 0.1 M). On the other hand, phosphate groups of **Pw** (300 mg) or **Sc** (6 pieces) were activated by immersion of the materials into a solution of EDC (1.25 g, 6.52 mmol) in PBS-EDTA 0.01 M buffer (10 mL). Finally, the solution of **2** or **3** was added to the scaffolds, and the samples were stirred for 24 hours at 37°C. Then, **Pw-3**, **Sc-3** and **Sc-2** were washed with water and acetone and dried under vacuum.

187

5.4.4 Bacterial viability assay

5.4.4.1 E. coli DH5α culture conditions

For bacterial viability studies, *Escherichia coli (E. coli) DH5a* cell culture was used. Bacteria cells were maintained in glycerol 15 % at -80 °C. For the assays, cells were grown for 24 hours at 37 °C and under constant stirring with 5 mL of Luria-Bertani Broth medium. Bacteria from 1 mL culture were collected by centrifugation for 30 seconds at 13000 rpm and re-suspended in 1 mL of PBS at pH 7.6.

5.4.4.2 Bacterial viability assay with Pw-3

E.coli bacteria were treated with different amounts of **Pw-3** in order to determine its antimicrobial potential. For this purpose, a suspension of 10^3 cells·mL^{-1} was stirred in the presence of 50, 5, 2, 1, 0.5, 0.35, 0.1, 0.05, 0.025, 0.005 and 0 mg·mL^{-1} of **Pw-3** for 15 minutes at 37 °C. 100 μL of the suspensions were seeded in LB plates (3 % agar) and incubated at 37 °C for 24 hours. Then, colony formation units (CFU) were counted. In order to compare the antibacterial activity of the materials with that of free vanillin (**1**), diamine (**2**) and the synthesized molecule (**3**), the same experiment was carried out with equivalent concentrations of **1, 2** and **3**. A control experiment was also carried out with **Pw** (without any functionalization) in order to demonstrate that the toxic effect was not due to the raw material.

5.4.4.3 Bacterial viability assay with Sc, Sc-2, Sc-3, and 1, 2, and 3

For testing the antimicrobial potential of the functionalized CaP scaffolds, suspensions of 10^3, 10^4 and 10^5 cells·mL^{-1} were prepared. Then, 1 mL of each suspension was stirred in the presence of **Sc-3** for 15 minutes at 37 °C. The suspensions were diluted with PBS in order to obtain a cell concentration easy to quantify, and 100 μL of the new dilutions were seeded in LB plates (3 % agar) and incubated at 37 °C for 24 hours. Then, colony formation units (CFU) were quantified. In order to determine that the antimicrobial behavior was due

to the presence of the modified vanillin molecule, similar experiments were carried out in the presence of non-functionalized scaffolds (**Sc**), diamine-functionalized scaffolds (**Sc-2**), and in the presence of equitoxic amounts of **1**, **2** and **3**. Triplicate experiments were carried out for each sample. Finally, untreated suspensions of 10^3, 10^4 and 10^5 cells·mL^{-1} were also used as a control.

5.4.4.4 Preparation of bacteria for FESEM

Bacteria treated with **Sc** and with **Sc-3** were filtered with PTFE 0.22 μm filters previously treated with a solution of 0.1 % ε-poly-L-lysine. Then, the filters were submerged into a solution of 2.5 % glutaraldehyde for 1 hour in order to fix the bacteria. Dehydration was carried out by submerging the filters in graded ethanol solution series (50, 70, 80, 95 and 100 %) for 10 minutes each. The samples were dried by critical point drying technique and coated with carbon for FESEM examination.

5.4.5 Cytotoxicity assays

5.4.5.1 Cell culture conditions

L929 fibroblast-like cells from American Type Culture Collection (ATCC-LGC Standards S.r.L., Milan, Italy) were maintained and expanded in DMEM supplemented with 10% FBS, 100 U·ml^{-1} penicillin and 100 μg·ml^{-1} streptomycin in standard conditions (37 °C, 5 % CO$_2$/95 % air, humidified atmosphere).

5.4.5.2 In vitro cell toxicity test

Before conducting cell toxicity experiments, samples (**Sc-3**, **Sc-2**, and **Sc** as reference) were washed with phosphate buffer solution (PBS), and sterilized for 15 minutes in ethanol 85 % and then 15 min in ethanol 70 %, by stirring. To assess cytotoxicity, L929 fibroblast-like cells were seeded at the density of 1.5·10^4 cells·cm^{-2} in 24-well plate and incubated for 24 hours. Triplicate wells were seeded for each sample, including negative and positive controls. The day

after **Sc**, **Sc-2** and **Sc-3** materials were carefully placed on the cell layer, ensuring that the specimens covered at least one tenth of the well bottom surface. A positive control (CTR+) was set up by adding 0.5 % phenol solution to the growth medium, and the negative control (CTR-) was represented by the only cell culture in complete DMEM.

In order to quantify cell viability at 24 and 48 hours, Alamar blue dye was added (1:10 v/v) to each culture, after removing the scaffold from wells, and incubated for 4 hours at 37 °C. The reagent is a dye which incorporates a redox indicator which changes its color in response to the chemical reduction of the growth medium resulting from cell growth. The results, in term of fluorescence, were expressed as relative fluorescence units (RFU).

At the same time points, the cell cultures supernatants were collected to detect LDH, which is a typical enzyme released by suffering and death cells. The procedures were performed following manufacturer's instruction. The developed colour, resulting by the activity of LDH, was spectrophotometrically read and the percentage of cytotoxicity for each sample type was calculated with the following formula:

$$\frac{ABS_{\text{sample}} - ABS_{CRL-}}{ABS_{CRL+} - ABS_{CRL-}} \, X \, 100$$

To observe the morphology of viable cells, a solution of 0.33 % Neutral Red dye in DMEM was added to each culture well (1:10 v/v) and incubated for 20 minutes at 37 °C. Viable cells typically incorporate the Neutral Red dye and preserve a normal morphology, while dead cells do not perform Neutral Red intake. Ten images of each culture were captured using a standard light microscope. The more significant images were analyzed according to the score reported below (UNI EN ISO 10993-5).

5.4.6 Biocompatibility assays

5.4.6.1 Cell culture conditions

Before conducting the biocompatibility assay, all samples (**Sc-3**, **Sc-2**, and **Sc** as reference) were sterilized in ethanol as previously described. MG-63 human osteoblast-like cells from American Type Culture Collection (ATCC-LGC Standards S.r.L., Milan, Italy) were used for biocompatibility experiments. Cells were maintained and expanded in DMEM supplemented with 10 % FBS, 100 U·ml^{-1} penicillin and 100 μg·ml^{-1} streptomycin, β-glicerophosphate (10^{-4} M) and ascorbic acid (50 μg·ml^{-1}) in standard conditions (37 °C, 5% CO_2/95% air, humidified atmosphere). At 80-90 % of confluence, the cells were detached by trypsinization and counted with Erythrosyn B vital dye to exclude dead cells. A suspension of $3\cdot10^4$ cells in 30 ☐l of medium was dropwise seeded on the scaffolds surface (equivalent to 10^5 cells·cm^{-2}).

The cell dispersion on the well bottom was minimized by carefully pipetting and repeating cell deposition and recovery. After 3 hours of incubation, 1.5 mL of medium were added to each well, so fully embedding the scaffolds. The same number of cells in 1.5 ml of medium was also seeded on polystyrene plates as control (CTR). The engineered constructs and the controls were cultured for 14 days by refeeding the culture medium twice a week.

5.4.6.2 Cell viability and morphology

In order to quantify cell viability at 24 hours, 1 week and 2 weeks, Alamar blue test was performed, as previously described for cell toxicity evaluation. Cell morphology and sample colonization were observed by LIVE/DEAD® assay according to the manufacturer's instructions. This mixture of fluorescent dyes includes calcein (suitable to label the vital cells), and ethidium homodimer (EthD-1, which goes through the damaged membranes of dead cells). Samples were visualized using an inverted microscope equipped with an epifluorescence set-up. The green and red fluorescence was typical of live and dead cells

respectively. Five images of each sample and control, at all time points, were captured using the digital camera, at 4x and 10x magnification.

5.4.6.3 Gene expression analysis

Gene expression was observed at 1, 2 and 3 weeks of culture. Total RNA was extracted by engineered constructs and controls using the commercial RNeasy Mini Kit and reverse transcribed using the Superscript Vilo cDNA synthesis kit. cDNA was diluted to the final concentration of 5 ng·µl^{-1}, and 10 ng of each sample were tested in duplicate. Gene expression was evaluated by qPCR, using the SYBR green PCR kit in a Light Cycler 2.0 Instrument. The protocol included a denaturation cycle at 95°C for 15 minutes, 25 to 40 cycles of amplification and a melting curve analysis to check for amplicon specificity. The following primer sets were used: GAPDH (forward: 5'-CTCTACCCACGGCAAGTTCAAC-3', reverse: 5'-GACATACTCAGCACCAGCATCAC-3'), ALPL (QuantiTect Primer Assay Hs_ALPL_1_SG), COL1A1 (QuantiTect Primer Assay Hs_COL1A1_1_SG), BGLAP (QuantiTect Primer Assay Hs_BGLAP_1_SG). The annealing temperatures were 55°C for all the primer sets except for GAPDH at 60°C. The mean threshold cycle was determined for each sample and used for the calculation of relative expression using the Livak method ($2^{-\Delta\Delta Ct}$), with GAPDH as reference gene and Sc samples as calibrators at each experimental time.[292]

5.4.7 Statistics

The statistical evaluation of data was performed using the software package SPSS/PC+ StatisticsTM 23.0 (SPSS Inc., Chicago, IL). The study is the results of three independent experiments and data are reported as mean standard deviations (SD) at a significance level of $P < 0.05$. After having verified normal distribution and homogeneity of variance, a one-way ANOVA was done for

---

[292] K. J. Livak, T. D. Schmittgen, Methods, **2001**, *25*, 402–408.

comparison between groups. Finally, post hoc multiple comparison test (Dunnett) was performed to detect significant differences among groups and controls. Student's t-test was used for the comparison between two groups.

6. Conclusions and perspectives

This thesis, entitled "Design of smart scaffolds for the treatment and prevention of bone infection", is focused on the development of smart organic-inorganic hybrid materials capable to perform controlled-delivery of drugs with biomedical purposes.

As it was stated in the **Introduction** chapter, the use of biomaterials with applications in biomedicine has experimented a rise upon the last years. Particularly, controlled-release systems that use mesoporous silica materials as a support have been widely studied and improved, resulting in meaningful applications as sensors, drug delivery systems, antitumoral designs or antibacterial devices. Apart from that, those biomaterials with bone regenerative properties, as mesoporous bioglasses or calcium phosphate ceramics, have also been studied and developed in order to adapt their use for specific disease cases. The main objective of this thesis was to develop innovative designs able to improve the features of the basic materials. This general objective was achieved. Thus, the conclusions of this thesis are:

-For the first time, mesoporous bioglasses have been equipped with molecular gates. In particular, a mesoporous bioglass was equiped with ATP and ε-poly-L-lysine molecular gates and the prepared material showed good performance in cellular and bacterial environments.

-Also, a gated bioglass to fight against bone infection was developed. This second material remarks the possibility to implement molecular gates in mesoporous bioglasses. The material conserved its bioactive properties, presented antibacterial behaviour and showed no toxicity to U-2 OS cells.

-A new device for the treatment of bone infection by *S.aureus* was developed. The material was able to release the cargo in the presence of *S.aureus* V8 protease and showed good selectivity to this enzyme.

-A calcium phosphate based material containing an essential oil component derivative was prepared. The material showed antimicrobial activity and good bone regenerative capabilities.

-All the synthesized solids show that it is possible to prepare functional materials against bone infection. The obtained results are promising, and could have meaningful applications in the biomedical field for the treatment of infection processes.

As we can observe, all the designs presented in this thesis have the scope of solving one of the most important medical problems related to bone surgery. As a proof of concept, organic-inorganic hybrid materials were prepared with the purpose of combining two strategies, as the ability of treat tumors and bacterial infection, and the ability of enhance bone growing. Thanks to the accurate design of the presented devices, this thesis contributes to the field of controlled delivery systems with promising results. Moreover, it has taken a step forward in the field of tissue regeneration, since the strategies developed in this thesis will help to avoid surgical problems as prosthesis infection or tumor growing. The need of an excesive antibiotic dosage after a surgery would not be necessary, since our designs are able to perform drug release in an efficient and localized way, avoiding complications related to high drug doses. From another point of view, the use of essential oil components presents an alternative for drugs treatment, which expands the horizons regarding to the treatment of infected tissues. In conclusion, this thesis has contributed to the field of biomedical devices and has helped to progress in the pathway to a new concept of a more advanced and personalized biomedicine.

199